THE UPTAKE AND ACCUMULATION OF CERIUM OXIDE NANOPARTICLES BY RAPHANUS SATIVUS L. (RADISH) IN HYDROPONIC AND SOIL SYSTEMS

A Dissertation

by

WEILAN ZHANG

Submitted to the Office of Graduate and Professional Studies of
Texas A&M University
in partial fulfillment of the requirements for the degree of

DOCTOR OF PHILOSOPHY

Chair of Committee,	Xingmao Ma
Committee Members,	Bill Batchelor
	Paul Schwab
	Qi Ying
Head of Department,	Robin Autenrieth

August 2017

Major Subject: Civil Engineering

ABSTRACT

Cerium oxide nanoparticles (CeO_2NPs) have received much attention recently because of their popular uses in industrial and commercial products. The accumulation of CeO_2NPs in the environment, especially in natural soils, becomes a potential risk to terrestrial plants. Although below-ground vegetables are most likely to accumulate the highest concentrations of CeO_2NPs, little work has been done to investigate the interactions between this plant group and CeO_2NPs. In this dissertation, the uptake and accumulation of CeO_2NPs by *Raphanus sativus* L. (radish) were evaluated in hydroponic and soil systems.

In the hydroponic system, the accumulation patterns and the effect of Ce on plant growth and physiological processes varied with the characteristics of Ce. While active transport appeared to be the primary pathway for ionic Ce accumulation in plant tissues, adsorption and diffusion of particulate Ce along the radial direction govern the accumulation of bulk CeO_2 and CeO_2NPs accumulation in radish storage roots. The intact CeO_2NPs could be taken up by the radish fine roots, but the upward transport was limited. Ce detected in radish shoots through root exposure is predominantly in the dissolved form. Importantly, the transformation of CeO_2NPs to ionic Ce on the radish fine root surface was first confirmed and the enhanced transformation was attributed to the organic acids with low molecular weight (e.g. malic acid) in the roots exudates of radish.

In the soil system, many soil properties, including the soil texture, mineral content, and organic matter content, affect the fractionation of CeO_2NPs in soil and their bioavailability to radish. Aging of CeO_2NPs in soil led to higher availability of dissolved Ce in the rhizosphere soil and greater accumulation of Ce in radish shoots. Efforts were also made to understand the interactions of CeO_2NPs with two major soil components (sand and clay). Experimental results and mathematical modeling results indicated that adsorption to sand and kaolin (a typical clay) particles had strong impact on the mobility of CeO_2NPs in soil. The surface properties of CeO_2NPs play a crucial role in these interactions.

DEDICATION

I dedicate this dissertation to my daughter, Diana.

ACKNOWLEDGEMENTS

I would like to thank my committee chair, Dr. Ma, and my committee members, Dr. Batchelor, Dr. Schwab, and Dr. Ying, for their guidance and support throughout the course of this research. I am very much thankful to Dr. Jason White of the Department of Analytical Chemistry at the Connecticut Agricultural Experiment Station for his help and support.

Thanks also go to my friends, colleagues, and the department faculty and staff for making my time at Texas A&M University a great experience. I also want to extend my gratitude to the U.S. Department of Agriculture for the research funding.

Finally, thanks to my parents for their encouragement and to my wife for her love.

CONTRIBUTORS AND FUNDING SOURCES

Contributors

Part 1, faculty committee recognition

This work was supervised by a dissertation committee consisting of Professor Xingmao Ma (advisor) and Professors Bill Batchelor and Qi Ying of the Department of Civil Engineering and Professor Paul Schwab of the Department of Soil and Crop Sciences.

Part 2, student/collaborator contributions

All work for the dissertation was completed by the student, in collaboration with Dr. Jason White of the Department of Analytical Chemistry at the Connecticut Agricultural Experiment Station and Professor Honglan Shi at Missouri University of Science and Technology.

Funding Sources

This work was made possible in part by the U.S. Department of Agriculture under Grant Number 2012-67005-19585.

Its contents are solely the responsibility of the authors and do not necessarily represent the official views of the U.S. Department of Agriculture.

TABLE OF CONTENTS

Page

Page

LIST OF FIGURES

Page

Page

Page

Page

Page

Page

LIST OF TABLES

Page

CHAPTER I

INTRODUCTION AND LITERATURE REVIEW

Nanotechnology and Nanoparticles

The concept of nanotechnology, which involves the manipulation of matter at nano-scale, was first introduced in 1959 by Dr. Richard Feynman and first used as a term by Professor Norio Taniguchi in 1974.[1] In 2015, the market values of nano-enabled products were estimated to be worth 3 trillion dollars, accounting for 15% of global manufacturing output.[2] The applications of engineered nanomaterials (ENMs), which is a critical subfield of nanotechnology, has attracted a large amount of attention recently.

ENMs are defined as engineered materials with at least one external dimension in the size range from approximately 1 – 100 nanometers.[3] ENMs with all three external dimensions at the nanoscale are termed engineered nanoparticles (ENPs).[3] Based on chemical composition, ENMs are usually classified into three categories: carbonaceous ENMs (primarily carbon nanotubes and fullerenes), polymeric ENMs (submicron-sized colloidal materials consisting of a polymer or copolymer), and metallic ENMs (including both elemental ENMs and metal oxide ENMs).

Carbonaceous ENMs are one of the key materials in nanotechnology and widely applied in the field of wastewater treatment processes, solar cells , microelectronics, energy storage, and coating and films, because of their high specific surface area, electrical conductivity, thermal conductivity, and tensile strength.[4] Most carbonaceous ENMs are incorporated into durable products in three different forms (nanotubes,

nanofibers, and nanoparticles) and are expected to be bound in the matrix throughout the life cycle of these products.[5] Among the three different forms, carbon nanotubes (CNTs) are the most widely used carbonaceous ENMs.

Over the last two decades, polymeric ENMs that have the properties of both nanomaterials and conventional polymer composites have also been widely applied in industry, especially in the aerospace/automotive engineering, renewable energy, and biomimetic sensor fields.[6] The significant mechanical and thermal properties of polymeric ENMs include gas impermeability, dimensional stability, and flame retardance.[6]

Compared with carbonaceous and polymeric ENMs, metallic ENMs, which have fascinated scientists and engineers for over a century, have the longest history and are now heavily utilized in the field of nanotechnology.[7] Currently, the metallic ENMs can be synthesized in desired size and shape, and modified with various chemical functional groups on the particle surface, which allow them to carry pharmaceuticals, proteins, enzymes, antibodies, and nucleotides.[7, 8] Thus, metallic ENMs potentially could be applied in biomedical technology, magnetic isolation, targeted drug delivery, and diagnostic imaging.[7]

Overall, the unique optical, electrical and chemical properties of ENMs are predominantly due to their very large specific surface area and the quantum nature of the energy state at nanometer scale. These novel properties lead to the potential for numerous applications of these ENMs in consumer, industrial, agricultural and

biomedical products. The applications of several most common ENMs are summarized in Table 1.1.

Table 1.1. Applications of several most common engineered nanomaterials (ENMs).

ENMs	Products/applications
Carbon Nano-Tubes (CNTs)	Composite fibers in materials to improve their mechanical, thermal and electrical properties[9]
	Tips for atomic force microscope probes[10]
	Scaffolding for bone growth[11]
Titanium Oxide Nanoparticles (TiO_2NPs)	Photocatalysis[12, 13]
	Contaminated water remediation[14]
	Food whitening[15]
	Cosmetic additive for ultraviolet radiation blocking[16]
Cerium oxide nanoparticles (CeO_2NPs)	Fuel additive/fuel-borne catalyst[17]
	Glass abrasive/grinding and polishing materials[18]
	Therapy material and nanomedicine[19-21]
Gold Nanoparticles (AuNPs)	Nanomedicine for diagnostic, drug delivery, and therapeutic purposes[22]
	Pollution sensing in agriculture[23, 24]
Silver Nanoparticles (AgNPs)	Antibacterial component in drugs and textiles to resist pathogens[25]
	Antibmicrobial component in pesticides[26]

Table 1.1. Continued.

ENMs	Products/applications
Zinc Oxide Nanoparticles (ZnONPs)	UV-absorbers in textiles[27]
	Additive in ceramics, glass, cement, rubber, paints, sunscreen and cosmetic[28]
	Chemical sensors and solar cells paints[29]
	Nano-fertilizer and nano-pesticides[28, 30]
Copper Oxide Nanoparticles (CuONPs)	Antimicrobial agent[31]
Iron(III) Oxide Nanoparticles (Fe_2O_3NPs)	Nano-fertilizer[32]
	Biomedicine[33]

In general, the possible fields for the applications of ENMs include advanced materials, display technologies, electronics, nutrition, cosmetics, medical drugs, and so on.[34] The wide applications of ENMs boost their production. The most produced ENMs worldwide include TiO_2NPs, SiO_2NPs, FeO_xNPs, AlO_xNPs, ZnONPs, CNTs, AgNPs, and CeO_2NPs. TiO_2NPs, as the ENMs with the highest production, are produced up to 10,000 tons per year.[34] FeO_xNPs, AlO_xNPs, ZnONPs, CNT, AgNPs, and CeO_2NPs are produced between 100 and 1,000 tons per year.[34] Such a large production of ENMs will understandably lead to their buildup in the environment during their manufacturing, uses, and disposal. Many previous studies have reported the detection of metallic ENMs in the waste to the environment.[35, 36] For example, CeO_2NPs can accumulate in the

environment from road runoffs that are contaminated by CeO_2NPs exhaust catalysts;[37] TiO_2NPs were reported to be released to the environment through industrial and urban effluents;[38] 75-100 μg/L of AgNPs have been detected in washing machine effluent after washing of AgNPs containing textiles.[39, 40]

The gradual increase of ENMs in the natural environment can be associated with potential risks. Although the understanding of the health and safety aspects of ENMs is still in its early stage, ENMs usually show more distinct toxicological properties than their bulk counterparts.[41] The toxicity of ENMs to organisms may stem from both the direct toxicity and indirect toxicity. In terms of the direct toxicity of ENMs, the toxic effects on organisms are caused by their high surface reactivity, because the large surface area of ENMs could intensify their reactivity and might cause catalysis of redox reactions with organic molecules.[36, 42] The indirect effects of ENMs on organisms can result from the release of their toxic ions or other toxic pollutants carried by ENMs [43]. In other words, the nano-scale dimension of ENMs is a key consideration in assessing their toxicological consequences to plants, animals, and human beings. Therefore, methods are required to assess the risks of ENMs in real world environments.

Over the last decade, due to environmental and health concerns of ENMs, the number of publications dealing with environmental implications of ENMs, including the interactions between ENMs and plants, increased dramatically. For example, as shown in Figure 1.1, the publications concerning the environment and ENMs rose fivefold during the last 10 years. To date, approximately 2200 peer-reviewed original publications addressing the environmental implications of ENMs are available in the

literature. Among these publications, the number of studies of the interactions between ENMs and plants jumped from 9 to 126 during the same period. More specifically, the number of investigations on the interactions between CeO_2NPs and plants increased from 2 to 36. Despite the increasing literature on ENMs, many questions remain. For example, the uptake pathways of ENMs by plants and the underlying mechanisms for ENM accumulation and transformation in plant tissues are still poorly understood.

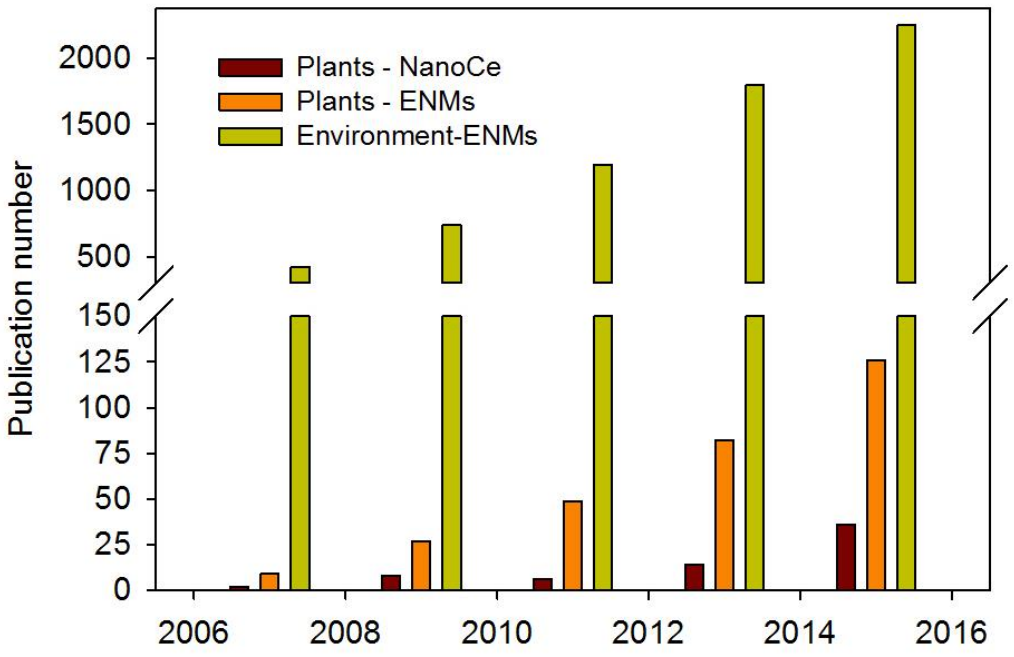

Figure 1.1. Number of peer reviewed research articles or book chapters on the topic of environmental implications of ENMs. Analyzed by using Web of Science. The search for the environmental impacts of ENMs: "topic= ((Environment) AND (nanoparticle OR nanomaterial))"; the search for the interactions between ENMs and plants: "topic= ((plant) AND (uptake OR interaction) AND (nanoparticle OR nanomaterial))"; the search for the interactions between CeO_2NPs and plants: "topic= ((plant) AND (uptake OR interaction) AND (nano* and Cerium))".

Physicochemical Properties and Applications of CeO_2NPs

Ce is a lanthanide metal and the most abundant (20-60 mg/kg) and reactive rare earth element. The oxide of Ce, CeO_2, is the most common form for Ce in the earth's crust. CeO_2NPs are also one of the most commonly used metallic ENMs in industry and consumer productions. Finely divided CeO_2 powder usually is used as a polishing agent for optical glass.[44, 45] CeO_2 can be also used in chemomechanical abrasives for insulating films due to its strong oxidizing active nature.[46] CeO_2NPs are also a key abrasive nanomaterial for chemical-mechanical planarization (CMP) of advanced integrated circuits.[47] In addition, CeO_2NPs are very effective in UV filtration. CeO_2 has a UV cut-off threshold at around 370 nm. Goharshadi et al.[48] demonstrated that most of the UV light (200-350 nm) can be blocked by CeO_2NPs, which renders CeO_2NPs a highly promising material for UV blocking in sunscreens and coating materials on sunglasses and parasols.

CeO_2 adopts the fluorite structure with a face-centered cubic unit cell. In the lattice structure of pure CeO_2, each Ce cation is coordinated with eight oxygen anions at the corner of a cube while each oxygen anion tetrahedrally coordinated with four Ce cations. Oxygen anions (O^{2-}) are removed from the lattice structure to form oxygen vacancies, depending on the temperature and oxygen partial pressure.[49, 50] The electrostatic balance caused by the loss of O^{2-} is offset by the reduction of two Ce^{4+} to Ce^{3+}. Ce^{3+} on the surface of CeO_2NPs could be oxidized back to Ce^{4+} caused by the oxidants in the environment. The density of oxygen vacancy and the percentage of Ce^{3+} on CeO_2NPs surface increase at smaller particle sizes.[51, 52] A recent study reported that

Ce^{3+} on the surface of uncoated CeO_2NPs jumped from 9.7% to 22.9% when the nanoparticle size was reduced from 64 to 9 nm.[53] Because of the unique redox chemistry between Ce^{3+}/Ce^{4+} on the particle surface, CeO_2NPs are one of the most important ENMs for a wide range of applications as described above.

The high capacity of CeO_2NPs to donating and storing oxygen can make CeO_2NPs an ideal catalyst in the diesel fuel to extend and improve fuel burn and reduce the ignition temperature.[54] Thus, CeO_2NPs in the diesel significantly enhance the efficacy of the diesel particulate filters to collect the burn-off soot and substantially decreases particle mass in the vehicle exhaust.[17, 54] Cassee et al.[17] reported that the most available commercial fuel borne catalysts (FBC) in the market, including Envirox (Energenics Pte Ltd.), Platinum Plus (Clean Diesel Technologies Inc), and Eolys DPX-9 (Rhodia), all contain CeO_2NPs with a size range of 5 to 40 nm. The addition of CeO_2NPs in the diesel fuel (final CeO_2NPs concentration is 5 mg/L [54]) makes diesel emissions inevitably contain Ce compounds, predominantly nanoscale CeO_2.[55] The released Ce would follow the runoff and eventually reach soil and natural water bodies.

The unique redox chemistry between Ce^{3+}/Ce^{4+} on CeO_2 surface also makes CeO_2NPs a potentially attractive nanomedicine because some previous research has demonstrated that CeO_2NPs can act as radical scavengers and redox cycling antioxidants. For example, Colon et al.[56] found that CeO_2NPs can protect gastrointestinal epithelium against radiation-induced damage by acting as radical scavenger and stimulating the production of superoxide dismutase 2 (SOD2) that converts superoxides into hydrogen peroxide. Das et al.[57] proposed that the presence of the mixed valence

states of Ce^{4+} and Ce^{3+} on the surface of CeO_2NPs makes the CeO_2NPs as a regenerative hydroxyl radical quencher. The mechanism is illustrated in Figure 1.2.

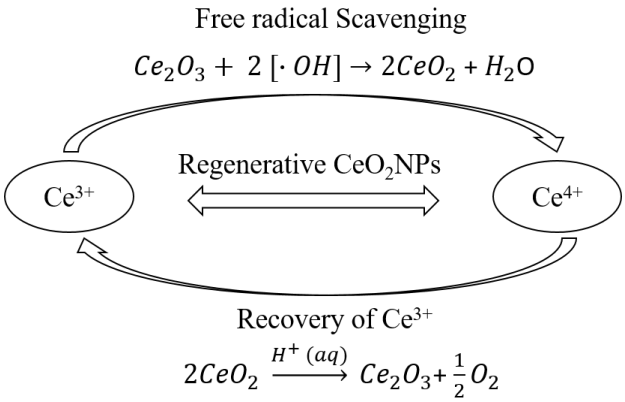

Figure 1.2. Schematic of the regenerative property and the ROS scavenging property of CeO_2NPs.[57]

Moreover, at higher Ce^{3+}/Ce^{4+} ratio (higher levels of Ce^{3+} on the particle surface), CeO_2NPs are efficient scavengers of superoxide ($O_2^{\cdot-}$) and display the superoxide dismutase (SOD) mimetic property:[58, 59]

$$O_2^{-\cdot} + Ce^{3+} + 2H^+ \rightarrow O_2 + Ce^{4+}$$

$$O_2^{-\cdot} + Ce^{4+} \rightarrow O_2 + Ce^{3+}$$

At relatively lower Ce^{3+}/Ce^{4+} ratios, CeO_2NPs were found to function as efficient antioxidant catalase (CAT) mimetics, which convert H_2O_2 to H_2O:[59]

$$H_2O_2 + 2Ce^{4+} + 2OH^- \rightarrow 2H_2O + O_2 + 2Ce^{3+}$$

SOD and CAT play paramount roles in maintaining the redox homeostasis in plants. Since CeO_2NPs could function as SOD or CAT depending on the Ce^{3+}/Ce^{4+} ratio on the particle surface,[60-62] it is reasonable to speculate that exposure to CeO_2NPs could affect the key biological processes in plants.

Human Exposure to CeO_2NPs

The highest exposure risk posed by CeO_2NPs for human beings occurs mainly through occupational activities. For example, workers have high risk to inhale CeO_2NPs during flame spray process used for coating and surface modification of materials.[63] In order to protect the workers, many countries have issued their own regulations to control this hazard. Although no information of CeO_2NPs workplace exposure limit (WEL) in the US was found, UK, Germany, and Netherlands proposed the WEL for CeO_2NPs to be 2×10^7 particles/m^3. [64] Also, Australia sets the WEL for CeO_2NPs to be 0.03×Australian inhalable WEL or 0.1×Australian respirable WEL.[64]

Aside from the occupational exposures, two other routes through which the general public can be exposed to CeO_2NPs may be possible: direct ingestion of CeO_2NPs through drinking water that is contaminated by CeO_2NPs and the consumption of foods which accumulate CeO_2NPs.[65] Plants as photosynthetic autotrophs form the foundation for many food webs. Consumption of plants represents the primary means by which many contaminants enter the food webs, including the human food supply.[66] In terms of the bioaccumulation of ENMs in food chains, evidence is growing that several food crops can accumulate CeO_2NPs.[36, 67-82] Given the concerns regarding the

environmental impacts and health risks of CeO_2NPs, understanding the interaction between plants and CeO_2NPs is critical. Evidence of Ce translocation from roots to shoots after plant exposure to CeO_2NPs and the propensity of roots to accumulate CeO_2NPs has been observed in some studies.[70, 83] These findings are important from a food safety and human health standpoint as they suggest a possible pathway of CeO_2NPs bioaccumulation in plant tissues. Based on the previous data, the belowground root, tubers, and bulb vegetables are more likely to accumulate increased concentrations of ENMs than above ground crops due to their direct contact with ENMs in soil. However, a small number of investigations in the literature have addressed the interactions of ENMs with belowground vegetables.

The Uptake of CeO_2NPs by Plants

Over the last two decades, especially after 2008, the bioaccumulation and transformation of ENMs in plants were broadly investigated to elucidate the risks of ENMs. Uptake and accumulation of ENMs in plants is an important aspect of plant-ENM interactions in terms of food safety. Mounting evidence has shown that ENMs (or elements of ENMs) can enter into plant root tissues and translocate to the shoots,[70, 83-85] despite the fact that ENMs aggregate in the environment and their particle sizes are often much larger than the pore sizes of plant cell walls.[86]

Plants develop mechanisms and exhibit specific barriers against intruders from the surrounding environment. For example, plant could excrete mucilage/exudates or create cell wall thickenings, such as papilla, callose, suberin and lignin deposits, to

physically intercept the mechanical intrusion of pathogens.[87, 88] Thus, nanoparticles may have to overcome the barriers created by plants to reach the vascular tissues. Based on previous observations, the pathway for ENMs to transport through the cell surface could be (1) passively diffusing through permeable regions of the cuticle, (2) facilitated transport due to ENMs surface properties, (3) facilitated transport by natural organic matter, (4) facilitated transport due to ubiquitous interactions between nanoparticles and microorganisms, and (5) facilitated transport by soil, sediment, or airborne particles.[86]

Nanoparticles crossing the cell wall thickenings through one of the pathways mentioned above then reach the cell wall. Previous studies show that the living plant cell wall, which is semipermeable, has pore sizes under 10 nm [88, 89] and represents a barrier for cellular uptake. So the uptake of ENMs across the cell wall largely depends on the nanoparticle size, and the pores of the cell wall. However, the pore sizes might be significantly underestimated. McCann et al.[90] claimed that the porosity of the cell wall is more flexible than previously thought and can be larger than 10 nm with a rare maximum of 20 nm. Even with the new finding on the pore size of cell walls, the physical size comparison of cell wall pores and ENMs is inadequate to interpret the accumulation of ENMs by plants. Numerous previous studies have shown that plants are capable of taking up ENMs that are larger than the physical pore sizes of root cell walls and membranes,[91] which contradict the common assumption that ENMs crossing the cell wall should be smaller than 20 nm in diameter. It remains unsettled why nanoparticles with much larger sizes than the physical openings of plant root cell walls can enter into

plant tissues. Partial dissolution and size reduction of nanoparticles may be necessary for plant uptake.[91]

After crossing the cell walls, ENMs may be transported apoplastically or symplastically inside the cells (Figure 1.3). In symplastic pathway, water/minerals and possibly ENMs can be transported from the cytoplasm of one cell to another through plasmodesmata, which consist of three main layers, including the plasma membrane, the desmotubule, and the cytoplasmic sleeve, and finally reach xylem tissue.[92, 93] During the division and differentiation of meristematic cells, plasmodesmata are formed as narrow threads of cytoplasm that pass through the cell walls of adjacent plant cells, allowing communication between cells.[94] So symplastic transport is strongly controlled by the plasmodesmata, which are the only connections of the cytoplasm of adjacent cells.[92] Based on the structure, there are two basic types of plasmodesmata: simple and branched.[95] Simple plamodesmata consist of a single channel traversing the cell wall, while branched plasmodesmata have two or more channels. The diameter of plasmodesmata are around 20 – 50 nm.[92, 96] The TEM images of ENMs or their aggregates in or near plasmodesmata in previous studies show that the nanoparticles fell in the size range of 15 to 40 nm in diameter can enter plasmodesmata (Figure 1.3).[91, 93] However, the AgNPs (20-40 nm) were found to be trapped by the plasmodesmata and posed a physical blockage of symplastic transport between cells in *Arabidopsis thaliana* plants.[91] Similarly, the AuNPs (15-25 nm) aggregated in the plasmodesmata and influence the transport of the subsequent AuNPs and other materials. The AuNPs, which could actually passed through the plasmodesmata and follow the symplastic pathway to

the xylem, constitute the major fraction of AuNPs transported upward in woody poplar plants (*Populus deltoids*).[93] Due to the scarce investigations and contradictory conclusions on the nanoparticles in the plasmodesmata, the significance of symplastic pathway for ENMs uptake is still unclear.

In apoplastic pathway, the apoplast consists of cell walls and intercellular spaces outside the plasma membrane, which is permeable.[97] Apoplast has little resistance to the movement of water, hence facilitates the transport of water and minerals flow in an upward direction to the xylem in the roots.[97] However, the apoplastic transport in the roots is interrupted by the Casparian strips in the endodermis, which block the passive flow of water and solutes to the xylem. The water and minerals flow are then move through the endodermis by the symplastic pathway (Figure 1.3). Nanoparticles, regardless of their surface charge, were mainly observed in the apoplast (cell wall, intercellular space, or middle lamellae of roots and the xylem),[91, 93, 98-100] indicating the transport of ENMs through the apoplastic pathway in the roots. Although the available literature has not confirmed the preference of nanoparticle transport (through the apoplast or symplast), a growing body of evidence supports the apoplastic pathway. Therefore, the apoplastic pathway was considered as the preferred route of the transport of ENMs within plants.[86]

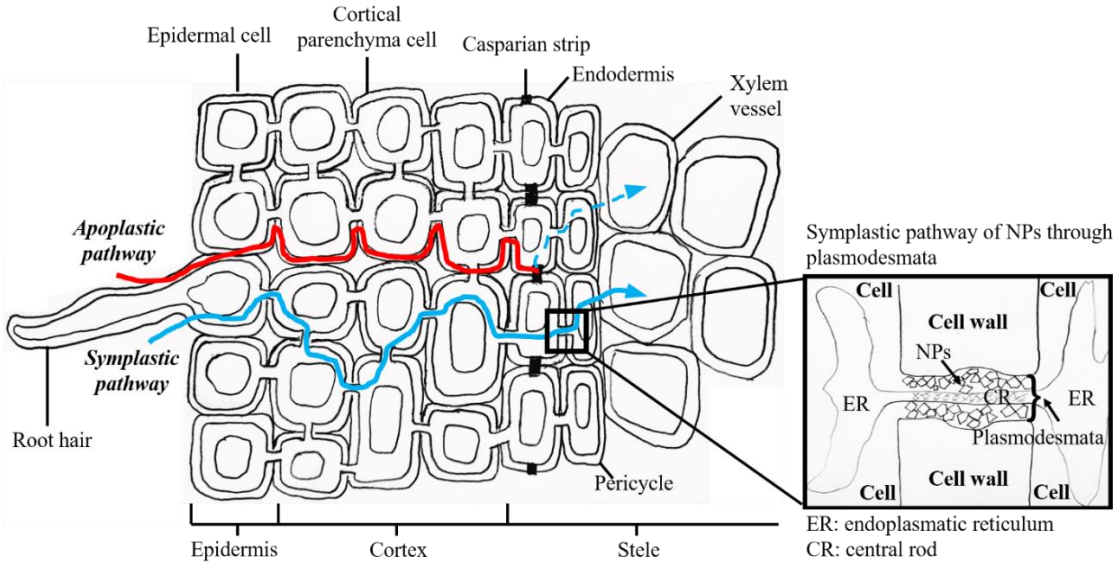

Figure 1.3. Key uptake pathways possible for nanoparticles (NPs) into the root and illustration of the possible NP pathway from cell to cell through plasmodesmata.[93, 95, 101]

In terms of CeO_2NPs, previous studies suggested that Ce element from CeO_2NPs can be taken up by plant roots and transported to shoots and the extent of transport is size and concentration dependent. Based on the literature, it is almost certain that CeO_2NPs up to 40 nm or even larger can be taken up by plant roots then translocated to other parts of plants. For example, after irrigating tomato (*Lycopersicon esculentum*) with solutions containing 10 mg/L of CeO_2NPs from seed germination to fruit bearing stage, Ce was detected in all tissues including tomato fruits.[84] The authors also noticed significantly higher Ce concentration in tomato seeds from treated plants than from control seeds. A separate study also indicated that Ce may cross the phloem membrane and accumulate in cucumber fruits.[85] However, whether the Ce detected in tomato or

cucumber (*Cucumis sativus*) fruits remained as CeO_2NPs or transformed products was not discussed in these studies.

Due to the low water solubility of CeO_2NPs, the detection of Ce in plant shoot tissues was previously interpreted as evidence that CeO_2NPs are taken up by plants as intact nanoparticles. The interpretation appeared to be supported by a previous study which showed that the oxidation state of Ce was unaltered in the root tissues after CeO_2NPs were exposed to four agricultural crops.[102] Moreover, López-Moreno et al.[70] confirmed the uptake of Ce by soybean (*Phaseolus vulgaris*) roots exposed to CeO_2NPs dispersion by using inductively coupled plasma optical emission spectroscopy (ICP-OES) and demonstrated the existence of Ce^{4+} in soybean roots with the help of synchrotron X-ray adsorption spectroscopy (XANES), also implying that no transformation of CeO_2NPs occurred during the uptake process. However, a different research group using soft X-ray scanning transmission microscopy (STXM) and near edge X-ray absorption spectrometry (XANES) analysis found measurable amount of $CePO_4$ in cucumber roots and Ce carboxylates in the shoot.[78] Zhang et al.[103] observed needlelike Ce clusters on root epidermis and in intercellular regions of cucumbers exposed to 2000 mg/L CeO_2NPs (40 nm) using TEM equipped with EDS, which were further confirmed to be $CePO_4$ by XANES. In addition, Ce carboxylates were detected in the cucumber stem and leaves, suggesting the transformation of CeO_2NPs to Ce^{3+} during CeO_2NPs uptake process. A subsequent study confirmed that Ce was present as CeO_2NPs and $CePO_4$ in the roots of lettuces exposed to CeO_2NPs while as CeO_2NPs and Ce carboxylates in the shoots.[104] Another study shows that Ce was primarily shown to

exist as CeO_2NPs in the root epidermis of kidney beans (*Phaseolus vulgaris*) exposed to CeO_2NPs, while 12% of nanoparticles was transformed to Ce^{3+} compound.[105]

The detection of transformed Ce in plant tissues sparked new debate on the uptake mechanisms of CeO_2NPs by plants. Recently, a new hypothesis has emerged which stated that CeO_2NPs are reduced to Ce^{3+} on root surface and then they are quickly oxidized back to Ce^{4+} to form CeO_2NPs once they are in plant tissues.[76] However, the proposition was solely based on the detection of dissolved Ce (assumed to be Ce^{3+} in the publication) with the help of X-ray Absorption Spectroscopy[83] or by determining the Zr (tracer) in plant tissues[76] and no mechanistic rationale or experimental evidence was provided. This is particularly fascinating considering that many layers of barriers such as the mucilage surrounding plant roots, the cell wall and the membrane must be crossed before CeO_2NPs can reach the xylem tissues for upward transport. The elucidation of the plant uptake mechanisms of CeO_2NPs has both significant scientific merit and tremendous broader impact because the ENM accumulation by plants represents an important pathway for human exposure to ENMs.

The Toxicity of CeO_2NPs to Plants

The toxicity of CeO_2NPs has been widely investigated for numerous plant species. From the plant physiology aspect, the impact of CeO_2NPs on plants was reported to be species and CeO_2NPs concentration dependent. Ma et al.[102] showed that exposure to 2000 mg/L CeO_2NPs (7.2 ± 0.7 nm) in hydroponic system for 5 days had no effect on the root elongation of radish (*Raphanus sativus*), rape (*Brassica napus*), tomato

(*Lycopersicon esculentum*), wheat (*Triticum aestivum*), cabbage (*Brassica oleracea*), and cucumber (*Cucumis sativus*), but inhibited root growth of lettuce (*Lactuca sativa*). The root elongation of alfalfa (*Medicago sativa*) and tomato (*Lycopersicon esculentum*) treated with 4000 mg/L CeO_2NPs was significantly reduced, although the two plants were not affected by CeO_2NPs exposure at 2000 mg/L.[83] The follow-up study from these authors showed that the CeO_2NPs higher than 2000 mg/L caused increasing of root elongation of soybean (*Glycine max*) seedlings.[70] Similar plant responses were reported in sand and soil cultivated plants. CeO_2NPs (16.5 ± 6.8 nm) higher than 1000 mg/kg in sand media diminished the chlorophyll content and significantly inhibited the biomass production of romaine lettuce (*Lactuca sativa*), while low CeO_2NPs (10 mg/kg) caused no toxic effects on plants.[104] An elevated nitrate-N level, which can be converted to nitrite and pose risks to human health, was detected in lettuce shoots exposed to CeO_2NPs higher than 500 mg/kg.[104] Zhao et al.[77] reported that the fresh biomass of large cucumber fruit (*Cucumis sativus*) exposed to 800 mg/kg CeO_2NPs (10 nm) in soil was reduced by 31.4%, while exposure to 400 mg/kg CeO_2NPs cause no difference in the biomass of plant fruits. These authors also found that CeO_2NPs at 800 mg/kg in soil changed the distribution of Ca in kernels of corn plants (*Zea mays*), altered quality of corn, and reduced the corn yield by 38%.[82] For plant exposed to CeO_2NPs aerosol, species dependent toxic effects were also observed. Hong et al.[106] found that foliar applied CeO_2NPs, either as powder (0.98 and 2.94 g/m^3) or as suspensions (20 – 320 mg/L), to cucumber (*Cucumis sativus*) leaves translocated to cucumber roots. The authors also reported that foliar application of CeO_2NPs at 200 mg/L altered the

nutritional status of cucumber fruit (reduced fruit Zn by 25%) and impacted cucumber photosynthetic parameter in seedlings (decreased photosynthesis rate and transpiration rate by 22% and 11% respectively).[107] Conversely, Birbaum et al.[108] found that foliar application of CeO_2NPs, either as powder at 0.178 g/m^3 or as suspension at 50 mg/L, resulted in no translocation of CeO_2NPs to other parts of corn plants and no physiological toxic effects on plant was observed.

In addition to the physiological responses, CeO_2NPs could induce genotoxicity to plants and cause molecular responses.[109] The genotoxicity of ENMs can be either direct or indirect. Direct genotoxicity results from physical interactions with DNA, such as influencing stacking forces among DNA bases, impacting phosphorylation, causing adduct formation, and altering gene expression/regulation, while indirect genotoxicity results from altered gene expression because of reduced DNA repair function or antioxidant depletion.[109] During ENM exposures, the mechanisms of ENM genotoxicity may indeed be more complex and work concurrently. Ma et al.[110] found that CeO_2NPs at 50-500 mg/L altered the expression of antioxidant related genes that regulate the sulfur assimilation and glutathione biosynthesis and induced genotoxicity to *Arabidopsis thaliana*. Pagano et al.[111] identified two genes that were consistently modulated by different ENM exposures (La_2O_3NPs, CuONPs, and CeO_2NPs): *BIP3* (005u) and *ORF31* (152u). The two genes can be considered potential biomarkers for ENM exposure and play a central role in ENMs genotoxicity and molecular response of plants. In summary, growing evidence shows that genotoxicity may be a common biotic response to ENM

exposure and should be considered when assessing the potential impacts of CeO_2NPs on plants.

Numerous studies proposed that the phytotoxic effects of CeO_2NPs on plants, including the physiology responses and molecular responses of plants to CeO_2NPs, were mainly caused by the oxidative stress incurred by CeO_2NPs and can be elucidated from the biochemical aspects.[73, 105, 106, 112-114] Under non-optimal conditions, such as pathogen attack, wounding, drought, salinity, waterlogging, heavy metal toxicity, nutrient deficiency and so on, plants may experience stress and the growth of plants may be affected.[115] Oxidative stress is induced if the reactive oxygen species (ROS) in plant tissues and the ability of plants to counteract or detoxify the harmful effects of ROS was imbalanced.[116] During the metabolism, respiration, photosynthesis and other biological processes in plants, ROS (e.g. superoxide radical ($O_2^{\cdot-}$), hydrogen peroxide (H_2O_2), hydroxyl radicals and singlet oxygen (O_2^*)) are continuously produced in mitochondria, chloroplasts, and peroxisomes.[117] ROS exhibit high chemical reactivity due to the unpaired electron on the oxygen atom.[118] Thus, ROS intend to acquire electrons from surrounding cells and molecules. Tightly regulated ROS are involved and exhibit critical functions in plants controlling processes such as growth, development, response to biotic and abiotic environmental stimuli, and programmed cell death.[119] However, excessive ROS in plant tissues may cause damage to plants. In general, the negative effects of ROS on plant cells include the damage of DNA, lipid peroxidation, oxidations of amino acids in proteins, and oxidative deactivation of specific enzymes.[120] In order to control the production of ROS and detoxify the excessive ROS, plants develop complex and

comprehensive mechanisms to scavenge ROS by means of antioxidants [117]. For example, $O_2^{-\cdot}$ can be converted to H_2O_2 catalyzed by superoxide dismutase (SOD), including MnSOD, FeSOD, and Cu/ZnSOD, through the following reaction:[121]

$$2O_2^{-\cdot} + 2H^+ \xrightarrow{SOD} H_2O_2 + O_2$$

In addition, peroxisomal enzyme, such as glycolate oxidase (GOX), can transfer O_2 molecules to H_2O_2.[122]

The H_2O_2 produced from $O_2^{-\cdot}$ and O_2 was then quenched and converted to H_2O catalyzed by catalase (CAT), ascorbate peroxidase (APX), guaiacol peroxidase (GPX), and some other peroxidases.[123, 124]

Besides the enzymatic antioxidants, nonenzymatic antioxidants, such as ascorbic acid, reduced glutathione, carotenoids, and flavonoids, have also been generated by plants against the oxidative stress.[123, 125] Similar to the enzymatic antioxidant, nonenzymatic antioxidants can serve as electron donors and detoxify ROS. The nonenzymatic and enzymatic antioxidants tightly coordinate to protect plants against various biotic and abiotic stresses.

The concentration of H_2O_2 and the activities of the antioxidants generated by plants, including SOD, GOX, CAT, APX, and GPX, are usually act as primary indicators of oxidative stress and are investigated in numerous previous studies. Zhao et al.[126] reported excessive production of H_2O_2 in corn plants (*Zea mays*) exposed to 400 – 800 mg/kg CeO_2NPs (10 ± 1 nm) in soil, demonstrating the oxidative stress in plant tissues. However, the up-regulation of several enzymes including the heat shock protein 70, CAT, and APX helped plants adapt to stress induced by CeO_2NPs and resulted in

minimum injury to plants. Rico et al.[127] reported that CeO_2NPs (8 ± 1 nm) treatment (500 mg/L) altered the enzyme activities of rice (*Oryza sative*) seedlings and caused membrane damage, oxidative stress, and photosynthetic stress in the shoots. Further investigation of the interaction between rice and CeO_2NPs showed that the CeO_2NPs at 500 mg/L led to higher production of H_2O_2 g, increased the peroxidase activities, and reduced the fatty acid and lignin contents in roots. The study on cilantro (*Coriandrum sativum*) exposed to 125 mg/kg CeO_2NPs (8 nm) in soil from the same research group showed that the activities of CAT and APX significantly increased in shoots and roots, suggesting that CeO_2NPs produced oxidative stress in cilantro plants.[112] This research group also showed that exposure of kidney bean (*Phaseolus vulgaris*) plants to suspensions of CeO_2NPs (8 ± 1 nm) at 62.5 and 125 mg/L increased the soluble proteins in roots by 204% and significantly enhanced the GPX activity in leaves, indicating an oxidative stress response of kidney bean plants to high concentrations of CeO_2NPs.[105] The romaine lettuce (*Lactuca sativa*) increased the antioxidant enzyme activities, including peroxidases and SOD, to defend the oxidative stress induced by CeO_2NPs at high concentrations (>1000 mg/L), but could not effectively attenuate the stress.[104] Ma et al.[114] found that exposure of CeO_2NPs at 10-100 mg/kg in soil led to a significantly higher H_2O_2 in plant tissues of *Brassica rapa* at floral stage . These authors further showed that the second and the third generation of *Brassica rapa* plants exposed to 10-1000 mg/L CeO_2NPs in soil generated even more H_2O_2 and experienced higher oxidative stress than their parental plants, demonstrating the chronic toxic impact of CeO_2NPs on plants.[113] Moreover, a report shows that even foliar CeO_2NPs application

can modify the antioxidant enzymatic activity, including CAT, APX, and dehydroascorbate reductase in in both shoot and root of cucumber (*Cucumis sativus*).[106]

From the literature, it appears that the biochemical responses of plants to CeO_2NPs is concentration dependent. While many negative physiological and biochemical effects of CeO_2NPs on plants have been reported as described above, the protective property of CeO_2NPs was also observed in relatively low concentrations. For example, CeO_2NPs at 0.1-10 mg/L had either an inconsequential or a slightly positive effect on tomato growth and production.[84] Exposure of rice (*Oryza sativa*) to CeO_2NPs from 62.5 to 125 mg/L decreased the H_2O_2 concentration in both roots and shoots, and the H_2O_2 generation in the rice roots exposed to 62.5 mg/L CeO_2NPs was reported to be reduced by 75%.[127] The beneficial effects on plant might be attributed to the radical scavenging ability of CeO_2NPs. The redox reaction between Ce^{3+} and Ce^{4+} ($Ce^{3+} \rightarrow Ce^{4+} + e^-$) are highly responsive to the surrounding pH.[128] Thus, the differential pH in the cytoplasm (~7.5) and in the extracellular and vacuolar spaces (~5.5)[129] allows the transition between Ce^{4+} and Ce^{3+} as illustrated in Figure 1.2. Das et al.[57] and Deshpande et al.[52] reported that the presence of the mixed valence states of Ce^{4+} and Ce^{3+} on the surface of CeO_2NPs allows CeO_2NPs to scavenge free radicals and makes the CeO_2NPs as a regenerative ROS quencher. The proposed reactions and mechanism of CeO_2NPs' ROS (e.g. H_2O_2, superoxide and hydroxyl radical) scavenging property was shown in previous section and illustrated in Figure 1.2. Data show that the radical scavenging ability of CeO_2NPs increases as the NPs size and concentration (as low as 10 μM) decrease.[130, 131] CeO_2NPs was reported to induce a protective cellular response in animal

cells at low concentration.[132, 133] Similarly, the ROS scavenging effect of CeO_2NPs could be predominant and beneficial in plants exposed to low concentration of CeO_2NPs.

Research Hypothesis and Goal

Because of the potential impacts of CeO_2NPs on plants, the risks of CeO_2NPs to plants can be significant and the Organization for Economic Cooperation and Development (OECD) has designated CeO_2NPs as a priority pollutant.[134] It should be realized that the concentrations of CeO_2NPs and other ENMs in the environment reported from mass flow models are frequently the average concentrations in certain media of a specific region and usually relatively low. The low model output makes the "hot spots", which is the primary sink of ENMs in the environment (soils and natural water bodies) with significantly higher ENMs concentrations, easy to overlook. For example, the average concentration of Ce in the in subsoil around London and in the North Yorkshire Dales was 36 - 45 mg/kg, but elevated Ce concentration (108 - 136 mg/kg) was found in the top 2 cm of soil alongside the M1, M6, and M25 motorways due to the exhaust-discharged CeO_2NPs from vehicles.[37]

In terms of ENM aggregation, surface manipulation in ENM synthesis often reduces aggregation. In addition, many factors in the environment (e.g. natural organic matters) actually stabilize ENMs.[135, 136] A key fact which should be emphasized that almost none of the previous studies investigating ENM accumulation in plants completely avoided aggregation, however, significant plant accumulation of ENM elements has been reported.[137] The results from previous studies raised several critical

questions: how do ENMs enter into plants against all the physical barriers plant roots have assembled? Will ENMs undergo any transformation during the plant uptake process and what are the mechanisms if transformation occurs? How do various environmental conditions such as soil properties play a role in the plant ENM interactions? The answers to these questions will provide more mechanistic insights into the interactions between plants and ENMs and may lead to more sustainable applications of ENMs in society. The dissertation aims to address these critical questions using CeO_2NPs as a model nanoparticle. Radish (*Raphanus sativus* L.) was selected as a model plant for this dissertation based on several factors, including the close relevance of this crop to US agriculture, the magnitude of consumption by US citizens, and the short growth cycle. More importantly, because the main edible tissue of radish is in direct contact with soil-borne or waterborne CeO_2NPs, it could accumulate higher concentrations of CeO_2NPs, resulting in higher potential risks to human health by consumption of the edible tissue.

The goal of this dissertation was to understand the uptake and accumulation CeO_2NPs by a selected belowground vegetable (radish) under different conditions. To achieve the overall goal, five hypotheses were developed:

Hypothesis 1: CeO_2NPs can be taken up by radish and the particle size plays a critical role in the CeO_2NPs-radish interaction.

Hypothesis 2: The transformation of CeO_2NPs occurs on the root surface during the uptake of CeO_2NPs by radish and plays a critical role in Ce uptake.

Hypothesis 3: Soil properties affect the fractionation of CeO_2NPs in soil and the bioavailability of CeO_2NPs to plants.

Hypothesis 4: The aging of CeO_2NPs in soil affects the fractionation of CeO_2NPs in soil and the bioavailability of CeO_2NPs to plants.

Hypothesis 5: Soil texture and CeO_2NPs surface charge are important factors that govern the mobility of CeO_2NPs in soil.

To test the above hypotheses, five experiments were conducted

(1) To examine the uptake and accumulation of CeO_2NPs and their bulk/ionic counterparts by radish in a hydroponic system.

(2) To determine the physicochemical properties of Ce in plants and investigate the uptake mechanisms of CeO_2NPs by radish in a hydroponic system.

(3) To study the impacts of soil properties on the bioavailability and translocation of CeO_2NPs to radish.

(4) To evaluate the aging effects of CeO_2NPs on their fractionation in soil and bioavailability to radish.

(5) To explore the underlying mechanisms of interactions between CeO_2NPs and soil particles.

Overall, the results of these five experiments established a framework for the potential risks of CeO_2NPs to belowground vegetables under different conditions.

CHAPTER II

THE UPTAKE AND ACCUMULATION OF CEO_2NPS AND THEIR BULK/IONIC COUNTERPARTS BY RADISH IN NUTRIENT SOLUTION*

Introduction

Concerns about the toxicity of ENMs to humans and the environment grow with the ever-expanding applications of ENMs. CeO_2NPs are released into the environment as a component in consumer products or during occupational activities, and are detected in wastewater streams and soils.[138] Because of the large specific surface area and the redox chemistry between Ce^{3+}/Ce^{4+} on the particle surface, CeO_2NPs exhibit unique physical, chemical, and biological properties compared with their bulk and ionic counterparts. The unique properties of CeO_2NPs that are missing from their bulk and ionic counterparts could be a double-edged sword: CeO_2NPs could introduce oxidative stress to plants at high concentrations but they could also function as an antioxidant to defend oxidative stress at low concentrations. Although the synthesis of CeO_2NPs adds desirable physical and/or chemical properties over the bulk or ionic forms, the potential environmental health and safety implications of CeO_2NPs use have become a serious concern.

---

* Part of this chapter is reprinted with permission from "Uptake and accumulation of bulk and nano-sized cerium oxide particles and ionic cerium by radish (Raphanus sativus L.)" by Zhang, W.; Ebbs, S. D.; Musante, C.; White, J. C.; Gao, C.; Ma, X., 2015. *Journal of Agricultural and Food Chemistry*, 63, 382-390, Copyright [2015] by American Chemical Society.

The potential toxicity of CeO_2NPs (6−40 nm, unmodified) to bacteria, fish, and mammalian cells has been reported.[139, 140] Plants, as a food source for humans, play a critical role in maintaining ecosystem health and function. Plant uptake of ENMs represents a plausible risk for human exposure to these nanoparticles through food consumption. Consequently, investigation of the uptake and accumulation of CeO_2NPs by agricultural crops is not only warranted but also critical to food safety and human health. Nanoparticles typically exhibit stronger effects on plants than their bulk counterparts. For example, following a 15 day hydroponic exposure, the biomass of zucchini plant exposed to silver nanoparticles was 75% less than that of plants treated with the same concentrations of bulk silver powder.[141] For CeO_2 particles, it is well accepted that the presence of highly mobile lattice oxygen on the surface could cause oxygen vacancy on the surface.[52] With the decrease of nanoparticle size, the specific surface area and consequently the density of the oxygen vacancy increase. The separation of oxygen from the lattice structure generates electrons, which can be used to reduce Ce^{4+} to Ce^{3+}. With increasing oxygen vacancy, the ratio of Ce^{3+}/Ce^{4+} will increase on the surface of CeO_2NPs.[51, 52] Because Ce^{3+} is about 14% larger than Ce^{4+},[52] the conversion of Ce^{4+} to Ce^{3+} will strain the lattice structure and increase the reactivity and superoxide dismutase (SOD) mimetic activity of the CeO_2 particles.[58, 59] Therefore, particle size is an important consideration in the assessment of the environmental toxicity of CeO_2. Unfortunately, information on the size effect of CeO_2 particles on radish development in the literature is very limited. Due to the potential dissolution of some metallic nanoparticles, another major question actively investigated in the

scientific community of nanotoxicology is the comparative toxicity of nanoparticles and the ionic form of the particles. Because of the low solubility of CeO_2NPs in liquid solutions, ionic Ce was generally not included in the experimental paradigms.[70, 73, 85, 142] However, recent investigations on the biotransformation of CeO_2NPs demonstrated the enhanced dissolution of CeO_2NPs when interacting with plants.[53, 71, 76, 104] Therefore, it is necessary to acquire a comprehensive understanding and comparison of the fate and phytotoxicity of ionic Ce.

Several studies have addressed the interactions of CeO_2NPs with terrestrial plants. The results from the previous studies showed that the biological responses of plants to CeO_2NPs are strongly species-dependent. For example, Gui et al.[68] reported that CeO_2NPs were taken up by lettuce plant and had a positive effect on plant growth at 100 mg/kg, but inhibited plant growth at 1000 mg/kg. Wang et al.[84] found that uncoated CeO_2NPs (<25 nm) at 0.1−10 mg/L had a slightly positive effect on tomato (*Solanum lycopersicum* L.) growth and yield; Ma et al.[102] stated that exposure to uncoated CeO_2NPs with an average diameter of 7.2 ± 0.7 nm in hydroponic system for 5 days had no effects on the root elongation of rape (*Brassica napus* L.), wheat (*Triticum aestivum* L.), cabbage (*Brassica oleracea* L.), tomato (*Lycopersicon esculentum* L.), and cucumber (*Cucumis sativus* L.) at 2000 mg/L, but inhibited root growth of lettuce (*Lactuca sativa* L.). Hernandez-Viezcas et al.[80] reported that mesquite (*Prosopis juliflora velutina*) had a higher degree of tolerance for the effect of CeO_2NPs (ceria cubic, rods ≈ 8 × 67 nm) than domesticated crop species and showed no visible signs of stress when exposed to 500-4000 mg/L CeO_2NPs suspensions. Rico et al.[73] indicated that uncoated

CeO_2NPs with an average size of 231 ± 16 nm up to 500 mg/L induced a concentration-dependent modification of the oxidative stress and antioxidant defense system in the rice seedlings. However, few of these studies focused on the uptake of CeO_2NPs by belowground vegetables, even though the edible tissues of the belowground plants often have direct contact with soilborne CeO_2NPs. In this chapter, radish (*Raphanus sativus* L.), which is a popular vegetable with high global consumption, was adopted as a model plant.

The objectives of this chapter were twofold: (1) to evaluate the effects of chemical forms (e.g. Ce particles vs. ionic Ce) and physical sizes (e.g. bulk CeO_2 and CeO_2NPs) of Ce on the growth of radish, and (2) to investigate the uptake and accumulation of Ce in different forms and sizes by radish tissues. With the two objectives, this chapter aimed to test the fundamental hypothesis that CeO_2NPs can be accumulated by radish. These results may provide in-depth understanding on the possible differential accumulation of Ce with different forms and particle sizes by plants for subsequent studies.

Materials and Methods

Chemicals and CeO_2NPs characterization

A laboratory investigation was conducted using hydroponics to minimize interferences from the growth media. To determine how different forms of Ce affect the growth of radish and the uptake of Ce by radish, four treatments were prepared, all in

one-fourth strength Hoagland solution[143]: (1) control (no Ce treatment); (2) 10 mg/L bulk CeO_2 suspension (Bulk); (3) 10 mg/L CeO_2NPs dispersion (NPs); (4) 10 mg/L $CeCl_3$ solution (Ion). Dispersion of uncoated CeO_2NPs (10 wt % in H_2O) and cerium (III) chloride heptahydrate were purchased from Sigma-Aldrich (St. Louis, MO). The bulk powder of CeO_2 was obtained from Strem Chemicals (Newburyport, MA). The size and morphology of CeO_2NPs and bulk CeO_2 were confirmed by a Hitachi H-7650 transmission electron microscope (TEM) (Hitachi, Tokyo, Japan). Hoagland solution (one-fourth strength) was prepared by dissolving an appropriate amount of the modified Hoagland basal salt mixture (Phytotechnology Laboratories, Lenexa, KS) with deionized water.

Seed germination and growth conditions

The radish seeds [Cherriette (F1)] were purchased from Johnny's Selected Seeds (Winslow, ME). Seeds were surface sterilized with 1.25% sodium hypochlorite solution for 10 min and then rinsed with deionized water three times. The sterilized seeds were germinated on moist filter paper in a Petri dish for 7 days (Figure 2.1a). Healthy young seedlings were then transferred to 50 mL polypropylene centrifuge tubes containing one-fourth strength Hoagland solution and were incubated in a growth cart with a 16-hour light/ 8-hour dark cycle (28 °C) to allow the seedlings to further develop (Figure 2.1b). The growth cart was equipped with four T5 fluorescent bulbs, providing a light intensity of approximately 104 μmol m^{-2} s^{-1} of visible light at the height of plant leaves. After 7 days, the seedlings were transferred from the centrifuge tubes to 100 mL glass jars containing the four treatment solutions respectively (Figure 2.1c). Each jar had a floating

lid made by Hareline 2 mm thin fly foam (Fishwest, Sandy, UT, USA) so that the plant roots were constantly submerged in the treatment solutions. Each treatment had 12 replicates. The solutions in the jars were carefully replenished without splashing on the leaves every other day with the same treatment solution to compensate for evapotranspiration. Plants were harvested 35 days after germination (21 days after treatment, Figure 2.1d).

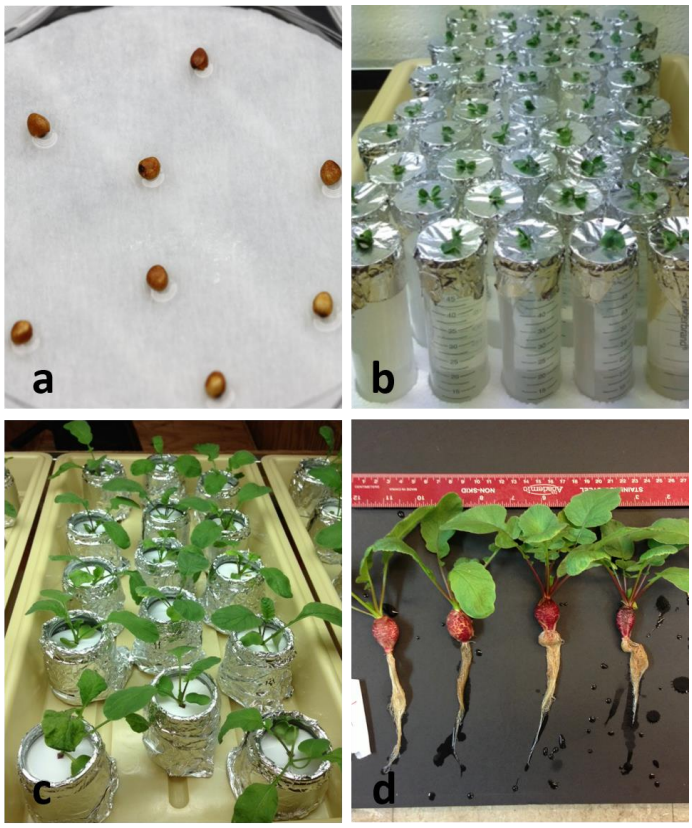

Figure 2.1. Hydroponic cultivation process of radish. (a) Seed germination in Petri dish, (b) development of seedlings in 50 mL centrifuge tubes, (c) development of plants in 100 mL glass jars, (d) plant harvest.

Plant physiological responses

The cumulative transpiration was calculated by summing the daily transpiration over the 21-day treatment period. The daily transpiration was recorded by measuring the water surface drop in the jar before the solution replenishment. Relative chlorophyll content was measured with a SPAD 502 Plus Chlorophyll Meter (Spectrum Technologies Inc., Aurora, IL) one day before harvest. The light-adapted *Y(II)* and dark-adapted F_v/F_M were measured by an OS 1p chlorophyll fluorometer (Opti-sciences Inc., Hudson, NH) on the same day the relative chlorophyll was measured. The electrolyte leakage of fine roots was conducted following the published procedures with some modifications.[144, 145] Briefly, the entire fine root system was submerged in 50 mL of deionized water and the initial conductivity C_w was measured immediately (Orion ROSS Ultra pH/ATC Triode Orion Star A325 Thermo Fisher Scientific, Waltham, MA). The conductivity of the solution was measured again as C_0 after 3 hours of incubation at room temperature. The entire fine roots were then autoclaved at 121 °C for 20 min with a Tuttnauer Brinkman 3850 M autoclave to release all electrolytes. The final conductivity C_t was measured after the samples cooled to room temperature. The percentage of electrolyte leakage was calculated as $E_L = (C_0 - C_w)/(C_t - C_w) \times 100$.

Ce uptake, accumulation, and distribution

At harvest, radish plants were separated into fine roots, storage root, and shoots. The fresh and dry biomass of each part were determined before and after drying in an oven at 75 °C for 7 days. The Ce concentration in each part of radish was quantified by using an inductively coupled plasma mass spectrometry (ICP-MS) after digesting the

plant tissues. The dry tissues were ground into fine powders, from which 0.25 g of the ground tissues was weighed and mixed with 4 mL of 70% v/v nitric acid. The mixture was heated at 95 °C for 20 min and then at 45 °C for 4 min, and the cycle was repeated five times. Afterward, 2 mL of hydrogen peroxide was added to the mixture and heated using the same temperature cycle until the solution was clear. The digest solution was then analyzed by an ICP-MS to obtain the Ce concentration in each radish sample.

The fresh fine root tips and sections of the storage roots from each treatment were observed under a Zeiss LSM 510 META confocal microscope to study the Ce distribution in the radish tissues. A laser excitation wavelength of 543 nm was used and an emission filter band-pass was set between 530 and 590 nm to collect both the laser reflection and the auto fluorescence in the excited region.

Data analysis

The results are reported as mean ± standard error of three replicates. One-way ANOVA analysis and Duncan's test for post hoc comparisons were performed with IBM SPSS Statistics V22.0 at $p<0.05$.

Results

Characterization of bulk CeO_2 and CeO_2NPs

Figure 2.2 shows the TEM images of bulk CeO_2 and CeO_2NPs in one-fourth strength Hoagland solution. Bulk CeO_2 were mostly at the micrometer scale, but the sizes were not uniform. Particles at the nanoscale were also detected in the bulk solutions. The sizes of bulk CeO_2 ranged approximately from 100 to 4000 nm.

Individual CeO_2NPs possessed irregular shapes with an average diameter ranged from 10 to 30 nm. The average particle size of CeO_2NPs, which was 17.2 nm, was obtained by measuring the diameter of individual nanoparticles in the TEM image with an imaging processing software ImageJ (ver 1.49). The nanoparticles aggregated considerably in the Hoagland solution, due to the high ionic strength. The hydrodynamic diameter of the nanoparticle aggregates was around 600 nm as measured by DLS. The zeta potential of CeO_2NPs in the Hoagland solution was approximately −11.9 mV, suggesting that the nanoparticles in the suspension were not stable.

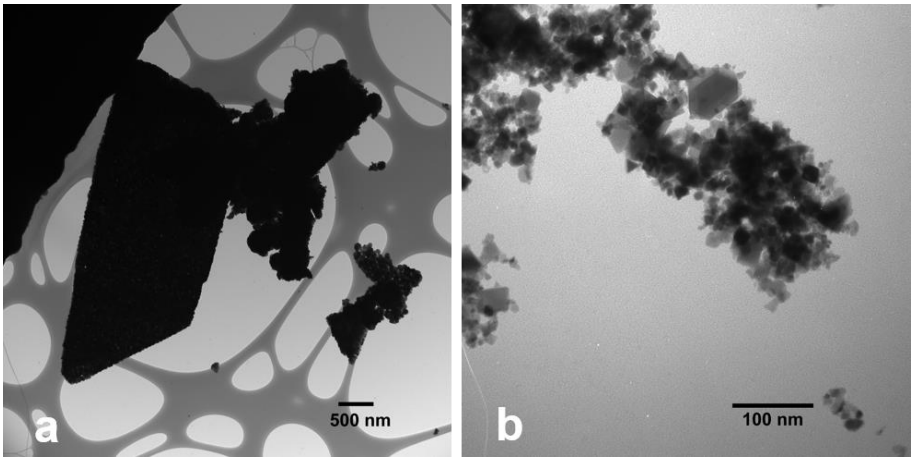

Figure 2.2. TEM images of CeO_2 particles (a: bulk CeO_2, b: CeO_2NPs).

Plant physiological status

The radish exposed to bulk CeO_2 had the highest total dry biomass, which was significantly greater than all other treatments (Figure 2.3a). The biomass of the CeO_2NPs

treated plants was not significantly different from the control plants. The plant biomass exposed to Ce ions was significantly lower than that of all other treatments. When the plant tissues were examined separately, the radishes exposed to bulk CeO_2, which had similar shoot biomass as radishes exposed to CeO_2NPs, had significantly higher dry shoot biomass than control and plants exposed to Ce ions (Figure 2.3b). The dry weight of storage roots across the treatments exhibited patterns similar to those of the total dry biomass (Figure 2.3c), but the dry biomass of fine roots did not differ significantly as a function of treatment (Figure 2.3d). The distribution of the biomass between the root (fine roots + storage root) and shoot compartments was significantly different in response to treatment. The shoot/root ratio of dry biomass of Ce ion treated radish (1.34 ± 0.11) was significantly higher than all other treatments, which had similar ratios (control: 1.00 ± 0.10; bulk CeO_2: 0.95 ± 0.06; CeO_2NPs: 1.07 ± 0.07). Visually, there was no apparent adverse effect of any of the Ce treatments on the growth and development of the radish plants except for the size differences (Figure 2.3e).

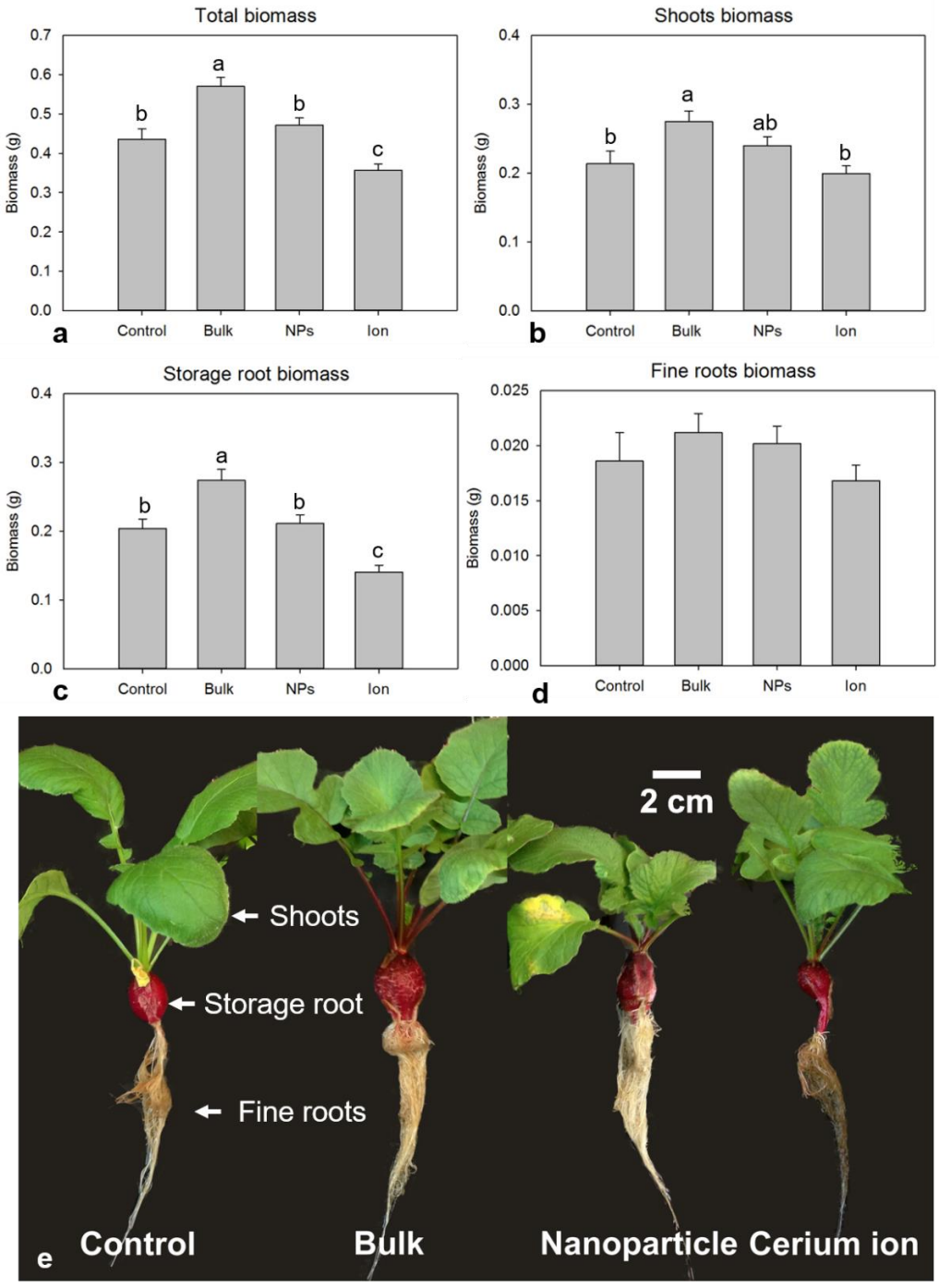

Figure 2.3. Dry biomass of total radish and different radish tissues treated with 10 mg/L of different forms of cerium (a−d). The reported values are the mean of 12 replicates, and the error bars represent standard error. Different letters represent significant differences between the treatments (p<0.05). (e) Images of typical radish plants from the different treatments.

In addition to the root biomass, the fine root membrane integrity was significantly affected by different forms of Ce. Figure 2.4 indicates that 10 mg/L of CeO_2NPs and ionic Ce resulted in significantly greater electrolyte leakage compared with the control roots. Leakage from fine roots exposed to bulk CeO_2 was not significantly different from control fine roots.

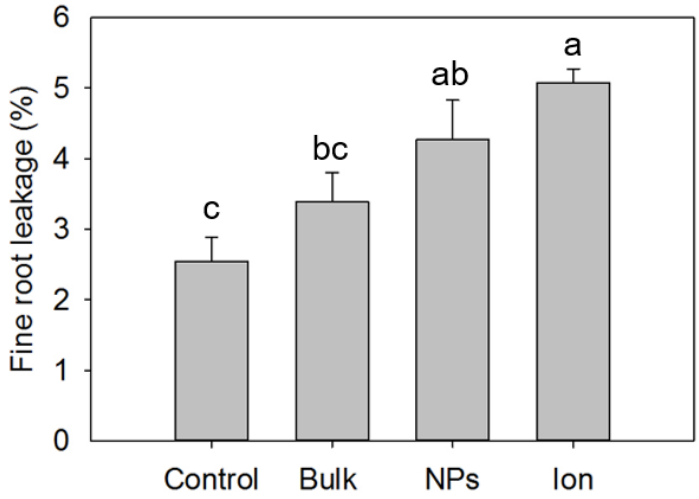

Figure 2.4. Electrolyte leakage from radish fine roots grown hydroponically in different solutions. The reported values are the average of five replicates in each treatment, and the error bars represent standard error. Different letters represent significant differences between the treatments (p<0.05).

The accumulative transpiration of radish for all treatments was comparable until day 21, then the accumulative transpiration of Ce ion treated radish became significantly lower than other treatment groups (Figure 2.5).

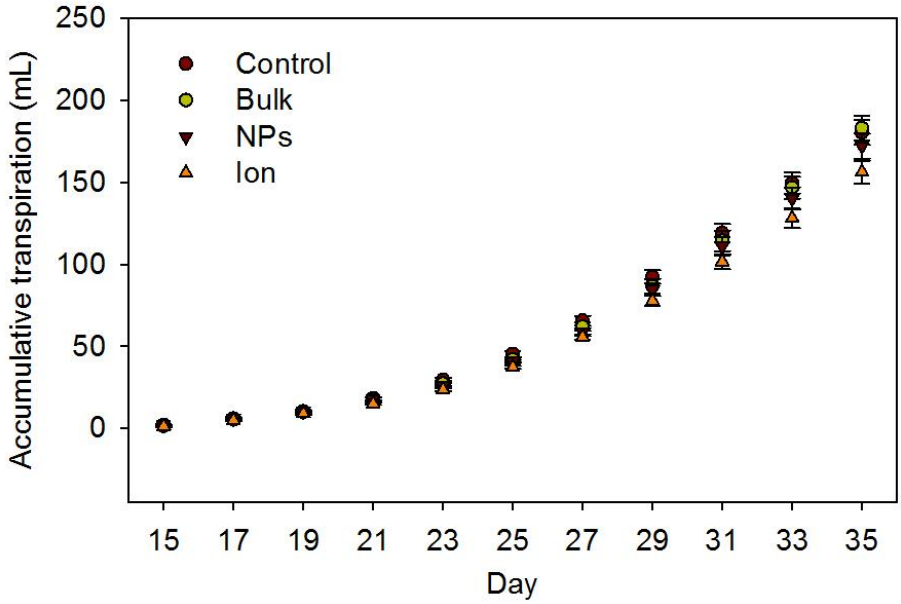

Figure 2.5. Average accumulative transpiration of radish treated with different forms and sizes of cerium, n=6.

The relative chlorophyll content expressed in percentage is shown in Table 2.1. Although all treated radishes had lower relative chlorophyll content, only the bulk CeO_2 and CeO_2NPs treated leaves had significantly lower chlorophyll content compared to the controls. The average quantum yield of photosystem II (*Y(II)*) and the F_V/F_M ratio for plants from different treatments are also shown in Table 2.1. The *Y(II)* was unaffected by the treatments. In contrast, only radishes exposed to bulk CeO_2 displayed a significantly lower value of the F_V/F_M ratio than the control plants. No significant differences were observed between the other Ce treatments.

Table 2.1. Relative chlorophyll content expressed as percentage of control of each treatment, average *Y(II)*, and F_V/F_M ratio, n=12. Different letters in the table represent significant differences between the treatments ($p<0.05$).

	Relative Chlorophyll (%)	Standard error	*Y(II)*	Standard error	F_V/F_M	Standard error
Control	100.00 [a]	2.67	0.774	0.007	0.830 [a]	0.003
Bulk	87.22 [b]	3.84	0.728	0.022	0.757 [b]	0.026
NPs	83.69 [b]	4.24	0.731	0.020	0.780 [ab]	0.016
Ion	91.51 [ab]	4.68	0.697	0.060	0.797 [ab]	0.020

Ce uptake and accumulation

Exposure to Ce resulted in significantly greater concentrations of Ce element in plant tissues. For the treated plants, the Ce concentration (mg Ce/kg tissue) and Ce (μg) content were significantly higher in the fine roots than in other tissues (Figure 2.6). Among different treatments, the concentration of Ce in the storage root was not significantly different between Ce treatments (Figure 2.6a). In the shoot tissues, radishes exposed to Ce ions had highest Ce concentration, followed by radishes exposed to bulk CeO_2 and then radishes exposed to CeO_2NPs. The fine roots of radishes exposed to CeO_2NPs had significantly higher concentration of Ce than the plants exposed to bulk CeO_2 and Ce ions. When the Ce content rather than the Ce concentration in different tissues was compared, Ce content in the storage roots of different treatments was still similar (Figure 2.6b). The Ce contents in the shoots of radishes exposed to bulk CeO_2 and Ce ions were not significantly different. However, the Ce content in shoots of radish exposed to CeO_2NPs was significantly lower than that of radishes exposed to bulk CeO2

and Ce ions. In the fine roots, the Ce contents demonstrated patterns similar to the Ce concentrations for different treatments.

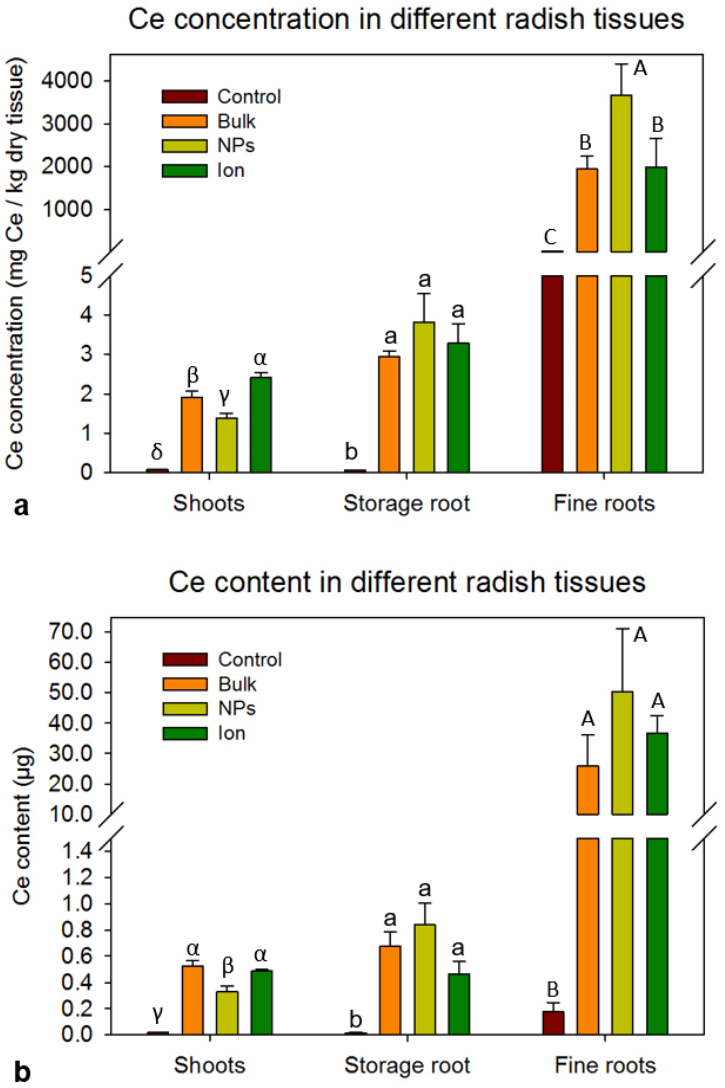

Figure 2.6. (a) Ce concentrations and (b) Ce contents in different radish tissues. The reported values in panel (a) are the average of four measurements. The reported values in panel (b) are the average of three measurements. Errors bars represent standard errors. Letters and Greek symbols above bars reflect their statistical grouping. Different letters and Greek symbols represent significant differences between the treatments (p<0.05).

Cerium localization and distribution in radish root and storage root

For the fine root tips, the confocal microscopic images were captured both on the root surface and at different depths from the root surface. The control had some weak signals either from the cerium content in the control tissues or from background excitation (Figure 2.7a). In contrast, plant roots from treated plants all generated stronger signals (Figure 2.7b− f). However, the signal patterns were noticeably different. On the fine root exposed to bulk CeO_2, the signals were only detected from the mucilage surrounding the root tip in both surface and deeper scanning images (Figure 2.7b, c). CeO_2NPs were detected on larger areas of the root surface as well as the mucilage on the root tip of the plants exposed to CeO_2NPs (Figure 2.7d). The signal was even more prominent in the deeper scanning planes (Figure 2.7e). For radish fine root exposed to Ce ions, the signals were predominantly detected in the surrounding areas of root surface. Neither the surface scan nor the deep scan detected significantly stronger signals than the controls within the root itself (Figure 2.7f). Figure 2.8 shows the confocal images of cut slices of radish storage roots. The control storage root showed little signal (Figure 2.8b). In comparison, storage roots from treated plants had strong signals. For radish exposed to bulk CeO_2, all signals came from the pigmented periderm with a random pattern (Figure 2.8c). For radish exposed to CeO_2NPs, stronger signals were observed in the pigmented periderm. In addition, the nanoparticles appeared to penetrate further into the storage root (Figure 2.8d). Ce was detected not only in the periderm but also in the secondary vascular tissues in the storage root of radish exposed to Ce ions (Figure 2.8e, f)

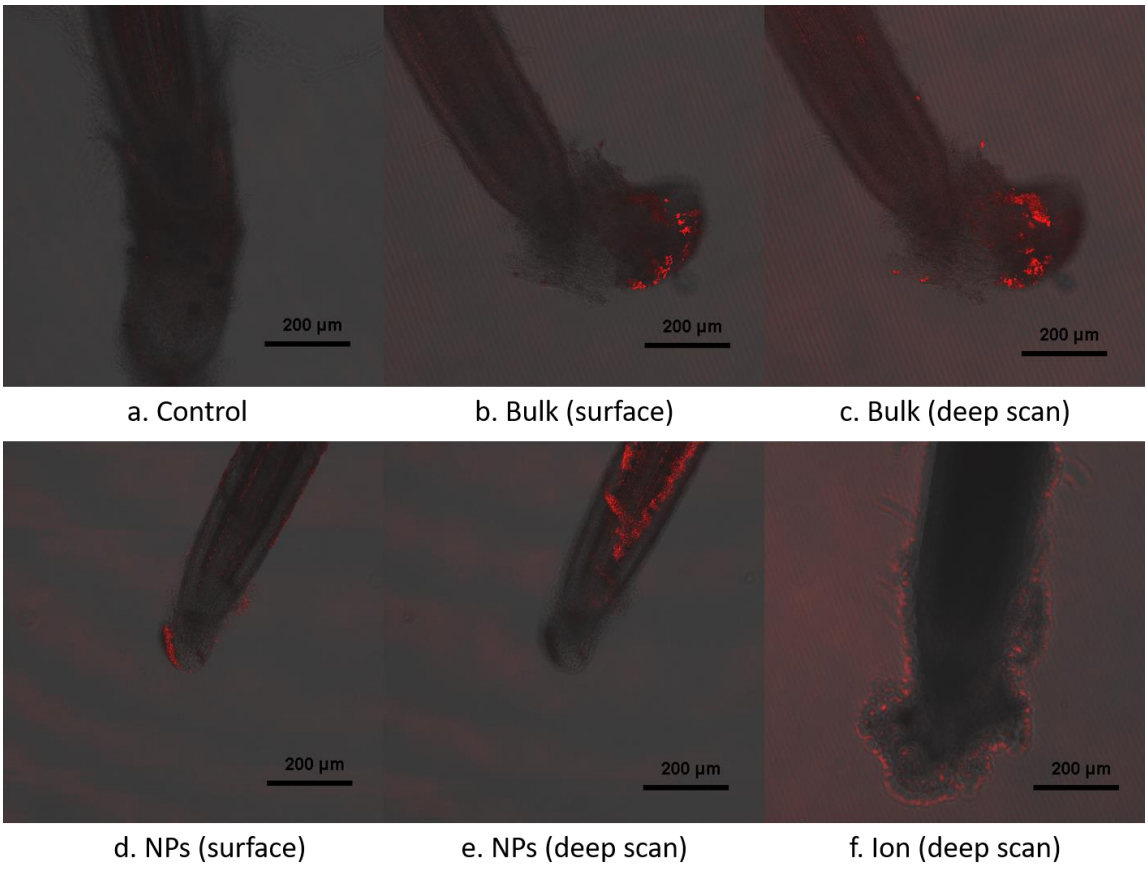

Figure 2.7. Confocal microscopic images depicting the accumulation of cerium in the fine roots of radish: (a) control root showing weak signals; (b, c) surface and representative deeper scan of fine roots treated by bulk CeO_2; (d, e) surface and representative deeper scan of fine roots exposed to CeO_2NPs; (f) deeper scan image of fine roots exposed to cerium ion. The deeper scan images shown were selected from a stack of deep scan images for different roots.

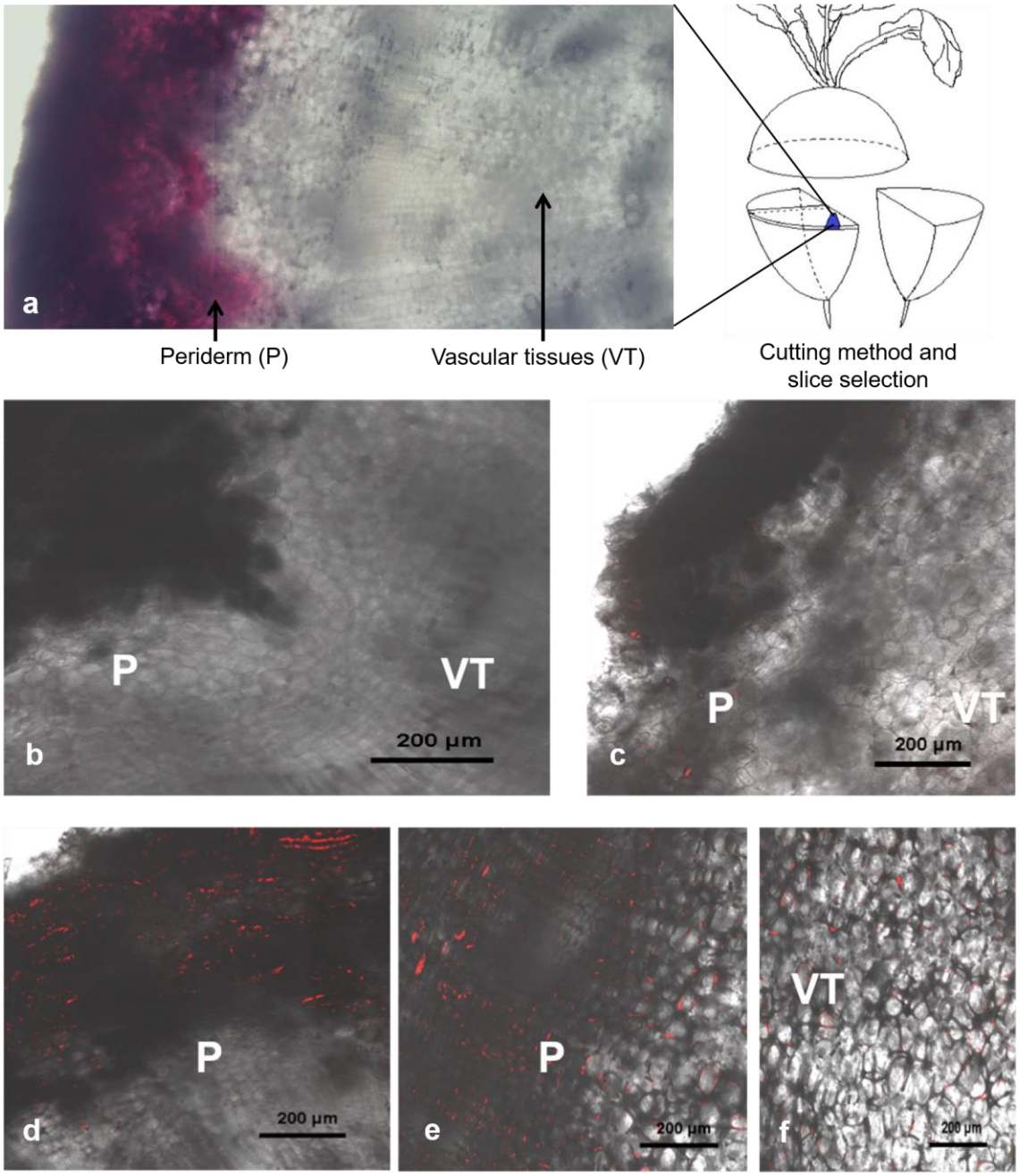

Figure 2.8. (a) Light microscopic image and confocal images of the transverse section of radish storage root treated with different types of Ce: (b) control; (c) bulk CeO_2 treated radish; (d) CeO_2NPs treated radish; (e, f) ionic Ce treated radish. P, periderm; VT, vascular tissues.

Discussion and Conclusions

The investigation in this chapter compared the fate and phytotoxicity of Ce in three different forms. Several physiological parameters, including the root membrane integrity, photosynthesis-related measurements, and biomass parameters, were affected by certain forms of Ce at the tested concentration. Whereas the specific mechanisms by which Ce compounds may compromise membrane integrity are not known and may differ, CeO_2NPs and Ce ions resulted in some damage to root membrane integrity as indicated by an increase in electrolyte leakage (Figure 2.4). However, the effect was significant only for CeO_2NPs and ionic Ce. The changes in the integrity of root membrane could also alter the membrane potential and potentially the function of the membrane.[144, 145] Altered plasma membrane integrity and potential are associated with changes in the ion fluxes into plant roots.[146] Hence, the alteration of membrane integrity could potentially influence the concentration of some essential macronutrients or micronutrients in radish.

For the bulk CeO_2 and CeO_2NPs, in addition to their impact on the membrane, physical adsorption on root surface and blockage of nutrient uptake by plant roots may also occur. It is possible that such impacts on the roots may have affected the uptake of elements such as magnesium or iron, two nutrients associated with the synthesis of chlorophyll. A decrease in the concentration of either of these essential nutrients might have contributed to the decrease in relative chlorophyll content observed in some treatments. Other aspects of chlorophyll synthesis or degradation could have been affected as well, and a more detailed study will be required to understand the extent or

severity of effects of Ce on chlorophyll metabolism. The significantly lower F_V/F_M values observed for the bulk CeO_2 treatment as compared to the control plants suggested that photosynthetic electron transport associated with photosystem II was stressed in those plants, but not for the other Ce treatments. These results differ from a study with plantlets of *Medicago arborea* in which CeO_2NPs was found to have a more negative effect on the F_V/F_M ratio than the same concentrations of bulk CeO_2.[147] Other studies have shown that the influence of Ce compounds on plant photochemistry differs depending on factors such as plant Mn status[148] and the presence of salt stress[149]. Definitive conclusions about the comparative phytotoxicity of the Ce ions and CeO_2NPs cannot be made without further investigation. Even so, the overall effects of all treatments on the two photosynthetic parameters measured were modest and perhaps not indicative of a significant stress imposed on the plants, particularly given that there were no effects observed for any treatments, including the ionic Ce and the CeO_2NPs treatments.

The only other indication of a negative effect of treatment with Ce was the decrease in biomass observed for the Ce ion treatment. The shoot/root ratio of radish was also affected by Ce, primarily through the change of the biomass of the storage roots. Because the root thickening is a result of the combined cell division and enlargement of secondary xylem and phloem cells that depends on the activity of the vascular cambium,[150] it is possible that different forms of Ce have different impacts on the activity of the vascular cambium. The bulk CeO_2 might have enhanced the activity of the vascular cambium, whereas ionic Ce inhibited it.

The concentration of $CeCl_3$ used in this study was very low, and the impact of chloride ion is not expected to be substantial. Parida and Das[151] investigated plant salt tolerance and salinity effects on plant growth and reported that under 100 mM NaCl (3.55 g/L Cl^-), chloride demonstrated limited influence on the osmotic adjustment of cell membrane. Marcelis and Van Hooijdonk[152] also reported that the growth of radish was limited by the availability of nutrients at low salinity level ($\leq$ 2 dS m^{-1}). The Cl^- in the ionic cerium solution used in this study was significantly lower than those reported values and was not expected to significantly contribute to the negative effect observed in the ionic treatment group. Consequently, the negative effect observed in the ionic treatment should be attributed to the ionic Ce. Another caveat about the results is that 10 mg/L was the concentration of the compounds of CeO_2 and $CeCl_3$, not the concentration of Ce as an element. Due to the different molecular weight percentage of cerium in CeO_2 and $CeCl_3$, the actual concentration of cerium as an element was 8.14 mg Ce/L in CeO_2NPs and the bulk and was only 5.68 mg Ce/L in the ionic form. Ce in CeO_2 was 43.5% higher than in the ionic form. If the equivalent concentration of Ce as an element was used, the ionic Ce may display an even stronger effect on plant physiology.

In addition to the yield of edible storage root, the potential accumulation of Ce plant tissues was examined. Exposed plants had detectable Ce in all plant tissues, including the fine roots, the storage root, and the shoots. The significantly higher Ce detected in the shoot tissues of exposed plants indicated that Ce translocation from roots to shoot had occurred. The upward transport of CeO_2NPs and ionic Ce from roots to shoots has been reported in the literature.[84, 85] However, no definitive evidence was

available to indicate the direct transport of CeO_2NPs from roots to shoots. The forms of Ce in these tissues, especially the plants exposed to CeO_2NPs, were unknown. As described in Chapter I, the symplastic pathway and the apoplastic pathways for CeO_2NPs transport could be blocked in the plasmodesmata and endodermis respectively. Several recent studies supported the notion of transformation of CeO_2NPs when interacting with plants.[53, 71, 76, 104] Dissolved Ce was reported to be released from CeO_2NPs on the root surface. Therefore, the Ce in the plant tissues exposed to CeO_2NPs might not be nanoparticles. The forms of Ce in plant tissues may affect both their toxicity and potential availability to plants and thus further investigation is deserved. For the bulk CeO_2, the upward transport to radish shoots was unexpected given the particle size. One possible source of the Ce detected from the bulk treated shoot tissues was the dissolved Ce released from nanoscale particles present in the bulk mixture if the transformation of CeO_2 did occur.

When the Ce localization in the storage root was investigated with the confocal microscope, signals of Ce in the vascular tissues were observed only in Ce ion treatment, suggesting that active transport may function as an important pathway of Ce accumulation only for ion treated radishes. In contrast, signals from the CeO_2NPs and bulk treated radish roots were mainly located on the periderms. Adsorption and diffusion of particulate Ce along the radial direction might be a more important pathway for CeO_2NPs and bulk accumulation in radish storage roots. The active transport of dissolved Ce transformed from CeO_2 particles and/or the diffusion of CeO_2 particles from the lenticels on the periderm may possibly occur, but more precise techniques are

needed to confirm these assumptions due to low quantity of the penetrated Ce. From the food safety point of view, the Ce accumulation in the edible storage root is more concerning, and although Ce concentration and content were similar across the Ce treatment, the distribution of cerium in the storage roots varied and, consequently, its availability to humans would vary. For example, the majority of particulate Ce accumulated in the edible tissue could be removed in the food preparation process, whereas ionic cerium in the storage roots is more likely to be consumed by humans with the storage root.

In summary, 10 mg/L Ce as CeO_2 or cerium chloride could affect the growth of radish and could accumulate in the edible storage root and shoot tissues. However, the impacts and accumulation patterns varied significantly by the size and chemical form of Ce. Ionic cerium displayed the strongest impact on radish root membrane integrity and growth, followed by CeO_2NPs and then the bulk. Whereas different forms cerium of all accumulate in radish tissues, their accumulation potential and distribution patterns differed considerably. As a result, potential exposure and risk to human health through diet exposure to different sizes and forms of Ce may vary, and these differences should be considered when the food safety of cerium in the environment is evaluated.

CHAPTER III

THE TRANSFORMATION OF CEO2NPS INTERACTING WITH RADISH*

Introduction

Previous investigations and results in Chapter II have shown that CeO_2NPs accumulated in radish and many other agricultural crops,[107, 153-156] hence enter the produce food chain and eventually accumulate in the human body and cause health risks. For example, Mittal and Pandey[157] demonstrated that exposure to CeO_2NPs (<25 nm) at 1 µg/mL - 100 µg/mL for 3 – 48 hours could cause morphological alterations, reduction of the antioxidant level, and DNA damage of human lung cells.

The results in Chapter II also demonstrated that different forms (e.g. particles vs. ion) of Ce may affect both toxicity and potential availability of Ce to radish. Due to the low solubility of CeO_2 and the limitation of detection instruments, a few previous studies reported that Ce in plant tissues remained as CeO_2NPs after plant uptake.[85, 142] However, several recent publications suggest that Ce transformation could occur when interacting with plants.[68, 76, 103, 158] Although Chapter II demonstrated the uptake of Ce by radish exposed to CeO_2NPs, the results were obtained through strong acid digestion, which only provided information on the total concentrations of Ce element. The unique features of CeO_2NPs were not obtained due to the digestion process. Because of the importance

* Part of this chapter is reprinted with permission from "Elucidating the mechanisms for plant uptake and in-planta speciation of cerium in radish (Raphanus sativus L.) treated with cerium oxide nanoparticles" by Zhang, W.; Dan, Y.; Shi, H.; Ma, X., 2017. *Journal of Environmental Chemical Engineering*, 5, 572-577, Copyright [2017] by Elsevier.

of the physicochemical states of Ce to its food safety implications, the physicochemical properties of Ce in plant tissues after plant exposure to CeO_2NPs need to be understood.

CeO_2 is generally deemed as a sparingly soluble compound that is chemically stable in the environment. However, dissolution does occur under certain circumstances. For example, Schwabe et al.[53] found that reductants in plant growth media could adsorb on CeO_2NP surfaces and reduce the surface Ce^{4+} to Ce^{3+}. The release of Ce^{3+} from CeO_2NPs was greater in plant rhizosphere than in the growth medium.[76] Zhang et al.[103] reported the detection of $CePO_4$ in cucumber roots and cerium carboxylates in cucumber shoots by investigating the chemical valence state of Ce using near edge X-ray adsorption fine structure (XANES) and X-ray scanning transmission microscopy (STXM). However, whether these compounds were formed after CeO_2NPs were taken up by plants or formed before they were taken up by plants was not discussed. Gui *et al*.[68] also found that Ce in lettuce roots treated with 50 – 1000 mg/kg CeO_2NPs in potting soil was present in the Ce(III) and Ce(IV) oxidation states. Because $CePO_4$ and Ce carboxylates were detected in lettuce roots but not in soil, the authors interpreted the results as evidence of *in-planta* transformation of CeO_2NPs. Very recently, Dan et al.[158] investigated the uptake of CeO_2NPs by four different plant species using a highly sensitive single particle inductively coupled plasma mass spectrometry (SP-ICP-MS) technology and reported common presence of dissolved Ce in plant tissues. In spite of these observations, questions remain concerning the mechanisms for CeO_2NPs uptake by plants and the location of transformation (*e.g*. within plant tissues or in the environment) as well as the composition of Ce in plant tissues following their uptake. Therefore,

further investigations are warranted of the physicochemical properties of Ce within and out of the plant tissues during CeO_2NPs uptake to gain more insights on the CeO_2NPs uptake mechanisms.

To study the physicochemical properties of Ce in plant tissues, a method that could effectively extract Ce from plant tissues without altering its properties is necessary. Enzymatic digestion by proteases or pectinases has been successfully used to solubilize biological materials and extract engineered nanoparticles.[159, 160] A recent breakthrough in extracting ENMs from plant tissues with Macerozyme R-10 provides a unique opportunity to elucidate the uptake mechanisms of CeO_2NPs by plants and to determine the chemical properties of Ce in plant tissues.[161, 162] In this study, the same enzymatic extraction method with Macerozyme R-10 was applied.

Three pathways of Ce uptake by radish are possibile: (1) the intact CeO_2NPs are taken up by the fine roots and the storage root of radish and translocated to the shoots; (2) the CeO_2NPs is transformed to dissolved Ce ions and taken up by the radish roots, then translocated to the shoots; (3) the CeO_2NPs which are taken up by the radish roots are transformed to dissolved Ce within the plant tissues, then translocated to the shoots. To help resolve the pathways of Ce uptake and transformation, this investigation is designed (1) to determine the physicochemical properties of Ce in radish following plant exposure to different types of Ce, and (2) to further investigate the mechanisms for CeO_2NPs plant uptake and *in-planta* speciation.

Materials and Methods

Ce preparation and characterization

A bench scale hydroponic experiment was conducted with radish. Four treatments were prepared: (1) control (no Ce treatment); (2) 10 (mg Ce)/L CeO_2NPs dispersion; (3) 10 (mg Ce)/L bulk CeO_2 suspension; (4) 10 (mg Ce)/L $CeCl_3$ solution. Dispersion of uncoated CeO_2NPs (10 wt% in H_2O) and cerium (III) chloride heptahydrate crystals were purchased from Sigma-Aldrich (St. Louis, MO). The bulk powder of CeO_2 was obtained from Strem Chemicals (Newburyport, MA). Dispersion of uncoated CeO_2NPs (10 wt % in H_2O) was filtered through a 10 kDa Amicon Ultra-4 Centrifugal Filter unit to remove the dissolved Ce in the dispersion. The CeO_2NPs residue on the filter was air-dried at room temperature. The bulk CeO_2 was filtered through a P8 grade filter paper and air-dried at room temperature. The dried CeO_2NPs and bulk CeO_2 were resuspended in water by sonication. The newly obtained dispersions were diluted to obtain suspensions of the targeted concentration. The size and morphology of CeO_2NPs and bulk CeO_2 were determined by a Tecnai G2 F20 transmission electron microscope (TEM) (FEI, Hillsboro, OR, USA) and a JEOL 6400 scanning electron microscope (SEM) (JEOL USA, Inc. Peabody, MA, USA) respectively. The TEM image of CeO_2NPs, SEM image of bulk CeO_2, and their corresponding particle size distributions are shown in Figure 3.1. Most CeO_2NPs fell in the size range of 10–40 nm, with an average size of 15.51 nm. The average particle size was obtained by measuring the diameter of over 100 individual nanoparticles with an

imaging processing software ImageJ (ver 1.49). Bulk CeO_2 particles had a broader size distribution ranging from 2 to 13mm, with an average size of 6.2 mm.

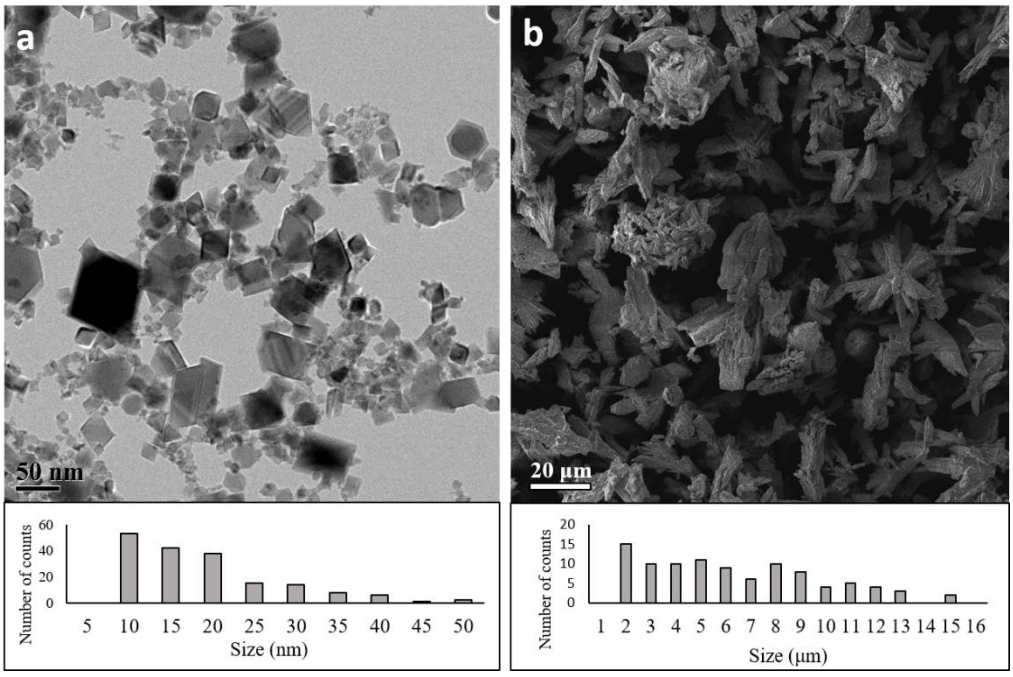

Figure 3.1. (a) The TEM image of CeO_2NPs, (b) the SEM image of bulk CeO_2, and the corresponding particle size distribution.

Plant cultivation and harvest

Sterilized radish [Cherriette (F1)] seeds, purchased from Johnny's Selected Seeds (Winslow, ME, USA), were germinated in Petri dish for 5 days. Healthy young seedlings were then transferred to 50 mL polypropylene centrifuge tubes containing quarter strength Hoagland solution (Phytotechnology Laboratories, Lenexa, KS, USA). Plants

were incubated in a growth cart with a 16-hour light/8-hour dark cycle (28 °C) to allow the seedlings to further develop. After two weeks, the seedlings were transferred to the prepared Ce suspension/solution for 5 days. Each treatment had three replicates. The suspension/solution in the tubes was replenished daily with the same suspension/solution to compensate for transpiration. The daily water consumption of each plant was recorded. The plants were sacrificed at day 24 after germination.

At harvest, plants were separated into three sections: fine roots, storage root, and shoots. The storage root and fine roots were washed with 50 mL $CaCl_2$ solution (5 mM) five times to remove the adhering Ce on the tissue surfaces. To determine the $CaCl_2$ washing effectiveness, plant roots collected from an individual plant were evenly divided into two groups, with one rinsed with DI water only and the other one rinsed with 5 mM $CaCl_2$ solution five times. The unwashed and washed fine roots were then observed under a Tescan Vega 3 scanning electron microscope (SEM) (Tescan USA Inc. Warrendale, PA, USA) to check the washing effectiveness (Figure 3.2). The SEM images indicated that the majority of Ce deposit on root surface was removed by washing. The washing solutions and the growth media were collected and filtered through 10 kDa Amicon Ultra-4 Centrifugal Filter units to separate the dissolved Ce from the particulate Ce. The concentrations of dissolved Ce in the filtrates of washing solutions and growth media were determined by a NexION 300 inductively coupled plasma-mass spectrometry (ICP–MS) (Perkin Elmer, Waltham, MA, USA). A fraction of the washing solution and the growth media was also acid digested to determine the total Ce in them. The acid digestion was performed using a DigiPREP MS hot block

digester (SCP science, Clark Graham, Canada). 5 mL of 70% (w/w) nitric acid (Certified ACS Plus) was add to 1 mL of the washing solution or the growth medium and heated at 95 °C for 4 hours. After cooling down to room temperature, 3 mL of 30% (w/w) H_2O_2 (Certified ACS) was added to the mixture and heated in the hot block at 95 °C for another 2 hours to completely digest the sample. The Ce was then quantified by an ICP-MS as the total Ce in the washing solution or the growth medium after proper dilution.

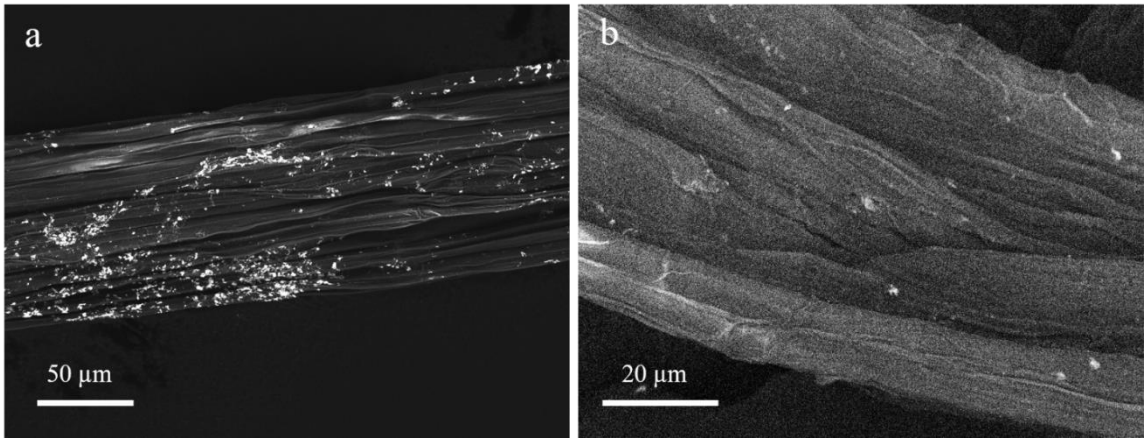

Figure 3.2 SEM images of (a) unwashed radish fine root exposed to CeO_2NPs and (b) $CaCl_2$ washed radish fine root exposed to CeO_2NPs. The bright spots on the root surface represent Ce element which were confirmed by EDS.

Enzymatic extraction, acid digestion, and ICP-MS detection of Ce from plant tissues

The enzymatic extraction of Ce from plant tissues in this study was conducted following the recently developed procedure.[161, 162] The washed tissues were cut into

small pieces with a blade, from which 0.5 g was weighed and mixed with 9 mL of 20 mM 2-(N-morpholino)ethanesulfonic acid (MES) buffer (pH = 5, adjusted by NaOH). The mixture was homogenized in a centrifuge tube using a handheld homogenizer. One mL of 30 mg/mL Macerozyme R-10 enzyme (prepared in 20 mM MES) was then added into the mixture. The mixture (10 mL) was shaken (250 rpm) at 37 °C for 24 hours. Afterward, 4 mL of the digestate was filtered through a 10 kDa Amicon Ultra-4 Centrifugal Filter unit. The Ce in the filtrate was quantified by ICP–MS as the dissolved Ce in plant tissues. Another 4 mL aliquot of enzyme digestate was acid digested to determine total Ce in plant tissues following the same protocol mentioned above.

TEM imaging of the enzymatic digestate

Drops of the last 2 mL of remaining enzymatic digestate were air-dried on a TEM copper grid and then observed under a Tecnai G2 F20 TEM equipped with an energy dispersive spectroscopy (EDS) at 200 kV to examine the physical and chemical form of Ce microscopically.

Artificial root exudates (ARE) study

The simplified ARE contained a mix of low molecular weight organics previously reported to occur in plant root exudates: glucose (50 mM), succinic acid (25 mM), malic acid (25 mM), and serine (12.5 mM).[163-165] The pH of the simplified ARE was measured (pH=2.45) by using a pH meter (Orion ROSS Ultra pH/ATC Triode Orion Star A325 Thermo Fisher Scientific, Waltham, MA). The simplified ARE, the four individual components at the same concentration as in the ARE, and HCl solution at the same pH with simplified ARE (pH=2.45) were mixed with 10 mg/L CeO_2NPs dispersion

in a centrifuge tube. The CeO_2NPs dispersion at 10 mg/L in DI water was prepared as a reference. The mixtures were shaken (250 rpm) on a shaker for 5 days (the same time frame as Ce exposure process of radish). Afterwards, the mixtures were filtered through 10 kDa Amicon Ultra-4 Centrifugal Filter units. The dissolved Ce in the filtrate was measured by ICP– MS. The total Ce in the mixtures were determined by acid digestion as mentioned above, followed by ICP–MS. The ratios of dissolved Ce to total Ce in the mixtures were then calculated.

Data analysis

The results are reported as mean ± standard error of three replicates. One-way ANOVA analysis and Duncan's test for post hoc comparisons were performed with IBM SPSS Statistics V22.0. Different letters in the Figures represent significant differences among the treatments when the *p* value was <0.05.

Results

Radish physiological status

The fresh biomass of different radish tissues was shown in Figure 3.3. The bulk CeO_2 had no impact on the biomass of radish. Exposure to CeO_2NPs resulted in significantly greater fresh biomass of the storage root than control. The fresh biomass of shoots and storage root exposed to Ce^{3+} ions was significantly lower than that of all other treatments. None of the treatments affected the fresh biomass of fine roots when compared to the control, but the fine root biomass of the bulk CeO_2 treated radish was significantly higher than that of radish exposed to Ce^{3+} ions.

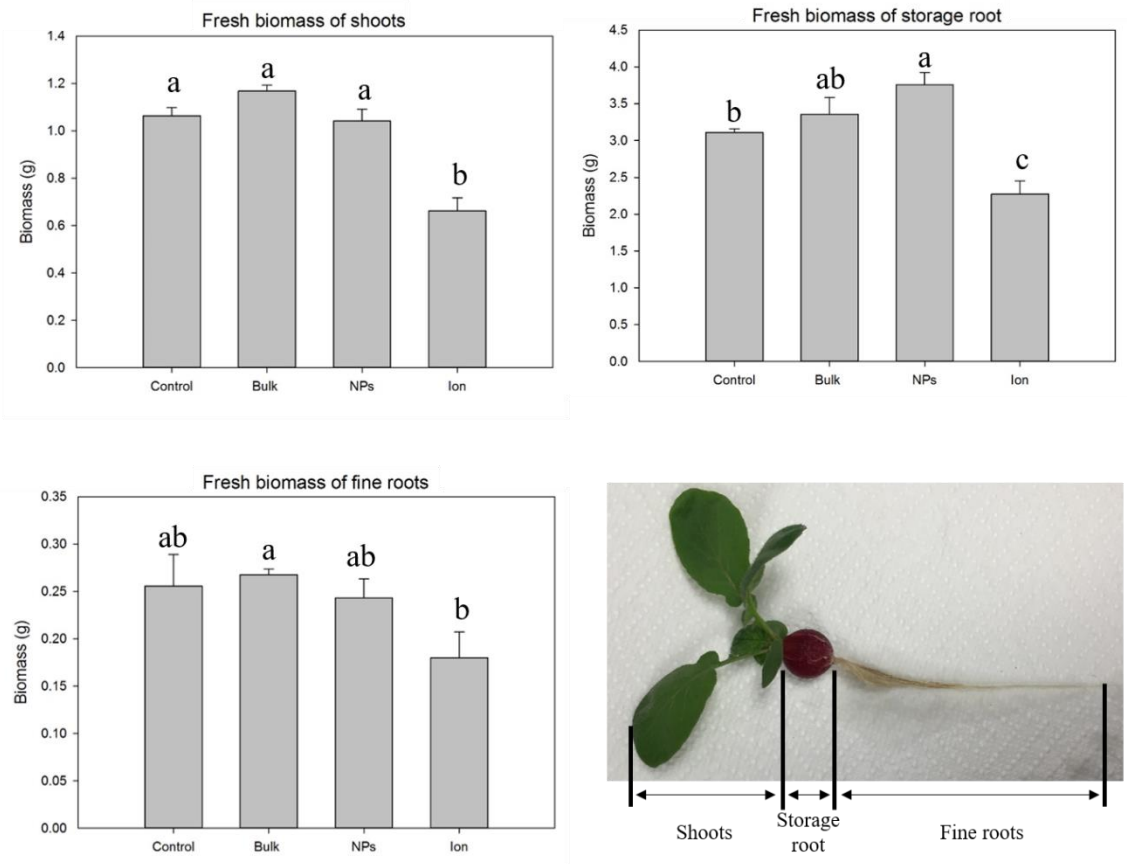

Figure 3.3. Average fresh biomass of radish tissues (n=3) and the illustration of radish separation. The error bars represent standard error. The data were statistically analyzed by one-way ANOVA and Duncan's test for post hoc comparisons. Different letters represent significant differences among the treatments (p<0.05).

Ce uptake and physicochemical transformation

The concentrations of Ce in plant tissues were shown in Figure 3.4. The total Ce concentration was highest in plant tissues exposed to Ce^{3+} ions, followed by the plants exposed to CeO_2NPs, which was significantly lower than Ce^{3+} treated plants but significantly higher than bulk CeO_2 treated plants or the control. The average concentrations of total Ce in the shoots exposed to both bulk CeO_2 and CeO_2NPs were

not statistically different from control plants (p>0.05 in one-way ANOVA analysis). Similar to the total Ce concentrations in plant tissues, exposure to Ce^{3+} ions resulted in significantly greater concentrations of dissolved Ce in all radish tissues, while no dissolved Ce was detected in the storage root and fine roots of the control radish. Dissolved Ce was also detected in tissues treated with bulk CeO_2 and CeO_2NPs. However, they were significantly lower than that detected in plant tissues exposed to ionic Ce^{3+}. The concentrations of dissolved Ce in the storage root and fine roots of bulk CeO_2 treated radish were significantly lower than those treated with CeO_2NPs, indicating a significant impact of particle size on the release of dissolved Ce from CeO_2 particles.

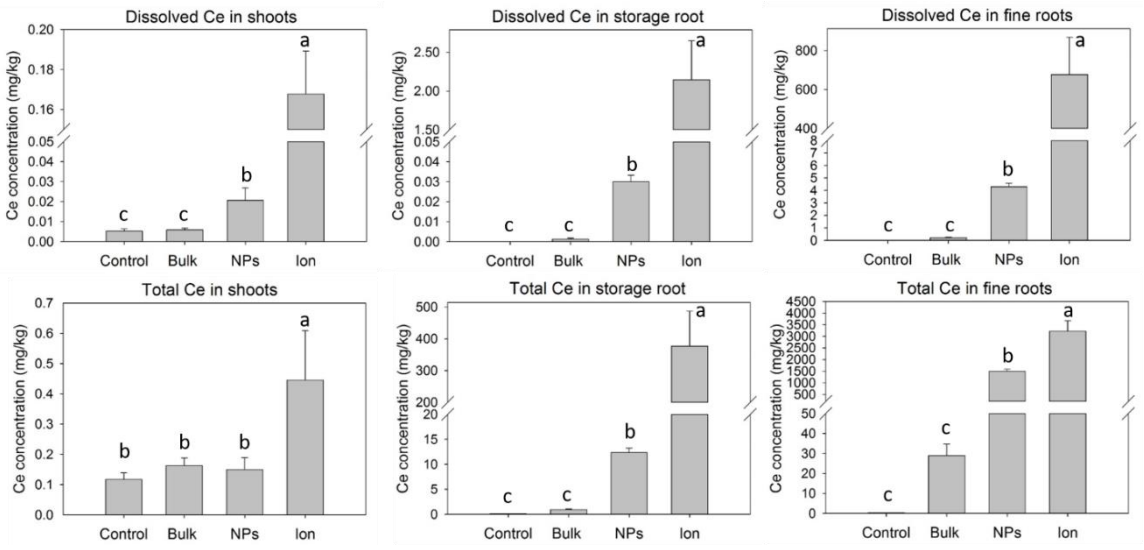

Figure 3.4. Average Ce concentration in radish tissues (n=3). The error bars represent standard error of the mean. Different letters represent significant differences among the treatments (p<0.05) determined by One-way ANOVA analysis followed by Duncan's test for post hoc comparisons.

The ratios of the dissolved Ce to total Ce in the growth media and washing solution at harvest are shown in Table 3.1. The concentration of dissolved Ce in the washing solution and growth medium of control plants was negligible. The dissolution of CeO_2NPs and bulk CeO_2 in the growth media was minimal. However, significant concentrations of dissolved Ce and higher ratios of dissolved Ce to total Ce were detected in the washing solutions of fine roots and storage root from CeO_2 treated plants compared with control. The washing solution of radish roots exposed to CeO_2NPs have significantly higher ratio of dissolved Ce to total Ce than that of radish roots exposed to bulk CeO_2.

Table 3.1. Concentrations of dissolved Ce and the ratio of dissolved Ce to total Ce in the growth media and washing solution at harvest (mean ± standard error, n=3).

Dissolved Ce	Control	Bulk	NPs	Ion
Washing solution (μg/L)	0.16±0.08	0.51±0.12	23.03±2.42	414.33±54.15
Growth media (μg/L)	0.22±0.11	0.45±0.18	0.21±0.14	2049.33±425.34

Dissolved Ce / Total Ce	Control	Bulk	NPs	Ion
Washing solution (%)	-	0.24±0.02	4.21±0.55	-
Growth medium (%)	-	0.02±0.00	0.024±0.01	-

CeO_2NPs were detected by SEM and confirmed by EDS in the unfiltered enzymatic digestate of fine roots exposed to CeO_2NPs (Figure 3.5a). However, no CeO_2NPs was found in the enzymatic digestates of shoots and storage root of radishes

exposed to CeO_2NPs (Figure 3.5b, c). No Ce particles were detected in any radish tissues exposed to bulk CeO_2.

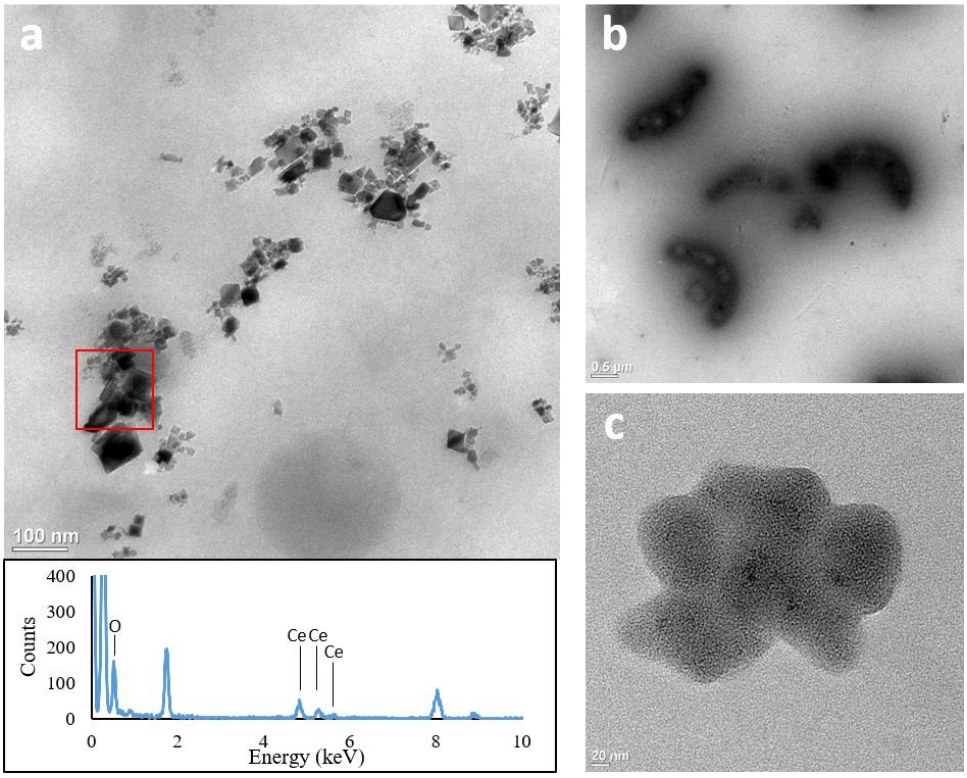

Figure 3.5. TEM images of (a) the enzymatic digestate of fine roots exposed to CeO_2NPs, (b) the enzymatic digestate of shoots exposed to CeO_2NPs, and (c) the enzymatic digestate of storage root exposed to CeO_2NPs. The EDS spectrums under the TEM images show the detected elements in selected areas (red frame in image).

Larger particles were found in the digestates of radish storage root and fine roots exposed to ionic Ce^{3+} only (Figure 3.6a, b). An X-ray analysis on the elemental composition of the particles indicated higher contents of P in addition to Ce, suggesting

that the particles might be in the form of $CePO_4$. No Ce particles were found in the enzymatic digestate of shoots exposed to Ce^{3+} ions.

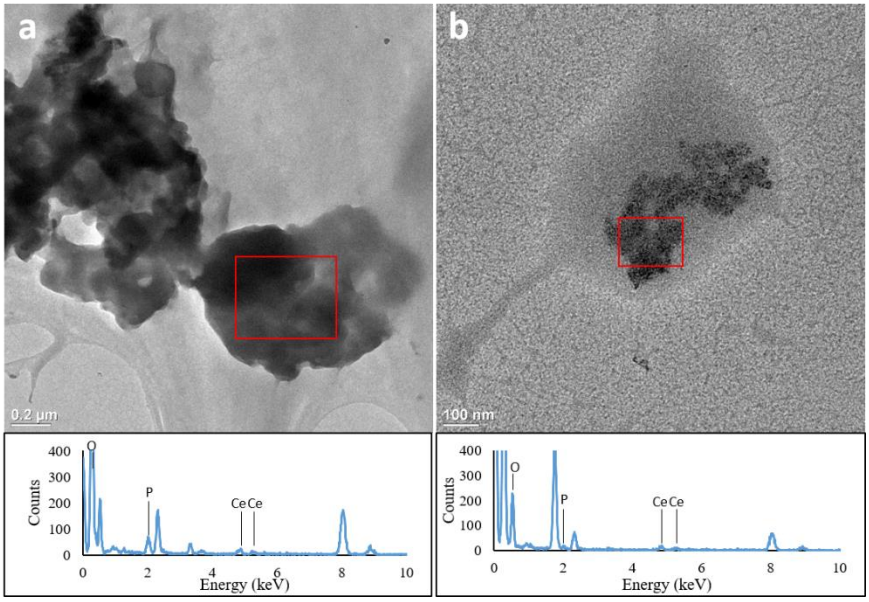

Figure 3.6. TEM images of (a) the enzymatic digestate of storage root exposed to Ce^{3+} ions, and (b) the enzymatic digestate of fine roots exposed to Ce^{3+} ions. The EDS spectrums under the TEM images show the detected elements in selected areas (red frames in images).

Artificial root exudates (ARE) in vitro study

The amount of dissolved Ce released from CeO_2NPs in water without any additive, glucose solution, and serine solution was insignificant after 5 days (Figure 3.7). In contrast, the dissolution of CeO_2NPs was significantly enhanced by succinic acid, malic acid, the simplified ARE, and HCl. The ratio of dissolved Ce to total Ce was

highest when CeO_2NPs mixed with the ARE, followed by the malic acid solution, the succinic acid solution, then the HCl solution at pH=2.45.

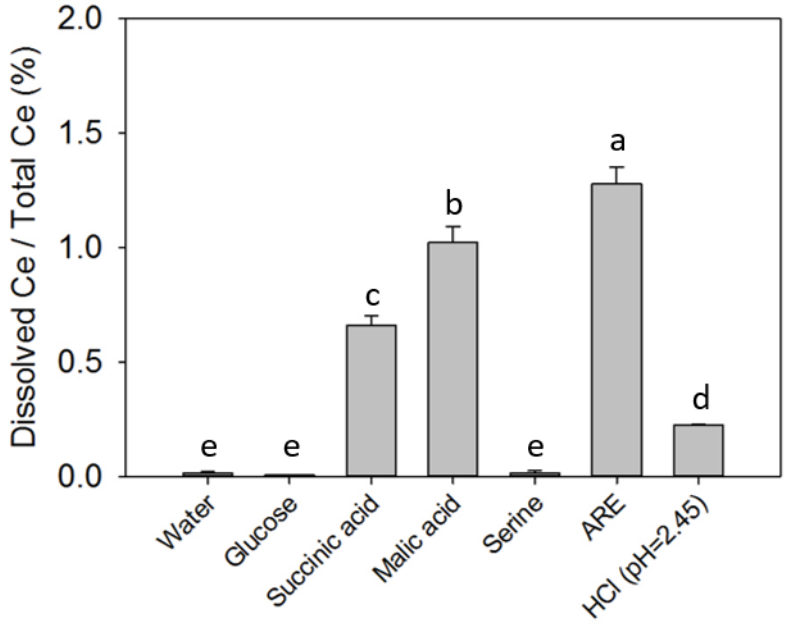

Figure 3.7. The ratios of dissolved Ce to total Ce in the reference (CeO_2NPs dispersion only) and in the mixtures of CeO_2NPs and artificial root exudates. Different letters represent significant differences among the treatments (p<0.05) determined by One-way ANOVA analysis followed by Duncan's test for post hoc comparisons.

Discussion and Conclusions

The results shown in the Figure 3.3 are consistent with our previous observation that the Ce^{3+} ions inhibited radish growth and demonstrated phytotoxicity at 10 mg/L. Meanwhile, CeO_2NPs at the tested concentration enhanced the growth of radish storage

roots. Several previous studies also reported that various concentrations of CeO_2NPs had positive impacts on the plants growth. Gui et al.[68] reported that lettuce (*Lactuca sative* L.) treated with 100 mg/kg CeO_2NPs in potting soil grew significantly faster than control plants. Rico et al.[74] found 500 mg/kg CeO_2NPs in potting soil could improve wheat (*Triticum aestivum* L.) growth, shoot biomass, and grain yield by 9.0%, 12.7%, and 36.6% respectively. The follow-up study of this research group revealed similar conclusions for tomatoes (*Solanum lycopersicum* L.) that 62.5 mg/kg CeO_2NPs in potting soil produced higher total number of tomatoes and 500 mg/kg CeO_2NPs increased the shoot length of tomatoes.[166] Yang et al.[167] found CeO_2NPs at 200 and 500 mg/L on agar plates stimulated root and shoot growth and root elongation of *Arabidopsis thaliana*. Similar to the CeO_2NPs, Ce^{3+} ions at low concentrations (0.1 - 2.5 mg/L) were observed to be beneficial for cowpea plants (*Vigna unguiculata* L.).[168] Thus, Ce at low concentrations was often used as an additive in micro-fertilizer to promote growth and development of crops.[169] However, negative impacts on the growth of cowpea plants were induced when Ce^{3+} ion concentration was above 10 mg/L. Liu et al.[170] showed that the growth of rice seedlings (*Oryza sativa* L.) was stimulated in the present of Ce^{3+} ions under 14 mg/L, but was significantly inhibited at the higher Ce^{3+} ion concentrations. Apparently, 10 mg/L was considered as high concentration for Ce^{3+} ions to introduce significantly negative effects on the fresh biomass of radish storage root and shoots.

Intact CeO_2NPs, which had a particle size distribution similar to the primary CeO_2NPs dosed in the growth medium (Figure 3.1), were detected in the unfiltered enzymatic digestate of fine roots exposed to CeO_2NPs (Figure 3.5a). The SEM images of

the unwashed and the washed radish fine roots (Figure 3.2) indicated that the majority of the CeO_2NPs adhered on the root surface had been removed by $CaCl_2$ washing. Therefore, the CeO_2NPs detected in the digestate of fine roots should be mostly from the nanoparticles penetrated into radish fine roots. Several previous studies have also demonstrated the uptake of CeO_2NPs by crop roots visualized by confocal microscope, TEM or μ-XRF [80, 142, 156, 171]. The detection of CeO_2NPs facilitated by TEM provided further evidence of direct uptake of CeO_2NPs by plant roots. However, no CeO_2NPs were found in the enzymatic digestates of shoots and storage root of radishes exposed to CeO_2NPs (Figure 3.5b, c), indicating that the upward transport of CeO_2NPs in radish was limited. Due to the detection of CeO_2NPs in plant fine roots and the dissolved Ce in all radish tissues treated with CeO_2NPs alone, there are two possibilities for the origin of the dissolved Ce: (1) CeO_2 dissolution within the fine roots after they entered into the root tissue or (2) part of the CeO_2NPs dissolved in the rhizosphere and both dissolved Ce and CeO_2NPs were taken up by plant fine roots, but only the dissolved Ce was transported from roots to shoots. Based on the concentrations of dissolved Ce and the ratios of dissolved Ce to total Ce in the growth media and washing solution at harvest shown in Table 3.1, dissolution of CeO_2NPs and bulk CeO_2 in the growth media was minimal. The results agreed well with the data in the artificial root exudates study that CeO_2NPs dissolution in water without plants was insignificant after 5 days (first column in Figure 3.7). Significant concentrations of dissolved Ce and higher ratios of dissolved Ce to total Ce were detected in the washing solutions of fine roots and storage root from CeO_2 treated plants. The concentration of dissolved Ce in the washing solution of

control plants was negligible. CeO_2NPs at 10 mg/L in this study were positively charged and the zeta potential of the nanoparticles was over +40 mV measured by a dynamic light scattering instrument (Malvern Zetasizer Nano-ZS90, Westborough, MA). $CaCl_2$ at 5 mM could reduce the Debye length of CeO_2NPs and cause CeO_2NPs aggregation, but they were not expected to cause dissolution of CeO_2.[172] Thus, the high concentrations of dissolved Ce in the washing solution reflected the higher percentage of dissolved Ce in the rhizosphere, indicating the dissolution of Ce from CeO_2 particles. The higher ratio of dissolved Ce to total Ce in the washing solution from CeO_2NPs treatment also indicated that the location of CeO_2NPs transformation was root surface. In addition, the quantitative calculation of the dissolved Ce in the collected washing solutions (250 mL) and plant tissues from CeO_2NPs treatment showed that the amount of dissolved Ce was highest in the surface deposit, followed by fine roots, storage root and then the shoots. These results suggest the dissolution of CeO_2NPs in the rhizosphere before ionic Ce was taken up by plant roots. This finding was consistent with the results reported by Schwabe et al.[76] that CeO_2NPs was more active to release Ce^{3+} on the root surface.

The enhanced dissolution of CeO_2 on root surface was attributed to the root exudates from radish. Plant roots release a wide range of compounds such as, ions, free oxygen, enzymes, mucilage, and a diverse array of carbon-containing molecules.[173] Among them, sugars, low molecular weight organic acids, and amino acid are the most common.[174] Lettuce root exudates improved the solubility of TiO_2NPs and Fe_3O_4NPs in the rhizosphere.[175] Stegemeier et al.[176] also found that the root exudates of Alfalfa (*Medicago sativa* L.) could partially dissolve Ag_2S-NPs, making the nanoparticles more

bioavailable to plants. In this *in vitro* study, we showed that the low molecular weight organic acids in root exudates including succinic acid and malic acid are primarily responsible for the enhanced dissolution of CeO_2NPs (Figure 3.7). Higher CeO_2NPs dissolution caused by organic acids with lower molecular weight in root exudates might be a primary mechanism for CeO_2NPs uptake and translocation to the shoots. Malic acid caused significantly higher CeO_2NPs dissolution than succinic acid. Malic acid has lower pK_{a1} (3.4) than succinic acid (pK_{a1}=4.2),[177] implying that pH might be one of the factors governing the CeO_2NPs transformation for two organic acids. This finding was consistent with a previous report that the percentage of Ce^{3+} ions released from CeO_2NPs (20 nm) increased from 0.25% to 3.1% as pH decreased from 7 to 4 in soil.[178] The dissolution of CeO_2NPs in acidic environment can be ascribed to the partial reduction of Ce^{4+} to Ce^{3+} and the dissolution rate increased with increasing reaction temperature and acid concentration:[179, 180]

$$4CeO_{2(s)} + 12H^{+}_{(aq)} \rightarrow 4Ce^{3+}_{(aq)} + 6H_2O + O_{2(g)}$$

However, the ratio of dissolved Ce to total Ce in the HCl solution at pH=2.45 was significantly lower than that in the ARE solution, the malic acid solution, and the succinic acid solution, suggesting that pH is not the only factor that caused the CeO_2NPs dissolution. According to the standard redox potential for Ce^{4+} at 25 °C is:[181]

$$Ce^{4+} + e^{-} \rightarrow Ce^{3+} \quad E^0 = +1.44\ \text{V}.$$

The standard redox potentials for the two organic acids are:[182]

$$Oxaloacetate + 2H^{+} + 2e^{-} \rightarrow malate \quad E^0 = -0.166\ \text{V}$$

$$Fumarate + 2H^{+} + 2e^{-} \rightarrow succinate \quad E^0 = +0.031\ \text{V}$$

The electrode potentials for the redox reactions between Ce^{4+} and the two organic acids are positive (1.606 V for Ce^{4+}/malate and 1.409 V for Ce^{4+}/succinate), suggesting the reactions proceed spontaneously. Therefore, the redox reactions between low molecular weight organic acids and CeO_2NPs are deemed as another factor contributing to the enhanced dissolution. Previous literature has also demonstrated that organic acids are able to reduce Ce^{4+} to Ce^{3+}. For example, the ascorbic acid can react with CeO_2 to form Ce^{3+}:[183]

$$2CeO_2 + 3C_6H_8O_6 \rightarrow Ce_2O_3 + 3C_6H_6O_6 + 2H_2O$$

Other organic acids, such as gallic acid, vanillic acid, caffeic acid are also reported as reductants to transform Ce^{4+} in CeO_2 to Ce^{3+}.[183] It is worth noting that root exudates for a plant species change with age. Therefore, the extent of CeO_2NPs dissolution may vary depending on the growth stage of exposure time. This might partially explain our previous observations that the phyto-impact of CeO_2NPs differ at different plant growth stages.

The concentrations of total Ce in all treated radish tissues were significantly higher than the concentration of dissolved Ce in the corresponding tissue, indicating the presence of undissolved Ce within plant tissues. Dan et al.[158] found particulate Ce in plant tissues spiked with dissolved Ce only using the same enzymatic extraction method adopted in this study. The authors attributed it to the attachment of dissolved Ce on the undigested plant tissue colloids so that the SP-ICP-MS mistakenly reported this adsorbed Ce as particulate Ce. Therefore, the concentration of measured dissolved Ce was probably lower than the actual concentration of dissolved Ce within plant tissues.

Another potential reason was the re-formation of particulate Ce. $CePO_4$ was reported as an undissolved form of Ce following the Ce^{3+} uptake process.[68, 103] The chemical speciation of Ce may change during the upward transport of dissolved Ce in the plant tissues. Larger particles were found in the digestates of storage root and fine roots of radish exposed to ionic Ce^{3+} only (Figure 3.6). An X-ray analysis on the elemental composition of the particles indicated higher contents of P in addition to Ce, suggesting that the particles might be in the form of $CePO_4$. If CeO_2NPs were reduced to Ce^{3+} in the rhizosphere and Ce^{3+} was taken up by plants and formed insoluble $CePO_4$, then Ce in plant tissues could be present as a mixture of intact CeO_2NPs, dissolved Ce, and Ce salts after plants are exposed to CeO_2NPs.

In summary, the conversion of CeO_2NPs to dissolved Ce, most likely on the root surface or in the rhizosphere and caused by the radish root exudates. The dissolved Ce and part of the CeO_2NPs could be directly taken up by radish fine roots. Particulate Ce salt such as $CePO_4$ was formed from Ce^{3+} ion exposure. Within radish root tissues exposed to CeO_2NPs, Ce could be present as a mixture of CeO_2NPs, dissolved Ce, and Ce salts. The co-existence of various forms of Ce complicates the health implications of Ce in plants and this phenomenon needs to be considered when the potential human exposure to Ce through plant consumption is investigated.

CHAPTER IV

THE IMPACT OF SOIL PROPERTIES ON THE FATE AND BIOAVAILABILITY OF CEO2NPS TO RADISH IN SOIL*

Introduction

Most previous studies on the uptake and accumulation of CeO_2NPs by plants, including the investigations reported in Chapter II and III, were conducted in hydroponic systems. The hydroponic cultivation could provide a sterile and controlled environment for plant development. However, while hydroponic studies provide valuable information on the potential mechanisms of plant uptake and accumulation of CeO_2NPs, increasing efforts are dedicated to elucidating the uptake and accumulation of CeO_2NPs by plants in soil systems to obtain a more realistic understanding of the fate and impact of CeO_2NPs on plants. For example, after tomato plants were irrigated with 0.1-10 mg/ L of CeO_2NPs solutions in soil, Ce was accumulated in tomato (*Solanum lycopersicum* L.) roots and shoots, including the edible tissues, with the root being the primary tissue of accumulation.[84] Zhao et al.[82] also reported low translocation of CeO_2NPs from root to shoot in corn plants (*Zea mays* L.) grown in soil and noticed that 800 mg/kg CeO_2NPs did not affect plant photosynthesis throughout the exposure but significantly reduced the corn yield. Another recent study demonstrated that CeO_2NPs did not affect the growth of

* Part of this chapter is reprinted with permission from "Bioavailability of cerium oxide nanoparticles to Raphanus sativus L. in two soils" by Zhang, W.; Musante, C.; White, J. C.; Schwab, P.; Want, Q.; Ebbs, S. D.; Ma, X., 2017. *Plant Physiology and Biochemistry,* 110, 185-193, Copyright [2017] by Elsevier.

lettuce (*Lactuca sativa* L.) at low concentrations (50 mg/kg and 100 mg/kg) in potting soil, but significantly inhibited biomass production and disrupted plant stress responses at 1000 mg/kg.[68] While these soil-based studies provide significant new information on the fate and impact of CeO_2NPs in the ecosystem, none of these studies has closely examined the impact of soil properties on the toxicity and bioavailability of CeO_2NPs to terrestrial plants.

Plant uptake of metals in soil depends on both the soluble fraction of total metal and the capability of soil to release the metals, and both factors can be affected by soil properties.[184] Previous studies have shown that metal mobility in soil, which is related to the bioavailability of the metal, is governed by many factors including the soil characteristics (e.g. soil texture, pH, organic matter content, acidification, and redox processes); the nature of contaminants (e.g. the chemical forms of pollutants and the binding state); and the environmental conditions (e.g. temperature and water regime).[185-187] Thus, the effects of soil properties on the fractionation of the CeO_2NPs in soil serves as an important focal point for assessing their bioavailability to plants.

In the past decades, several extraction methods were developed to evaluate the mobility and fractionation of metals in soil. Sequential selective extraction, which is one of the most applied techniques in soil analysis, is defined as the use of a series of selective reagents to solubilize the solid material successively into specific fractions.[188] A three-step sequential extraction procedure for soil and sediment analysis known as the BCR (Bureau Commune de Reference of the European Commission) method, proposed in 1993[189] and later modified by Rauret et al.[190] is widely used for the determination of

extractable trace metals in soils and sediments. This three-step sequential extraction method separates the metal of interest into four fractions: the exchangeable, water/weak acid soluble metal (F1); the metal bound to Fe-Mn oxides (F2); the metal bound to organic matter (F3) and the metal bound to silicate minerals in the residual fraction (F4). The assignment of chemical pools of these fractions is functional and not literal. Very little has been done to attempt to demonstrate that the portions of metals removed by the given extractants actually belong to the assigned chemical pools. Zhong et al.[187] suggested that the first three fractions of the metals in soil were the potentially bioavailable and hazardous fractions to plants. According to the research of Li et al.[184], F1 represents the most active, mobile and bioavailable phase of the metal. These authors used the BCR method to study the bioavailability of Zn, Cu, Pb Cd, Hg, and As in topsoil and found that soil physicochemical properties (e.g. pH, organic matter, and clay content) affected metal fractionation in soil and their bioavailability to plants. The successful application of the BCR method to estimate the bioavailability of heavy metals in soil to plants provides a potentially useful method to evaluate the availability of engineered metallic nanoparticles under similar exposure scenarios.

Chapter II and III demonstrated that Ce from CeO_2NPs could be taken up from hydroponic solutions by radish and accumulated in the radish tissues, introducing potential health risks to humans through the food chain. Similar experiments need to be conducted in soils to provide further clues on the interactions between CeO_2NPs and plants in a realistic environment.

The objectives of this investigation were to (1) use an effective soil sequential extraction method (BCR method) to evaluate the fractionation of CeO_2NPs in soils with different properties; (2) to assess the bioavailability of CeO_2NPs to radish in soils; and (3) to determine the impact of soil properties on the distribution of Ce in plant tissues.

Materials and Methods

CeO_2NPs characterization

Dispersion of uncoated CeO_2NPs (<25 nm; 10 wt% in H_2O) was purchased from Sigma-Aldrich (St. Louis, MO, USA). The shape and size distribution were determined by a Tecnai G2 F20 transmission electron microscope (FEI, Hillsboro, OR). The hydrodynamic diameter and zeta potential of CeO_2NPs at 500 mg/L in water were measured by a dynamic light scattering instrument (Malvern Zetasizer Nano-ZS90, Westborough, MA). The surface speciation of CeO_2NPs was investigated with an X-ray photoelectron spectroscopy (XPS) (Omicron multriprobe MXPS system, Scienta Omicron, Germany).

Soil characterization and preparation

Two types of soil were used in this study: commercially-purchased topsoil (Timberline Top Soil, Oldcastle Inc., Atlanta, GA) and an agricultural soil (Alfisols) collected from a farmland in Carbondale, IL (Figure 4.1a). The weight percentages of sand, silt and clay of the two soils were determined through wet sieve analysis and hydrometer test.[191] The commercial topsoil was classified as loamy sand and the farmland soil was classified as silt loam according to the USDA soil texture classification. The ASTM D2974 method (Standard Test Methods for Moisture, Ash,

and Organic Matter of Peat and Organic Soils) was used to determine the organic matter content in soil. The soil was first dried in an oven at 105 °C for 24 hours. The dry soil was weighed and then combusted at 440 °C for 24 hours. The loss in mass was assumed to be due entirely to the oxidation of organic matter. The soil routine analyses, including the measurements of pH, conductivity, nitrate-N, and some macro- and micronutrients, were conducted in the Soil, Water and Forage Testing Laboratory at Texas A&M University following established protocols. Briefly, soil pH and conductivity were determined with a slurry with a 1:2 soil:deionized water ratio. The slurry was vigorously stirred and then allowed to settle for a minimum of 30 min at room temperature before the measurements. Both the pH and the conductivity were determined with an Orion Star A325 pH/conductivity portable multiparameter meter (Thermo Scientific, Beverly, MA). Nitrate-N was extracted from soil with a 1 N KCl solution and reduced to nitrite through a cadmium column and then quantified by an UV−*vis* spectrophotometer in a FIAlab-2500 analyzer system (FIAlab Instruments, Inc., Bellevue, WA). The micronutrients (Cu, Fe, Mn, and Zn) were extracted using a solution containing 5 mM diethylenetriaminepentaacetic acid (DTPA), 10 mM $CaCl_2$, and 100 mM triethanolamine. The phosphorus, K, Ca, Mg, Na, and S were extracted using the Mehlich III extractant. The extracted micronutrients, phosphorus, K, Ca, Mg, Na, and S were determined by an inductively coupled plasma optical emission spectroscopy (ICP-OES) (SPECTRO Analytical Instruments, Kleve, Germany).

The growing pots for radish were established by adding 150 g of dry soil to a plastic container. CeO_2NPs dispersion and deionized water were added to the container

in different proportions so that the soil was saturated to 100% of field capacity and at the same time reached the targeted concentration of CeO_2NPs homogeneously. Four concentrations of CeO_2NPs were prepared for each type of soil: control, 100, 500, and 1000 (mg Ce)/(kg dry soil). The concentrations were chosen based on the most frequently used concentrations in the literature for the fate and phytotoxicity study of metal oxide nanoparticles to terrestrial plants.[192] Each treatment had six replicates. Altogether, 24 such containers were prepared for each soil. The soil were incubated for one day before radish seeds were sowed.

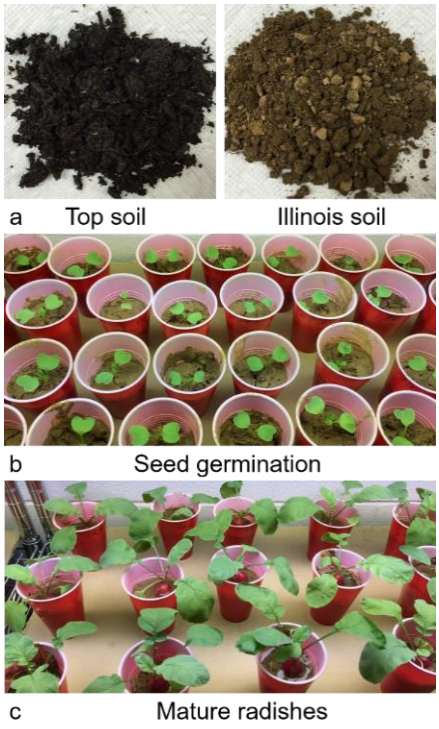

Figure 4.1. (a) Commercially-purchased topsoil and an agricultural soil collected from a farmland in Carbondale, IL. (b) Radish seeds germination. (c) Mature radishes before harvest.

Seed germination and growth conditions

Radish seeds [Cherriette (F1)] were purchased from Johnny's Selected Seeds (Winslow, ME). Three seeds were placed approximately 15 mm beneath the soil surface in each container with soils containing different concentrations of CeO_2NPs. After germination, each container was thinned to one seedling (Figure 4.1b).

Plants were irrigated with quarter strength Hoagland's solution to a constant mass (230 g after irrigation) daily from Day 6 to Day 15 after sowing. The soil was then irrigated to the same constant mass with half strength Hoagland's solution until harvest (Day 31). Quarter and half strength Hoagland solution were prepared by dissolving an appropriate amount of the modified Hoagland's basal salt mixture purchased from Phytotechnology Laboratories (Lenexa, KS) in deionized (DI) water. Plants were incubated on a growth cart with a 16 hours photoperiod at 28 °C and ambient humidity. The growth cart was equipped with four T5 fluorescent bulbs, providing a light intensity of approximately 104 mmol/m^2 s at the height of plant shoots. Relative chlorophyll content was measured with a SPAD 502 Plus Chlorophyll Meter at Day 26 and was expressed as a percentage of the control plants. Plants were harvested at Day 31 (Figure 4.1c).

Ce fractionation in soil

At harvest, plants were gently removed from the soil for further analysis (details described below). The soil was homogenized and then three samples were randomly collected from three containers in each treatment and extracted with the modified BCR method to determine the fractionation of CeO_2NPs in soil. The dry soil sample was first

extracted with 20 mL of 0.11 M acetic acid solution by shaking at 250 rpm for 16 hours at 22 ± 5 °C and centrifuged at 3000 g for 20 min to obtain the exchangeable fraction (F1). The residue was then resuspended and extracted by 20 mL of 0.5 M hydroxylamine hydrochloride solution at pH 1.5 and shaken at 250 rpm for 16 hours at 22 ± 5 °C. The mixture was centrifuged similarly as described above to obtain the reducible fraction (F2). The residue was then resuspended and mixed with 30% H_2O_2 and shaken at 250 rpm for 1 hour at room temperature, followed by another hour of shaking at 250 rpm at 85 ± 2 °C with a closed cap. The volume of the mixture was reduced to less than 1.5 mL by further heating at the same temperature without cap. Following the volume reduction, an aliquot of 5 mL of 30% w/v H_2O_2 was added and the heating process was repeated until the volume was reduced to about 0.5 mL. Afterwards, 25 mL of 1 M ammonium acetate solution at pH 2 was mixed with the residue for 16 hours at 22 ± 5 °C and the mixture was centrifuged at 3000 g for 20 min to extract the oxidizable fraction (F3). The residue fraction (F4) was extracted by aqua regia following the ISO 11466 protocol; 4.5 mL of HCl (12.0 M) and 1.5 mL of HNO_3 (15.8 M) was added drop-wise to 0.5 g of residue from the F3. The mixture was left at room temperature for 16 hours and then was transferred to a 50 mL reaction vessel connected to a reflux condenser. The reaction vessel was heated until reflux conditions were reached and was continuously heated for 2 hours (the condensation zone is lower than 1/3 of the height of the condenser). The condenser was further rinsed with 10 mL HNO_3 (0.5 M) and the rinsing solution and additional HNO_3 (0.5 M) were collected and added to the reaction vessel until they reached the 50 mL scale line. The supernatant solution of each fraction was analyzed for

Ce by an Agilent 7500ce Inductively Coupled Plasma Mass Spectrometry (Agilent Technologies, Santa Clara, CA).

SEM characterization of Ce in soil

To visualize and characterize the Ce in soils, air dried control and 1000 mg/kg treated loamy sand and silt loam soils were fixed on a double-sided adhesive tape, which was adhered to the specimen holder, and were analyzed using FEI Quanta FEG450 scanning electron microscope (SEM) equipped with an Energy Dispersive X-ray Spectroscopy (EDS). The SEM imaging of soil samples was performed by applying accelerating voltages of 10 kV. The concentration of 1000 mg/kg CeO_2NPs, the highest concentration used in this study, was selected to ensure the detection of CeO_2NPs by SEM.

Plant uptake and accumulation of Ce

After plants were carefully removed from the soil, they were separated into shoots, storage root and fine roots. The separated tissues were rinsed with deionized water to remove all adhering soil particles and dried in an oven at 105 °C for 30 min, then at 75 °C for seven days prior to dry weight determination. After drying in the oven, three replicates in each treatment were randomly chosen. The dried shoot, storage root, and fine root tissues were ground into fine powders and digested in 4 mL of 70% (v/ v) nitric acid. The nitric acid digest was heated at 95 °C for 20 min and then at 45 °C for 4 min. The cycle was repeated until all the dry tissues was dissolved. Afterwards, 2 mL of H_2O_2 was added to the mixture. The mixture was heated using the same temperature cycle until the solution was clear. The digest solutions of storage roots and shoots were

then analyzed by an Agilent 7500ce ICP-MS (Agilent Technologies, Santa Clara, CA). The digest solution of fine roots was analyzed by a Thermal Scientific iCAP 6500 Inductively Coupled Plasma Optical Emission Spectrometry (ICP-OES) due to the high cerium concentration in the fine root tissue.

Distribution of Ce in radish shoots and storage roots

Rest three replicates from the control and 500 mg/kg treatment group grown in both soils were used as representatives to illustrate the Ce localization in the radish storage roots and shoots. The whole fresh storage root was divided into three layers with a precision knife: the periderm (Peri), the intermediate layer (L1), and the inner layer (L2). The thicknesses of the periderm and the intermediate layer were approximately 1 mm and 5 mm respectively. Each fresh shoot was divided into two sections: the edges (S1) and the main leaf area (S2). The width of the edges was about 5-7 mm. The cutting method is illustrated in Figure 4.2. The subsections of the storage roots and shoots were oven dried and digested as described above for the whole tissues. The digest solutions were analyzed by ICP-MS.

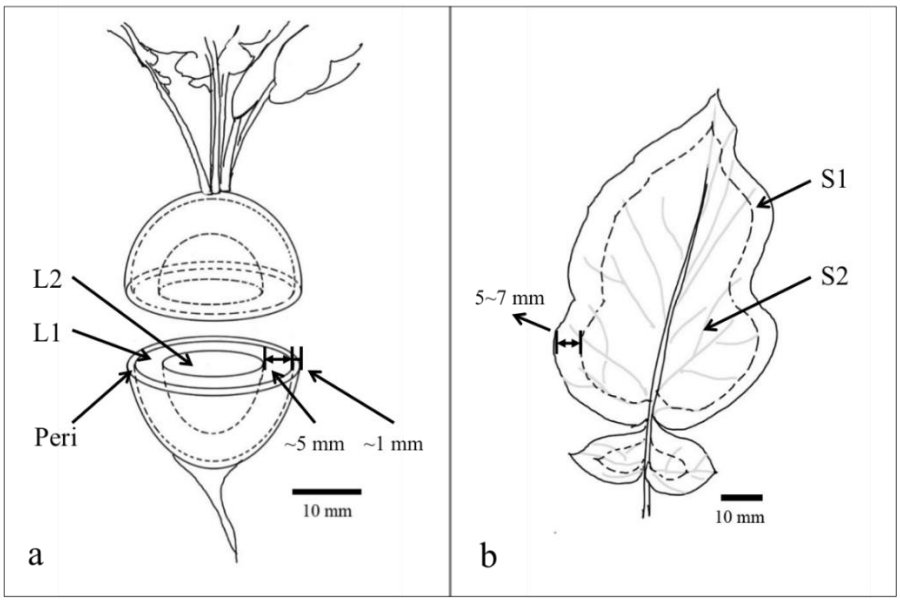

Figure 4.2. Schematic illustration of the cutting method of the radish storage root and shoot used for Ce uptake distribution. Peri: the periderm; L1: the intermediate layer; L2: the inner layer; S1: the edges of leaves; S2: the main leaf area.

Data analysis

The statistical analyses of experimental data were one-way and two-way ANOVA using IBM SPSS Statistics V22.0. The Duncan test was conducted for post hoc comparisons. A student t test was conducted to determine the significance of soil impact at the same concentration. Statistical significance was accepted when $p < 0.05$.

Results

Ce and soils characterization

The TEM image of CeO_2NPs and the size distribution of the CeO_2NPs are shown in Figure 4.3a & b. The size distribution was obtained by measuring 112 individual

nanoparticles on the TEM image with ImageJ. Most of the nanoparticles had quadrilateral or polygonal shapes and fell in the size range of 10-25 nm in diameter with an average nanoparticle size of 19.1 nm. The hydrodynamic diameter and zeta potential of CeO_2NPs at 500 mg/L in water were 107.3 nm and 45 ± 0.41 mV respectively. The XPS spectra of Ce on the surface of CeO_2NPs are shown in Figure 4.3c. 12.4% of Ce on the surface was in the form of Ce^{3+}, as calculated through the XPS peak fitting software XPSPEAK 4.1.

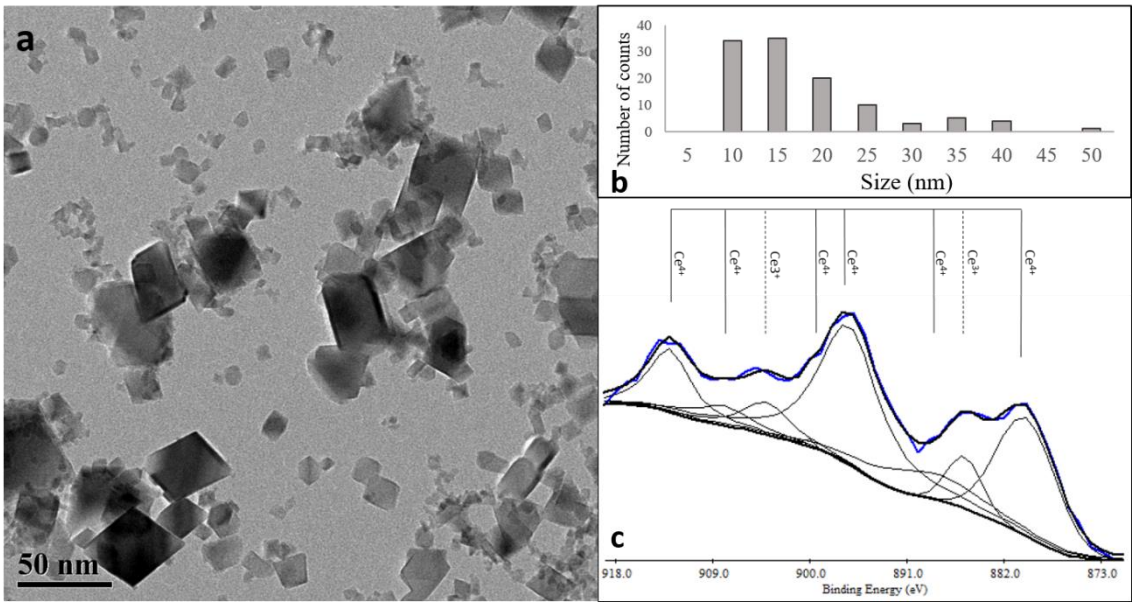

Figure 4.3. Characterization of CeO_2NPs. (a) TEM image of CeO_2NPs; (b) the size distribution of the CeO_2NPs in the TEM image; (c) the XPS spectra of Ce on the surface of CeO_2NPs. Ce^{3+} and Ce^{4+} produced characteristic sets of XPS peaks at characteristic binding energy values shown in (c).

The average organic matter contents were 11.87± 0.56% for loamy sand and 2.21 ± 0.04% (average ± standard error, n = 3) for silt loam. The weight percentages of sand, silt, and clay are listed in Table 4.1. The results of the soil routine analyses conducted in the Soil, Water and Forage Testing Laboratory at Texas A&M University are listed in the Table 4.2.

Table 4.1. The percentages of sand, silt, and clay in two types of soil.

	Topsoil	Illinois soil
Clay	6.27%	19.06%
Silt	18.13%	65.14%
Sand	75.60%	15.80%
Classification	Loamy sand	Silt loam

Table 4.2. Properties and concentrations of common elements in two soils.

Analysis	Units	Loamy sand	Silt loam
pH	-	6.87	6.58
Conductivity	umho/cm	358	275
Nitrate-N	mg/kg	2	13
Phosphorus	mg/kg	46	16
Potassium	mg/kg	213	111
Calcium	mg/kg	3620	3660
Magnesium	mg/kg	391	241
Sulfur	mg/kg	61	10
Sodium	mg/kg	39	11
Iron	mg/kg	40.33	11.95
Zinc	mg/kg	4.86	0.84
Manganese	mg/kg	9.94	8.22
Copper	mg/kg	1.60	0.52

Plant physiological status

The dry biomass of storage roots and shoots are shown in Figure 4.4. For both soils, treatment with 100 and 500 mg/kg CeO_2NPs were not associated with significant differences between the treated plants and their controls. Plants exposed to 1000 mg/ kg CeO_2NPs had significantly greater dry biomass of the storage root than all other treated and control plants in loamy sand. The same treatment led to significantly lower dry biomass of storage roots than that of 500 mg/kg treated radishes in silt loam but was not statistically different than the control. When the biomass of radishes grown in two soils at the same concentration was compared, the storage roots of control, 100 mg/kg, and 500 mg/kg CeO_2NPs treated radishes were significantly greater in silt loam than in loamy sand. At the highest concentration, the difference of the storage root biomass between the two soils was not significant. In contrast to the storage root biomass, the shoot biomass was not affected by CeO_2NPs exposure for either soil. However, significant differences were noticed between the soil types at control and 100 mg/kg treatment. Radishes grown in silt loam soil from the two concentration groups had significantly higher shoot biomass than the plants grown in loamy sand. The relative chlorophyll contents, expressed as percentages of controls, are shown in Table 4.3. No significant differences were observed across the treatments.

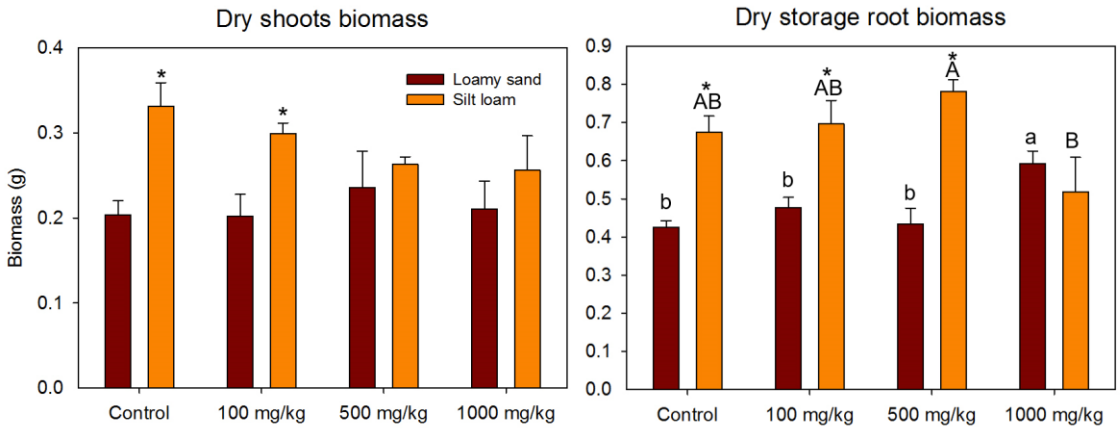

Figure 4.4. Dry biomass of radish tissues treated with different concentrations of CeO_2 NPs in two different soils. The error bars represent standard error (n=4). Different letters in lower case and upper case represent significant differences between the treatments in loamy sand and silt loam respectively ($p<0.05$). Asterisks indicate significant differences between two soils at same CeO_2 dosing concentration ($p<0.05$).

Table 4.3**.** The relative chlorophyll content of treated radish shoots expressed as the percentage of controls, data represent the mean and standard error (n=7).

	Control (%)	100 mg/kg (%)	500 mg/kg (%)	1000 mg/kg (%)
Loamy sand	100±3.14	102.35±1.61	101.49±1.62	100.68±1.88
Local	100±2.26	98.82±2.82	99.98±2.03	102.72±3.27

Ce fractionation in soil

The percentage of each fraction in the two soils is illustrated in stacked bars in Figure 4.5. F4 was the dominant fraction of CeO_2NPs in both soils. The percentage of F4 was higher in silt loam (60.8-78.2%) than in loamy sand (58.6-70.5%) at the same concentration, but only the difference at 100 mg/kg was statistically significant. F1 was the smallest fraction and accounted for less than 0.11% in loamy sand and 0.22% in silt

loam. While the relative percentage of F2 was comparable between the two soils, the loamy sand always contained significantly higher oxidizable fraction (F3) than silt loam at the same concentration (15.8-17.8% for loamy sand vs. 9.07-11.8% for silt loam). The distribution of CeO_2NPs among these four fractions changed with concentration. In general, with the increase of concentration, the percentage of F1 and F2 decreased while the percentage of F4 increased in both soils. The percentage of F3 was relatively stable across the concentration ranges employed in this study.

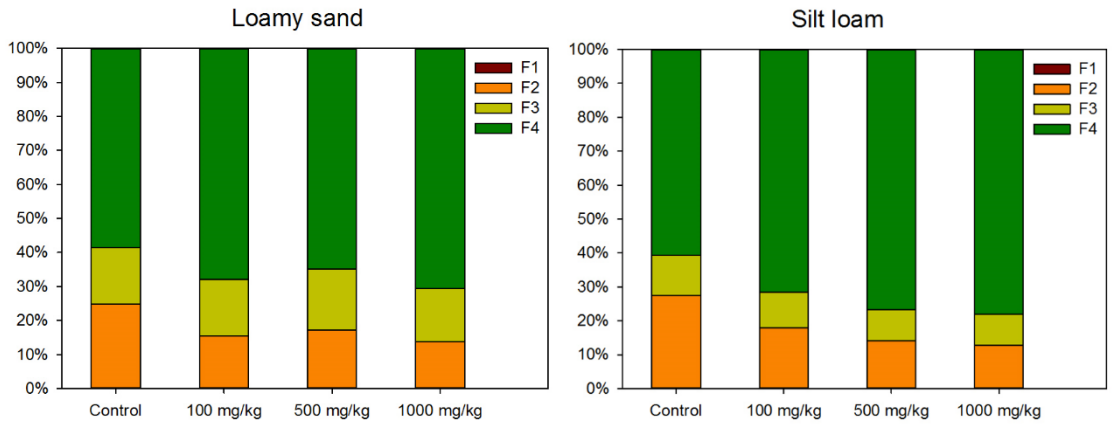

	F1 (%)	F2 (%)	F3 (%)	F4 (%)
Control	0.11±0.057	24.62±1.12	16.72±0.78	58.55±1.60
100 mg/kg	0.093±0.0048	15.32±0.21	16.68±0.61	67.92±1.21
500 mg/kg	0.048±0.0034	17.15±0.75	17.87±0.53	64.93±1.33
1000 mg/kg	0.027±0.0034	13.64±0.44	15.80±0.74	70.54±1.27

	F1 (%)	F2 (%)	F3 (%)	F4 (%)
Control	0.22±0.0053	27.27±0.47	11.82±0.48	60.69±5.85
100 mg/kg	0.16±0.024	17.74±0.54	10.58±0.69	71.51±0.49
500 mg/kg	0.11±0.0031	14.04±0.79	9.07±1.09	76.78±12.18
1000 mg/kg	0.08±0.014	12.68±0.1.90	9.08±1.31	78.16±17.26

Figure 4.5. Percentage of cerium fractionation in (a) loamy sand and (b) silt loam determined by the modified BCR sequential extraction procedure. The results shown on the table beneath the figures represent the average and standard error of three replicates. The F1 fraction was too small to see in the treated soils.

The actual concentrations of individual fractions are presented in Fig. 4.6a. As the most abundant rare earth element on the earth's crust, both soils contained high background concentration of cerium. The background Ce was 52.5 ± 1.87 mg/kg dry soil in the loamy sand and 77.2 ± 5.25 mg/kg dry soil in the silt loam respectively. Due to the high background concentrations of Ce, the fractionation of dosed CeO_2 was calculated by subtracting the Ce concentration in each individual fraction of the control soil from the concentrations in the corresponding fractions of the treated soil. The results are presented in Figure 4.6b. Both the dosing concentration and soil type were significant factors affecting the fractionation of CeO_2NPs in soil according to the two-way ANOVA analysis. In general, the silt loam contained higher F1 than the loamy sand and the difference was significant for 500 mg/kg treatment (Figure 4.6b). The silt loam contained significantly lower F2 and F3 than the loamy sand in 500 and 1000 mg/kg treatment. The silt loam had significantly higher F4 than the loamy sand in 100 mg/kg but the differences in F4 were not significant in higher concentrations (Figure 4.6b). It has been reported that CeO_2NPs cannot be fully dissolved in aqua regia.[193] Therefore, it is likely that some Ce residues remained in the soil and was not included in the four fractions reported here.

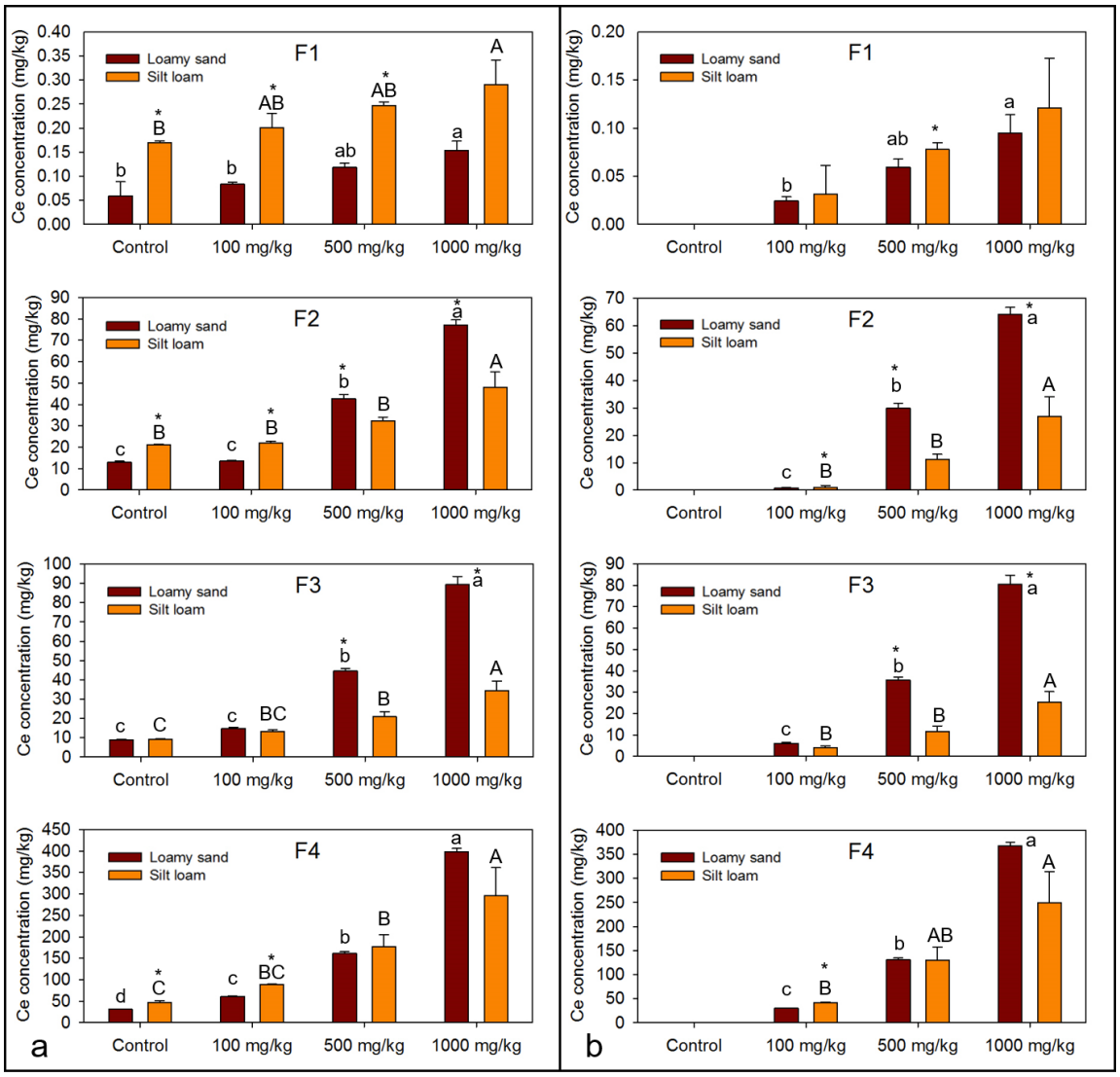

Figure 4.6. (a) The actual Ce concentrations in different soil fractions and (b) the adjusted Ce concentrations by subtracting the Ce concentration in corresponding fraction of the control soil. The error bars represent standard error (n=3). Different letters in lower case and upper case represent significant differences between the treatments in loamy sand and silt loam respectively (p<0.05). Asterisks indicate significant differences between two soils at the same CeO_2NPs dosing concentration (p<0.05).

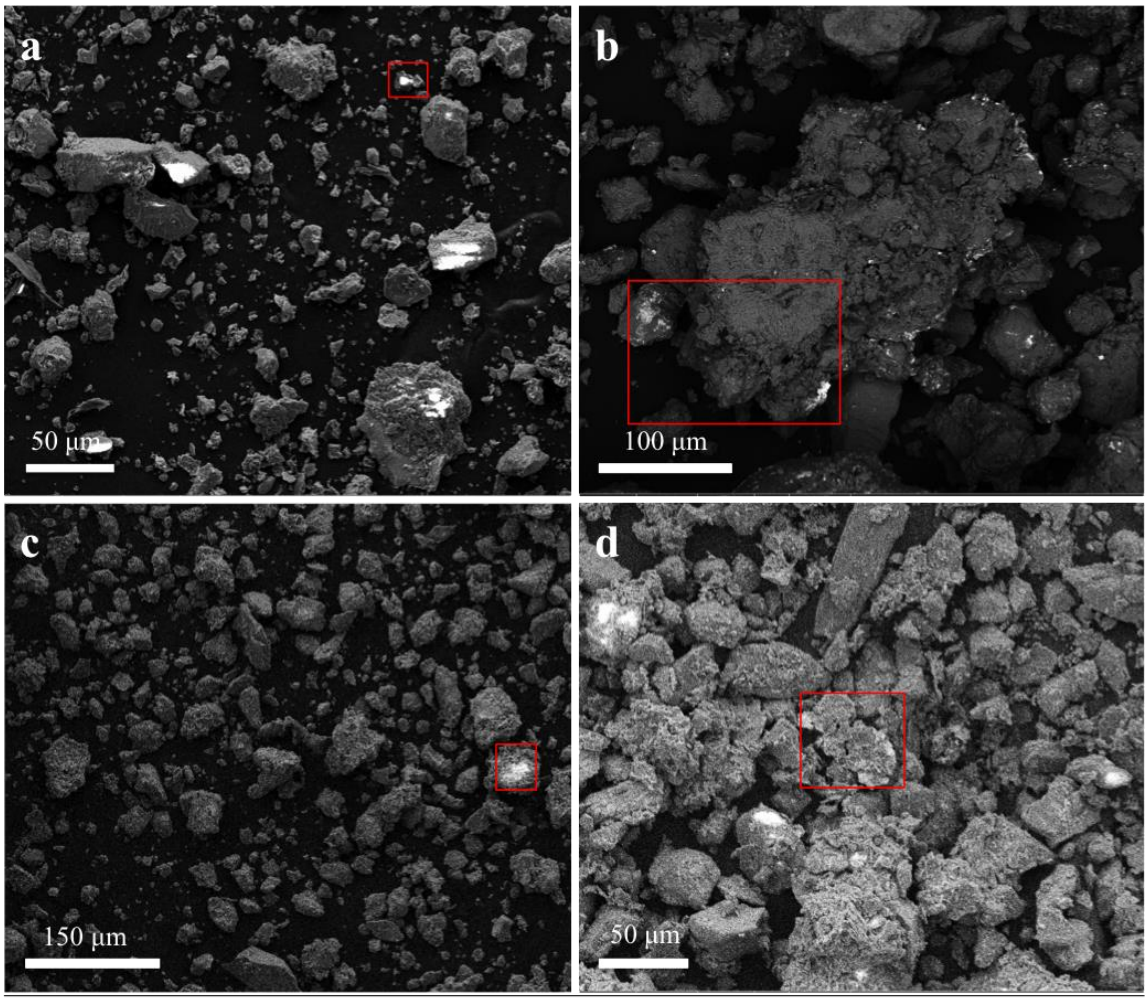

Element	Weight% in a	Weight% in b	Weight% in c	Weight% in d
O	61.56	56.49	62	55.32
Al	2.48	4.04	4.85	4.43
Si	34.85	28.65	30	30.03
K	N/A	0.73	3.15	0.72
Ca	N/A	0.76	N/A	N/A
Fe	1.11	2.1	N/A	1.45
Ce	N/A	7.23	N/A	8.05
Total	100	100	100	100

Figure 4.7. SEM images of soil samples of. (a): loamy sand control; (b): loamy sand 1000 mg/kg; (c): silt loam control; (d): silt loam 1000 mg/kg. Table below images shows the weight percentage of detected elements in selected area (red frames in images).

To further probe the differences of CeO_2NPs behaviors in the two soils, SEM analysis was conducted. The SEM images shown in Figure 4.7 were acquired with samples from control and 1000 mg/kg treatment. EDS analysis was conducted in the selected area (red frames in the images) to detect the component elements. The main components of the two soils were silica and oxygen. In control samples from both soil types, no Ce was detected by the EDS even though ICP-MS analysis showed that both soils contained high background Ce. However, in 1000 mg/kg treatment, the Ce weight percentages were 7.23% and 8.05% in loamy sand and silt loam, respectively. The Ce signals in both soil indicate that the CeO_2NPs were mainly attached to the edge of soil particles. Individual particle aggregates could be seen in the treated loamy sand, but not in the silt loam soil.

Ce uptake and accumulation

Ce was detected in all plant tissues; however, the total accumulation of Ce in plant biomass was relatively small compared with the total Ce added to the system. The concentrations and the total mass of Ce in different plant tissues are presented in Figure 4.8a. Due to the high background Ce concentration in control plants, the accumulation of the dosed Ce in different plant tissues was calculated by subtracting the Ce concentration in different plant tissues of the control plants from the corresponding tissues of treated ones and the results are presented in Figure 4.8b. Even though the accumulation of Ce in all tissues increased with increasing concentration in general, a dose response relationship was not apparent, especially for the shoot tissues. The comparison of Ce accumulation by plants grown in two soil types indicated that the radish fine roots and

storage root from the loamy sand usually possessed higher Ce concentration than the same tissues collected from the silt loam. The Ce concentration in the shoot showed opposite trend between these two soils. However, none of these differences were significant except for the Ce in the fine roots from 100 mg/kg treatment.

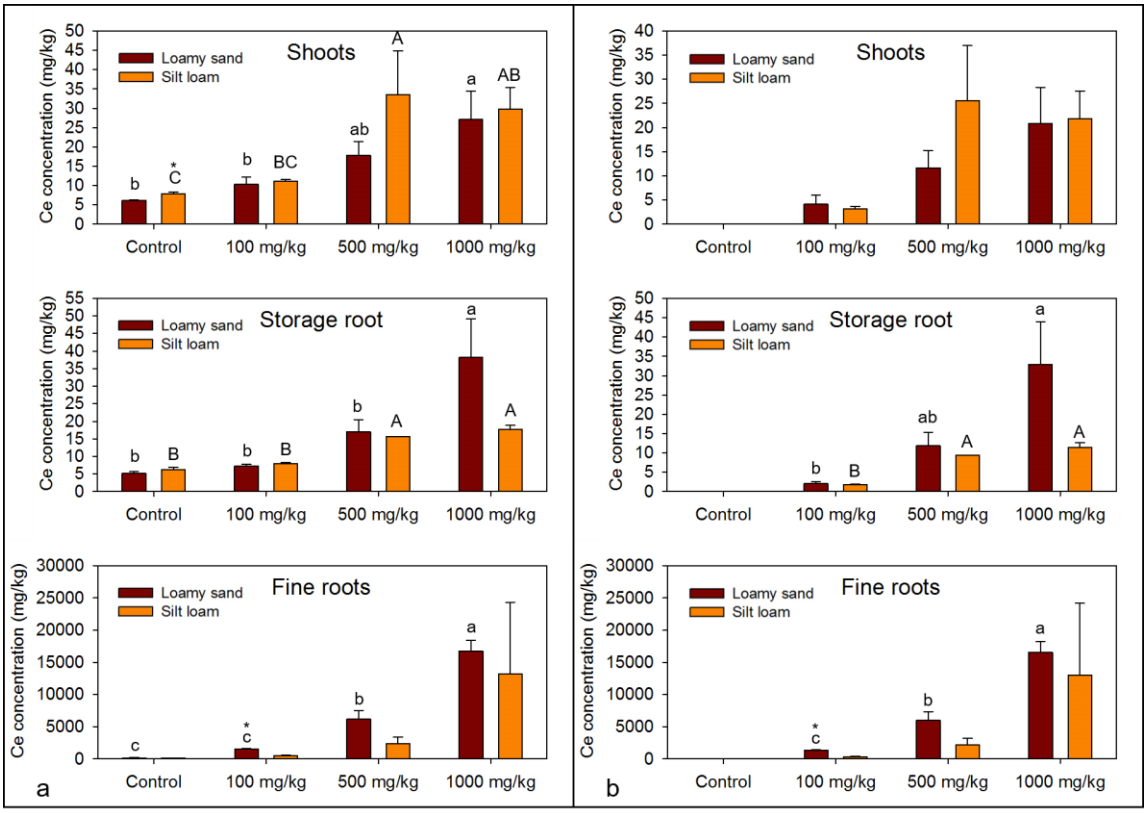

Figure 4.8. (a) The actual Ce concentrations in different radish tissues and (b) modified Ce concentrations in different radish tissues after the Ce concentrations in the control plants were subtracted from the corresponding tissues of treated plants. The error bars represent standard error (n=3). Samples without error bars indicate that the error bars are too small to see on the figures. Different letters in lower case and upper case represent significant differences between the treatments in loamy sand and silt loam respectively (p<0.05). Asterisks indicate significant differences between two kinds of soil at same CeO_2NPs dosing concentration (p<0.05).

Ce localization in radish storage roots and shoots

The Ce concentrations in different sections of radish storage roots and shoots are shown in Table 4.4. The average Ce concentration in the periderm (Peri) of radish storage roots from 500 mg/kg was more than ten times higher than that of control in both soils. However, large variations were observed between replicates from the same treatment group. Ce concentrations in the intermediate layer (L1) and the inner layer were comparable to the control plants in both soils. In radish leaves, the Ce concentrations in the edge section (S1) of treated and control plants were similar for both soils. However, the average Ce concentration in the main leaf area (S2) was significantly higher (almost three times) from 500 mg/kg treated radish than from control plants in the silt loam. No difference was observed for the main leaf area in control plants and 500 mg/kg treated plants in loamy sand.

Table 4.4. The cerium concentration in different parts of radish, data represented the mean and standard error (n=3). Different letters represent significant differences between the treatments.

Soil Type	Treatment	Peri (mg/kg)	L1 (mg/kg)	L2 (mg/kg)
Loamy sand	Control	11.40±3.06	7.45±1.38	11.09±1.83
	500 mg/kg	112.90±52.35	10.88±1.61	9.40±1.67
Silt loam	Control	8.91±0.76	10.43±2.09	8.07±2.97
	500 mg/ kg	127.06±56.25	11.49±1.18	8.61±0.32

Soil Type	Treatment	S1 (mg/kg)	S2 (mg/kg)
Loamy sand	Control	18.83±1.67	8.85 ± 0.42^{ab}
	500 mg/kg	23.12±0.49	9.81 ± 1.57^{ab}
Silt loam	Control	22.90±4.23	7.00 ± 0.52^{b}
	500 mg/ kg	18.26±3.14	20.58 ± 7.29^{a}

Discussion and Conclusions

Although plant uptake of CeO_2 NPs from soil has been observed previously, the influence of soil properties on CeO_2 NPs bioavailability has not been fully understood. However, once Ce enters soil through wastewater irrigation or biosolid amendment, particle bioavailability may depend heavily on the physical and chemical properties of soil, as noted for other elements.[186] The results of this study confirmed that the accumulation and translocation of CeO_2NPs in plant tissues could be affected by soil type due to the impact of soil on CeO_2NPs fractionation.

CeO_2NPs are generally perceived as stable in the environment, but dissolution under certain circumstances (e.g. interacting with plants) have been reported. The presence of chelating agents in the soil may also enhance the dissolution by forming complexes with Ce^{3+} on the surface of CeO_2NPs.[53] F1 was considered to include both the dissolved ions and dissolved nanoparticles. Due to the low solubility of CeO_2NPs and possibly the rapid adsorption of dissolved ions to the solid phase, F1 represented a negligible fraction in both soils in this study even though the concentration of F1 increased with concentrations (<0.16% for the dosed CeO_2NPs). Water soluble Ce at low concentration is generally not considered as toxic and has been used as an additive to fertilizer.[169] The F1 in silt loam was invariably higher than that in loamy sand at the same concentration (difference was not significant at 1000 mg/kg). Therefore, the differences of F1 may partially explain the generally higher dry biomass of radish storage root and shoots in silt loam than in loamy sand (Figure 4.4). This observation

was also consistent with the finding in Chapter III that CeO_2NPs at low concentration could improve the biomass of radish storage root.

Fe-Mn oxides, considered as secondary minerals, exist primarily in the clay fraction.[194, 195] The concentrations of Fe in two soils listed in Table 4.2 implied that loamy sand contained significantly higher Fe oxides than silt loam. Therefore, higher F2 in loamy sand was expected. The results (Figure 4.6b) showed that F2 in the loamy sand was significantly higher than that in the silt loam at higher CeO_2NPs dosing concentrations (500 and 1000 mg/kg), suggesting the significance of mineral content on the fractionation of Ce in soils.

The oxidizable fraction (F3) of CeO_2 is believed to be associated with organic matter in soil. The higher organic matter content in loamy sand soil is consistent with the generally higher F3 in this soil than in the silt loam. Natural organic matter can enhance the mobility of NPs in porous media by increasing charge and steric stabilization.[196] Zhao et al.[126] studied the uptake of CeO_2NPs by corn grown in soils and concluded that organic matter improved the mobility and bioavailability of CeO_2NPs to corn, resulting in higher accumulation of Ce in corn roots. The consistently higher Ce concentration in the fine roots and storage roots of radish grown in loamy sand was consistent with the relative organic matter contents in these two soils. These findings support the theory that natural organic matter plays an important role in regulating the mobility and bioavailability of engineered nanoparticles to plants.[196]

One intriguing observation of this study was the disparity of roots and shoots with regard to CeO_2NPs accumulation from different soils. As described above, the

radish storage roots and fine roots generally contained higher Ce concentration in loamy sand. However, the concentrations of Ce in shoot tissues followed the opposite trend between the soils. It is postulated that the low translocation of Ce in the loamy sand is associated with the low F1 in that soil. Previous research suggested that engineered nanoparticles in plant roots are translocated up through the xylem tissues along with water,[194] which makes the water soluble fraction more readily transferred to the shoot tissues. The study in Chapter III also indicates that the dissolved Ce is easier for plants to transport from roots to shoots. A recent study also demonstrated that negatively charged humus colloids in soil could chelate with positively charged CeO_2NPs and reduce their mobility and bioavailability in soil.[72] Consequently, the upward transport of CeO_2NPs from root to shoot will be limited in soil grown plants and the extent of transport may depend significantly on the amount of water soluble fraction. Our results agreed with the observation of the low root to shoot translocation of CeO_2NPs in organic matter enriched soil, but contradicted a previous study which indicated that organic matter enriched soil facilitated the uptake and translocation of CeO_2 NPs by corn.[126] The discrepancies may derive from the use of different CeO_2NPs and different plant species and require further investigation.

Following the uptake of Ce, whether the different soil fractionation would affect the distribution of Ce in different plant tissues was evaluated. Consistent with the previous investigation in Chapter II, Ce was predominantly accumulated in the pigmented periderm of radish storage roots for both soils (Table 4.4). Another recent study on the interactions between CeO_2NPs and carrot (*Daucus carota* L.) also reported

that the accumulation of Ce principally in the taproot peel and the shoots, with significantly lower Ce concentration in the edible flesh.[197] Notably, even though the average concentration in the periderm was ten times higher in the 500 mg/kg treated radish than the control radish in this study, high variability between the replicates of treated radish was noticed (51.7-217 mg/ kg dry tissue for loamy sand and 45.5-236 mg/kg dry tissue for silt loam). The high variability likely was due to the unequal adsorption of CeO_2NPs on the skin surface of the storage root and the incomplete rinsing process during harvest. The similar Ce concentration in the intermediate and inner layers of the treated and control plants suggested that Ce accumulation in the flesh is limited. Altogether, the results indicate that a primary pathway for Ce accumulation in radish storage roots was physical adsorption on the surface and radial diffusion toward the center which is minimal in this study. The Ce concentration in S2 section of the shoot tissue grown in silt loam was three times higher than their corresponding controls, but such difference was not observed in the sandy loam. Our finding is consistent with the higher shoot concentration in CeO_2NPs treated radish in silt loam and substantiates our earlier contention that F1 was more readily translocated from radish roots to shoots. A previous study indicated that the Ce taken up from roots is transported to leaves through leaf vein vasculature with the transpiration stream[78] and our results appeared to support that conclusion. However, the results from this study suggested that most of the Ce transported with the transpiration stream is in the dissolved form, not the nanoparticles.

In summary, soil characteristics were shown to be an important factor affecting the soil fractionation and subsequent bioavailability of CeO_2NPs to plants. The

accumulation of Ce in radish belowground tissues correlated well with the sum of the first three fractions (R^2=0.98 and 0.78 for loamy sand and silt loam respectively), suggesting that these fractions were bioavailable to plant roots. However, only the exchangeable fraction correlated well with the element amounts shown to transport from roots to shoots (R^2=0.97 and 0.89 for loamy sand and silt loam respectively). In addition to their bioavailability, the distribution of Ce in different plant tissues was also affected by the physicochemical properties soils, indicating that the specific soil properties must be an important consideration in the assessment of the fate and transport of engineered nanoparticles in the environment.

CHAPTER V

THE AGING EFFECTS ON THE FATE AND BIOAVAILABILITY OF CEO2NPS TO RADISH IN SOIL*

Introduction

The wide application of CeO_2NPs in industry and consumer products inevitably leads to the release of these ENMs to the environment. CeO_2NPs likely will continue to build up in the environment, and the prospect of high CeO_2NPs concentrations in the environment has raised concerns because of their potential impact on the ecosystem. Although numerous studies on the interactions between CeO_2NPs and plants have been conducted, almost all of them used freshly prepared CeO_2NPs. A more realistic scenario is that CeO_2NPs would persist in the soil or sediment for a long period of time after releasing into the environment. Increasing evidence shows that the properties of metal contaminants including engineered metallic nanoparticles change with time due to various physical, chemical and biological processes in the environment.[198-200] Thus, understanding the aging effect of CeO_2NPs in soil on their fate and bioavailability is necessary for assessing the environmental risks of CeO_2NPs.

Current understanding on the aging process of ENMs is still in its fledgling stage but developing rapidly. Coutris et al.[199] found that the bioaccessibility of uncoated

---

* Part of this chapter is reprinted with permission from "Effects of aging on the fate and bioavailability of cerium oxide nanoparticles to radish (Raphanus sativus L.) in soil" by Zhang, W.; Dan, Y.; Shi, H.; Ma, X., 2016. *ACS Sustainable Chemistry & Engineering*, 4, 5424-5431, Copyright [2016] by American Chemical Society.

AgNPs increased due to the continued release of Ag^+ from nanoparticles. Diez-Ortiz et al.[201] also reported that the bioavailability of uncoated AgNPs to earthworm in soil increased during aging process (52 weeks in soil) as a result of dissolution. Although CeO_2 has low solubility and is not expected to dissolve extensively in bulk soil, higher dissolution of CeO_2NPs has been reported in the rhizosphere of plant roots[53] and was demonstrated in Chapter III. The presence of chelating agents in the soil may also enhance the dissolution CeO_2 by forming complexes with Ce^{3+} on the surface of CeO_2NPs.[53] So whether CeO_2NPs would behave similarly as AgNPs during aging process needs to be specifically examined.

Numerous studies have shown that the bioavailability of dissolved, adsorbed, and solid phase metallic ions in soil change with time because of the various physical and chemical processes.[198] The adsorption of heavy metal ions onto the soil particle surface occurs through three mechanisms: inner-sphere surface complexation due to the siloxane cavity, outer-sphere surface complexation, and adsorption due to diffuse ion swarm (or diffuse layer).[202] The first mechanism, which is also described as “specific adsorption”, takes place in permanent charge clay minerals and on the surface of metal oxides and organic matter. The latter two, which are relatively weaker and generally described as “nonspecific adsorption”, occur at pH dependent mineral surfaces, including the edges of individual kaolinite platelets, Fe-Mn oxides, aluminum hydroxide, and organic matter. Outer-sphere complexes can transform to inner-sphere complexes over time, and solid phases can increase in crystallinity, both of which decreases solubility and bioavailability of heavy metal ions.[202] Precipitation can immobilize the metal ions by

decreasing the solubility of the metal compounds. Because of these metal ion retention mechanisms, the bioavailability of contaminant metal ions usually decreases during the aging process.[200] In addition to dissolution, CeO_2NPs also display unique surface redox chemistry between Ce^{3+} and Ce^{4+} on the NP surface, depending on the surrounding environment. For example, Kuchibhatla et al.[203] found that Ce^{3+} could be formed from Ce^{4+} in the presence of hydroperoxy species:

$$Ce^{4+} + HO_2 \rightarrow Ce^{3+} + H^+ + O_2 .$$

Those processes that could take place after the release of CeO_2NPs suggest that aged CeO_2NPs may display fates and impacts on the environment quite differently from those of fresh CeO_2NPs. However, no studies have been performed to examine the effects of aging of CeO_2NPs on the fate and bioavailability of CeO_2NPs to plants. By applying a well-established sequential extraction method, the effect of aging on CeO_2NPs fractionation in soil was evaluated. From the fractionation results, information on how aging process affects the interactions between CeO_2NPs and soil particles and their bioavailability could be derived. In this chapter, the fractionation of CeO_2NPs in soil was assessed with the modified BCR (Bureau Commune de Reference of the European Commission) sequential extraction method[190] and an EDTA partial extraction method.

The objectives of this study were (1) to investigate the aging effects of CeO_2NPs on their fractionation in soil; (2) to determine the aging effects on the bioavailability of CeO_2NPs to radish; and (3) to examine the effects of aging effects on the nutritional status of radish bulbs.

Materials and Methods

CeO_2NPs characterization

Uncoated CeO_2NP powder (10−30 nm) was purchased from US Research Nanomaterials (Houston, TX). The shape and size of NPs were confirmed by a Tecnai G2 F20 transmission electron microscope (TEM) (FEI, Hillsboro, OR). An X-ray photoelectron spectroscope (XPS) (Omicron multiprobe MXPS system, Scienta Omicron, Taunusstein, Germany) was used to investigate the surface speciation of CeO_2NPs.

Soil characterization and preparation

The same agricultural soil collected from a farmland in Carbondale, IL, as used in the previous chapter, was used in this study. On the basis of the weight percentages of sand, silt, and clay (Table 4.1), the soil was classified as silt loam according to the U.S. Department of Agriculture soil texture classification. The soil routine analyses, including the measurements of pH, conductivity, nitrate-N, and some macro- and micronutrients, were conducted in the Soil, Water and Forage Testing Laboratory at Texas A&M University following established protocols. Briefly, soil pH and conductivity were determined with a slurry with a 1:2 soil:deionized water ratio. The slurry was vigorously stirred and then allowed to settle for a minimum of 30 min at room temperature before the measurements. Both the pH and the conductivity was determined with an Orion Star A325 pH/conductivity portable multiparameter meter (Thermo Scientific, Beverly, MA). nitrate-N was extracted from soil with a 1 N KCl solution and reduced to nitrite through a cadmium column and then quantified by an UV−vis spectrophotometer in a FIAlab-

2500 analyzer system (FIAlab Instruments, Inc., Bellevue, WA). The micronutrients were extracted using a solution containing 5 mM diethylenetriaminepentaacetic acid (DTPA), 10 mM $CaCl_2$, and 100 mM triethanolamine. The extracted micronutrients were then determined by inductively coupled plasma optical emission spectroscopy (ICP-OES) (SPECTRO Analytical Instruments, Kleve, Germany). The organic matter content was determined by measuring the loss of mass during combustion at 440 °C for 24 hours, following the ASTM D 2974 method (Standard Test Methods for Moisture, Ash and Organic Matter of Peat and Organic Soils). The average organic matter content was 2.21 ± 0.04% (average ± standard error; n = 3).

Three treatment scenarios were prepared: control soil (no addition of CeO_2NPs), soil with 1000 mg of freshly spiked CeO_2NPs as Ce element per kilogram of dry soil (Fresh soil), and soil with the same concentration of CeO_2NPs but aged for 7 months (Aged soil). The CeO_2NPs aging was performed as follows. The soil was first mixed with a known amount of CeO_2NPs manually in a covered container to achieve the targeted concentration (1000 mg/kg) and shaken on a shaker table at 250 rpm for 2 months. The mixture was then stored in a covered container for an additional 5 months. The water content of Aged soil was maintained at 20%. The Fresh soil was prepared by mixing the soil with CeO_2NPs similarly and shaking on a shaker table at 250 rpm for 24 hours before the experiment.

Ce fractionation in soil

Before seeds were sowed, the fractionation of CeO_2NPs in the soils described above was analyzed following an established BCR extraction protocol with slight

modifications.[190] A half-gram of dry soil was randomly collected from each prepared soil and transferred to a 50 mL centrifuge tube. The soil was mixed with 20 mL of a 0.11 M acetic acid solution by being shaken at 250 rpm for 16 hours at room temperature. The mixture was then centrifuged at 3000g for 20 min. The Ce in the supernatant was considered as the exchangeable fraction (F1). The residue was then resuspended and extracted with 20 mL of a 0.5 M hydroxylamine hydrochloride solution at pH 1.5 by being shaken (250 rpm) and centrifuged under conditions similar to those described above to obtain the reducible fraction (F2). The residue from F2 was again resuspended and mixed with 30% (w/v) hydrogen peroxide (H_2O_2). The mixture was kept at room temperature with a loosely closed cap for 1 hour. The container was then closed and heated at 85 ± 2 °C in a water bath for an additional hour. Afterward, the volume of the mixture was reduced to less than 1.5 mL by further heating in a water bath without a cap. Another aliquot of 5 mL of 30% (w/v) H_2O_2 was added, and the heating process was repeated. The oxidizable fraction (F3) was then extracted with 25 mL of a 1 M ammonium acetate solution at pH 2 by being shaken at 250 rpm for 16 hours and centrifuged at 3000g for 20 min at room temperature. The ISO 11466 protocol was applied to extract the residual fraction (F4) by further digesting the residue from F3 using aqua regia. A mixture of 4.5 mL of HCl (12.0 M) and 1.5 mL of HNO_3 (15.8 M) was added to the centrifuge tube that contained the residue from F3. The residue was resuspended in the aqua regia and transferred to a 50 mL reaction vessel that was connected to a reflux condenser. The reaction vessel was heated on a hot plate for 2 hours under reflux. Afterward, the condenser was rinsed with HNO_3 (0.5 M). The rinsing

solution and additional HNO_3 (0.5 M) were collected and added to the reaction vessel until the solution level reached 50 mL. The Ce in the supernatant of each fraction was quantified by a NexION 300 inductively coupled plasma mass spectrometry (ICP-MS) (PerkinElmer, Waltham, MA). Three replicates were prepared and analyzed for each treatment.

In addition, the concentration of Ce^{3+} in each soil was determined through a separate ethylenediaminetetraacetic acid (EDTA) partial extraction. Previous research has shown that both the dissolved Ce^{3+} ions and the Ce^{3+} adsorbed or precipitated with PO_4^{3-} on the surfaces of CeO_2NPs and soil particles can be successfully extracted with EDTA.[53, 204] Briefly, an additional 0.5 g of dry soil was randomly collected from each prepared soil and transferred to a 50 mL centrifuge tube. Twenty milliliters of 100 μmol/L EDTA acid disodium salt dehydrate was added to the soil. The mixture was shaken at 250 rpm for 7 days at room temperature. Then the mixture was centrifuged at 3000g for 20 min. The supernatant was collected and filtered through a 10 kDa Amicon Ultra-4 Centrifugal Filter unit (EMD Millipore, Darmstadt, Germany) for 45 min at 4000 rpm. The soluble Ce in the filtrate was quantified by ICP-MS. For each soil, three replicates were analyzed.

Seed germination and growth conditions

The growing pots were established by adding 150 g of dry soil to a plastic container (total volume of ~266 mL). Deionized water was added to the growing pots to saturate the soil to 100% of field capacity. Radish seeds [Cherriette (F1)], purchased from Johnny's Selected Seeds (Winslow, ME), were geminated in Petri dishes for 5

days. Healthy seedlings were transferred to the growing pots incubated on a growth cart with a 16 h photoperiod at 28 °C. The light in the growth cart was provided by four T5 fluorescent bulbs. The light intensity was approximately 104 μmol m^{-2} s^{-1} at the height of growing pots. Radishes in the growing pots were irrigated daily with a quarter strength Hoagland's solution to a constant mass (230 g after irrigation for the whole pot) from day 6 to day 30 after sowing. Daily Hoagland's solution usage was recorded to estimate the cumulative transpiration of plants. Nine radish seedlings were grown for each treatment.

Ce uptake and accumulation in plants

On day 30 after sowing, plants were carefully removed from soil and rinsed with deionized water and then a 5 mM $CaCl_2$ solution three times to remove the adhering soil particles and Ce on the root surface. A separate study in our lab suggested that the adopted washing procedure can remove approximately 93.9 and 67.0% of Ce from the surface of storage root and fine roots, respectively. After washing, the radishes were divided into shoots, storage root, and fine roots. The separated plant tissues of three replicates were randomly chosen from each treatment and dried in an oven at 95 °C for 7 days before the dry weight measurement. The dry tissues were digested using a DigiPREP MS hot block digester (SCP science, Baie-d'Urfe, QC, Canada). Four milliliters of 70% (v/v) nitric acid (Certified ACS Plus) was mixed with the ground plant tissues, and the mixture was held at room temperature overnight to predigest the tissues. Then the mixture was digested in the hot block at 95 °C for 4 hours. After the mixture had cooled to room temperature, 2 mL of 30% (w/v) H_2O_2 was added, and the mixture

continued to be digested at 95 °C for an additional 2 hours, following the procedures reported in previous chapters. Finally, the Ce concentration in the mixture was quantified by ICP-MS.

Plant nutritional status

The storage roots of three other replicates were randomly chosen from each treatment and dried similarly as described above. The measurement of the total protein (calculated from the N percentage) and some common minerals in the dry tissues was conducted at the Soil, Water and Forage Testing Laboratory at Texas A&M University. The plant nitrogen is determined by a high-temperature combustion process. Nitrate in plant tissues was first extracted with a 1 M KCl solution and then reduced to nitrite through a cadmium column before it was quantified by an UV−*vis* spectrometer in the same FIAlab-2500 analyzer system as mentioned above. Plant minerals were determined by a SPECTROBLUE FMX26 ICP-OES instrument after digestion with 70% (v/ v) nitric acid.

Data analysis

The experimental data are presented as means ± the standard error of three or more replicates. One-way analysis of variance and Duncan's test for post hoc comparisons were performed with IBM SPSS Statistics V22.0. Statistical significance was attained when the $p<0.05$.

Results

CeO_2NPs and soil characterization

The TEM image of CeO_2NPs and the size distribution of the CeO_2NPs were shown in Figure 5.1a & b. Most nanoparticles have an irregular polygonal shape. A few nanorods were also found in the powder. The size distribution and average size were obtained by measuring 185 individual NPs with image processing software ImageJ version 1.49. Most CeO_2NPs fell in the size range of 6−24 nm (Figure 5.1b), with an average size of 10 nm. The XPS spectra of Ce on the surface of CeO_2NPs was shown in Figure 5.1c. The results indicated that around 8% of the Ce on the nanoparticle surface was in the form of Ce^{3+}, as determined by the XPS peak fitting software XPSPEAK version 4.1.

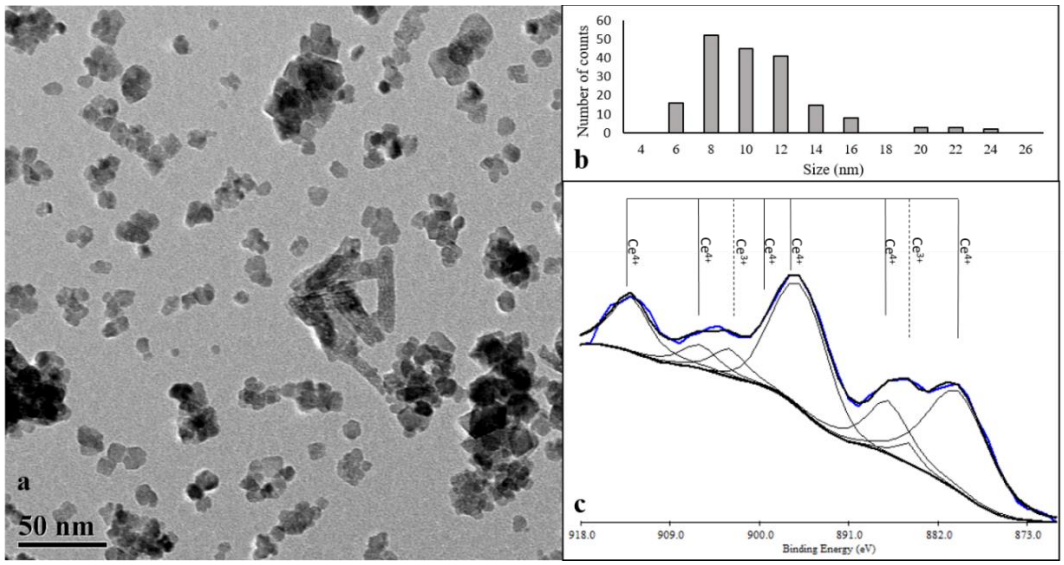

Figure 5.1. Characterization of CeO_2NPs. (a) TEM image of CeO_2NPs; (b) size distribution of CeO_2NPs; (c) XPS spectra of Ce on the surface of CeO_2NPs.

The results of the soil routine analyses conducted in the Soil, Water and Forage Testing Laboratory at Texas A&M University were listed in the Table 5.1.

Table 5.1 Properties and concentrations of common elements in the soil used in this study.

Analysis	Units	Results
pH	-	7.50
Conductivity	umho/cm	279
Nitrate-N	mg/kg	12
Phosphorus	mg/kg	16
Potassium	mg/kg	103
Calcium	mg/kg	3672
Magnesium	mg/kg	244.67
Sulfur	mg/kg	10
Sodium	mg/kg	12
Iron	mg/kg	11.93
Zinc	mg/kg	0.83
Manganese	mg/kg	9.43
Copper	mg/kg	0.52

Ce fractionation in soil

The percentages of different Ce fractions in soils are illustrated in stacked columns in Figure 5.2. F4 was the predominant fraction for all soils. F1 was considered to include both the suspended CeO_2NPs and Ce^{3+}. It was the smallest fraction and accounted for only <0.73% of all treatments because of the low solubility of CeO_2NPs and its low dissolution rate. After dosing CeO_2NPs to the soils, the percentage of F2 decreased dramatically, while the percentage of F4 significantly increased.

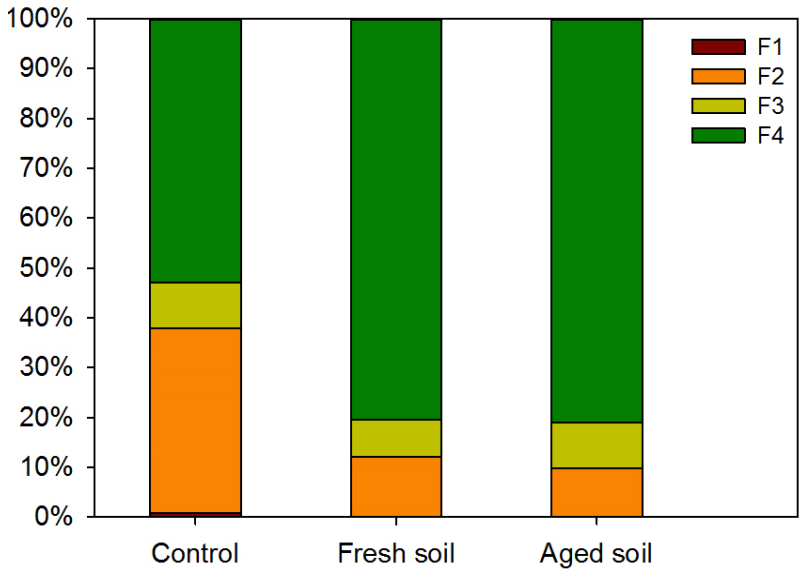

	F1 (%)	F2 (%)	F3 (%)	F4 (%)
Control	0.73±0.08	37.05±1.53	9.31±0.37	52.90±1.13
Fresh soil	0.14±0.015	11.87±1.61	7.59±0.45	80.41±1.41
Aged soil	0.10±0.016	9.66±2.29	9.23±1.17	81.01±9.78

Figure 5.2. Percentage of Ce fractionation determined by the modified BCR sequential extraction procedure. The results shown on the table beneath the figures represent the average and standard error of three replicates (n=3). The F1 fraction was too small to see in the treated soils.

The measured concentrations of individual fractions for each treatment are presented in Figure 5.3. Ce is the most abundant rare earth element in the earth's crust.[205] As expected, the control soil contained high background concentration of Ce. The summation of four Ce fractions in control soil by BCR method was 39.2 ± 1.2 mg/kg. Both the Fresh and Aged soil have Ce concentrations significantly higher than those of the control soil in F1, yet no significant difference was observed between these two treated soils. The sum of the first three fractions in the control soil, the Fresh soil

and the Aged soil was shown in Figure 5.4. No significant difference between the Fresh soil and the Aged soil was found either.

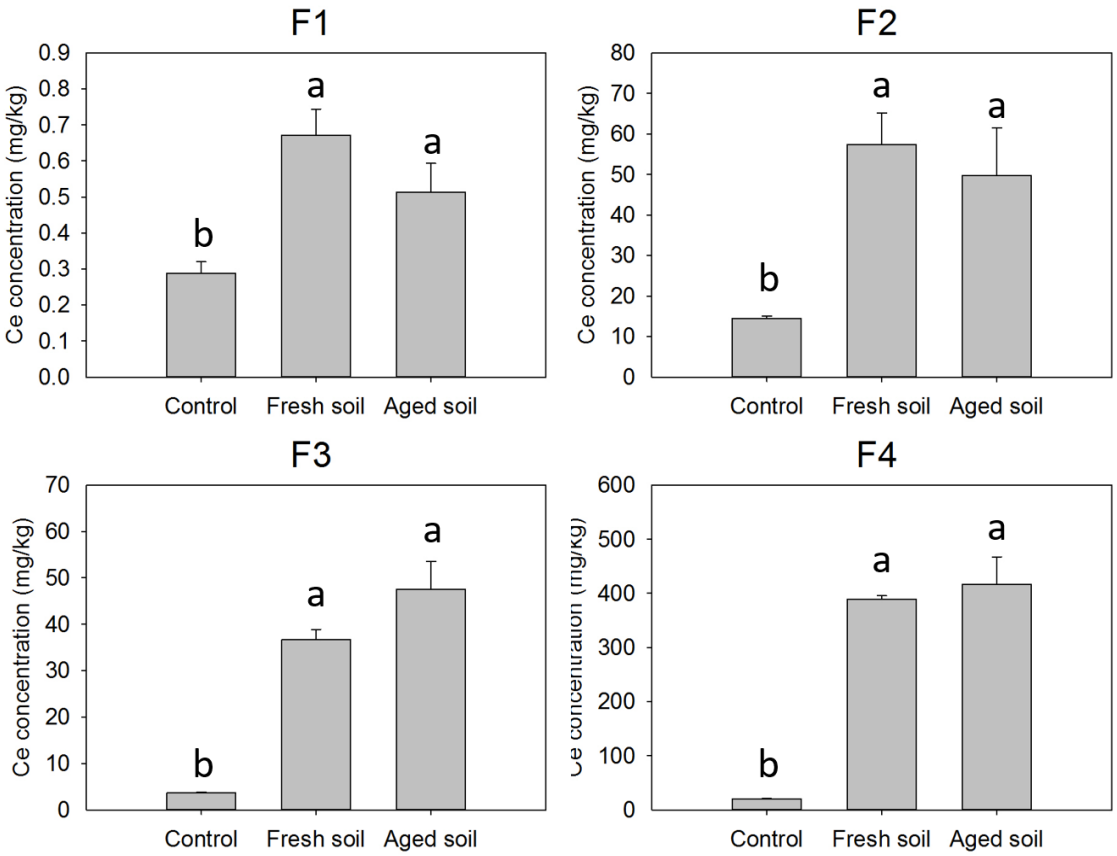

Figure 5.3. Average concentrations of Ce in different fractions of soil as determined by the BCR sequential extraction. The error bars represent the standard error (n = 3). Different letters represent significant differences among the treatments ($p < 0.05$). Samples without error bars indicate that the error bars are too small to see in the figures.

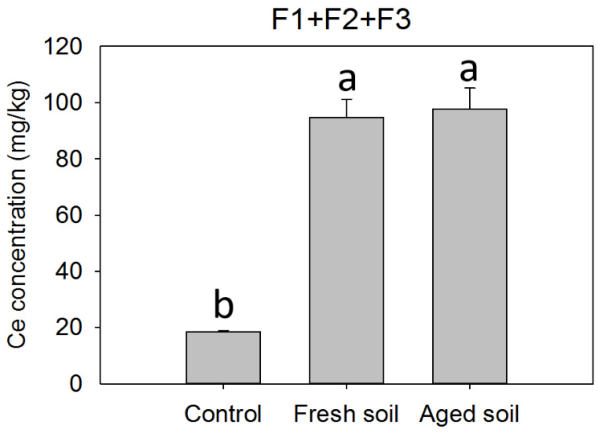

Figure 5.4. The sum of the first three fractions extracted by modified BCR method in three different soils. (n = 3). The error bars represent the standard error (n = 3). Different letters represent significant differences among the treatments ($p < 0.05$).

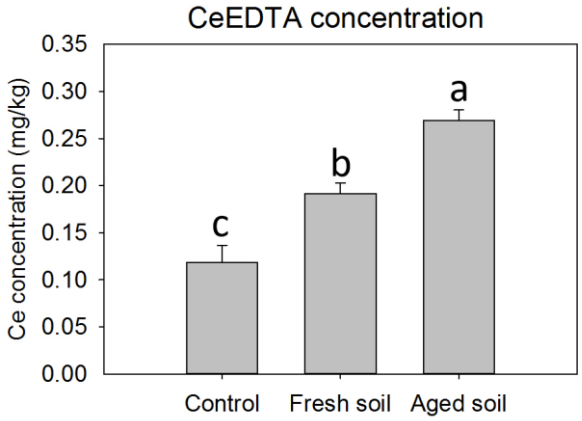

Figure 5.5. Average concentrations of CeEDTA in three different soils (n = 3). The error bars represent the standard error (n = 3). Different letters represent significant differences among the treatments ($p < 0.05$).

The results from the EDTA partial extraction are illustrated in Figure 5.5. The Aged soil had the highest Ce^{3+} concentration, followed by that of the Fresh soil. Control

soil had the lowest Ce^{3+} concentration. The differences of Ce^{3+} in the three soil were significant ($p<0.05$).

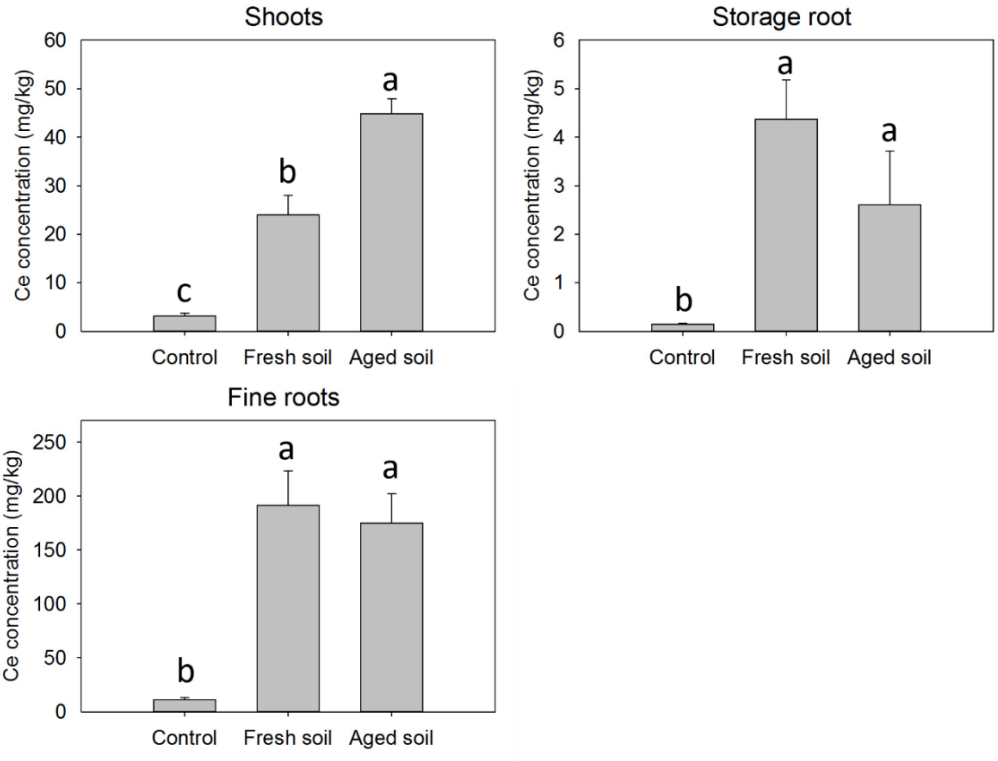

Figure 5.6. Average concentrations of Ce in different radish tissues (n = 3). The error bars represent the standard error (n = 3). Different letters represent significant differences among the treatments ($p < 0.05$).

Ce uptake and accumulation

Ce was detected in all plant tissues, including the radish tissues from controls. The concentrations of Ce in different plant tissues are presented in Figure 5.6. Exposure to both Fresh and Aged soils resulted in Ce concentrations significantly higher than

those in control plants. No significant difference in Ce concentration was found in the storage root or fine roots of plants grown in the Fresh and Aged soils. However, the radish shoots grown in Aged soil contained a Ce concentration significantly higher than that in the shoots in Fresh soil.

Plant physiological and nutritional status

The accumulative transpiration of radishes in three different soils is illustrated in Figure 5.7. Neither the freshly spiked nor the aged CeO_2NPs caused any significant differences in plant transpiration.

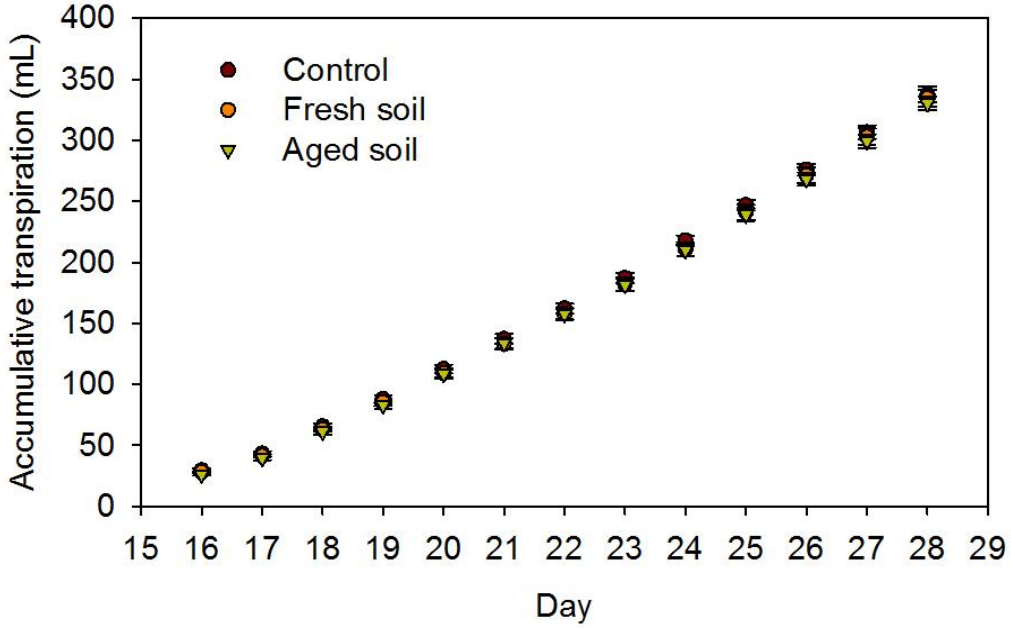

Figure 5.7. The Average accumulative transpiration of radish grown in three different soils (n=9). Error bars represent standards error. No significant difference was detected between different treatments.

The treatment with freshly spiked and aged CeO_2NPs increased the average fresh biomass of radish shoots by 5.65 and 10.41%, respectively, and the biomass of fresh storage root by 1.27 and 6.10%, respectively, compared with control plants, even though the increase was not statistically significant (Figure 5.8). Table 5.2 shows the concentrations of several major macro- and micronutrients in storage roots. There were no significant differences among three treatments. CeO_2NPs at 1000 mg/kg did not cause any significant changes in plant nutritional status.

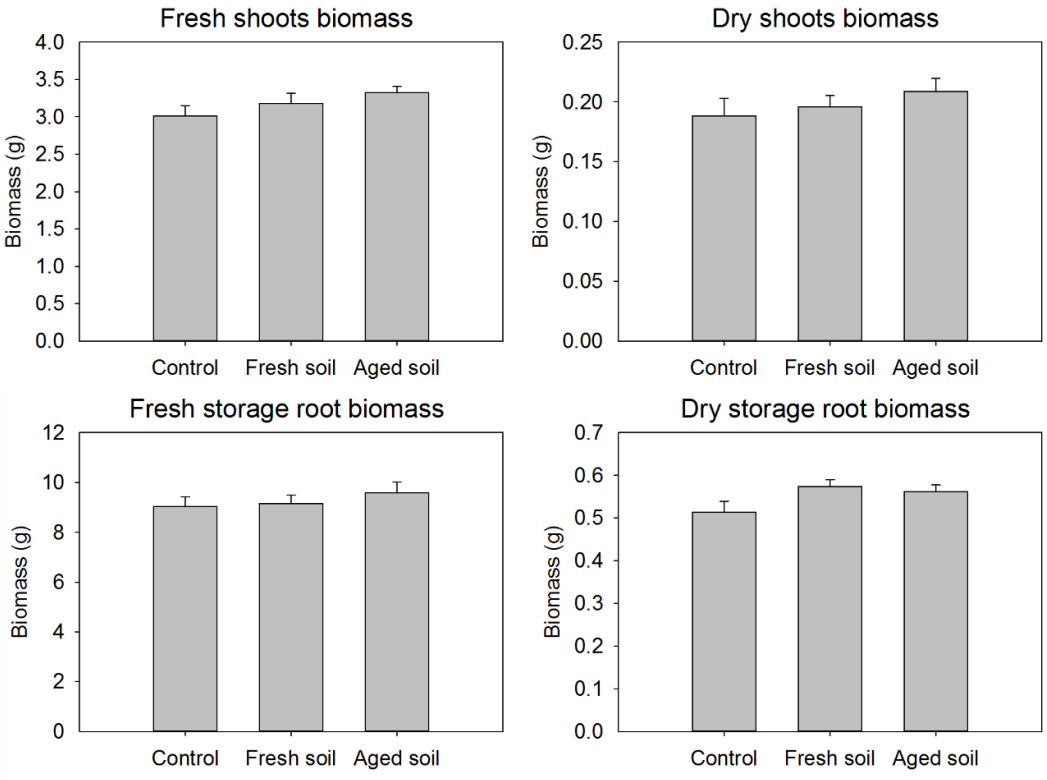

Figure 5.8. Average fresh and dry biomass of radish tissues grown in three different soils (n = 9). The error bars represent the standard error. Different letters represent significant differences among the treatments ($p < 0.05$).

Table 5.2. Protein and minerals in the storage roots of radishes grown in three different soils. The results shown on the table represent the average and standard error of three replicates.

	N (%)	Protein (%)	P (ppm)	K (ppm)	Ca (ppm)
Control	1.86±0.09	11.62±0.56	2774±140	31878±1615	3994±161
Freshly spiked	1.84±0.12	11.51±0.74	2828±189	32377±1432	4126±341
Aged	1.94±0.22	12.20±1.40	2581±139	32953±3763	4196±311

	Mg (ppm)	Na (ppm)	Zn (ppm)	Fe (ppm)	Cu (ppm)
Control	1298±145	3634±406	10.81±0.84	159±68	2.32±0.17
Freshly spiked	1350±157	3696±440	10.62±2.24	126±20	2.23±0.23
Aged	1485±108	4951±1391	10.81±2.19	127±20	2.11±0.18

	Mn (ppm)	S (ppm)	B (ppm)
Control	10.42±1.68	6233±451	13.64±0.62
Freshly spiked	10.43±1.23	6404±700	13.22±0.93
Aged	10.61±1.45	6234±633	13.32±1.69

Discussion and Conclusions

In this chapter, the effect of aging on CeO_2NPs fractionation and environmental transformation in soil was evaluated. Although F1 extracted by BCR method represented the most bioavailable fraction, it did not contain all Ce^{3+} ions in the soil. Rare earth phosphates, including Ce phosphate, have been reported as insoluble materials in soil because of their very low solubility products ($\log K_{sp}^0$ = -26.2±0.15 for $CePO_4$).[206] The phosphorus concentration in the soil used in this study was 16.33 mg/kg (Table 5.1). Inorganic phosphorus in soil was mainly in phosphate form.[207] So the Ce^{3+} dissolved in the liquid phase or on the CeO_2NPs surface (Figure 5.1c) could potentially form particulate $CePO_4$ and precipitate out of the solution. This part of Ce^{3+} in the $CePO_4$ may

not be accounted for in the determination of F1 due to the low solubility of $CePO_4$ in water or acetic acid.[204] However, this fraction of Ce^{3+} could still be available to plants due to the interactions between plant roots and $CePO_4$. It should be noted that while the sum of the first three fractions of Ce based on BCR extraction can be bioavailable to plant roots, it is the F1 fraction that are most likely to be transported to plant shoots and the total concentration of Ce^{3+} reflects the transportable Ce from roots to shoots.[208] Hence, F1 could not be a sufficiently reliable indicator of Ce bioavailability to plant shoots when studying aging effects. Therefore, the independent EDTA partial extraction was conducted to determine the total concentration of Ce^{3+} in different soils. Golden and Wang[209] reported that the Ce-acetic acid complex formation constant at 25 °C (log K_f) is 1.68, while the log K_f of Ce-EDTA complex is 16.80. So EDTA can strongly bond to all Ce^{3+}, including the Ce^{3+} in $CePO_4$ (if present) and those attached to CeO_2NPs surfaces, and form soluble Ce-EDTA complex.[204] The results from the EDTA partial extraction showed that the Aged soil had the highest Ce^{3+} concentration, followed by the Fresh soil, and then control soil (Figure 5.5). These results indicated that the dosed CeO_2NPs were able to release Ce^{3+} ions, and aging increased the release of Ce^{3+}. A possible explanation for the heightened Ce^{3+} in the Aged soil might be the oxidation state switching of Ce between +3 and +4 on CeO_2NPs surface. The oxidation state of Ce on the nanoparticle surface strongly depends on the environment and time.[203] After adsorption of a reductant or an oxidant onto the metal compound, an electron transfer may occur between the metal and adsorbate gradually.[202] For example, Schwabe et al.[53] concluded that the ferrous iron in the growth media could be adsorbed onto the CeO_2NPs surface and

reduce the surface Ce^{4+} into Ce^{3+}. Over time, the Ce^{3+} could dissolve in soil solution or be complexed with the organic matter in soil. The complex then detached and equilibrated with the soil solution. The decreasing percentage of Ce^{3+} on the nanoparticle surface might drive the reduction process producing more Ce^{3+} from Ce^{4+}. The observation in Chapter III suggests that the low molecular organic acids in the soil (if present) could enhance the release of Ce^{3+} from CeO_2NPs during aging process. Other processes such as the microbial activities in soil might also contribute to the higher Ce^{3+} concentration in the Aged soil and the detailed mechanisms for higher release of Ce^{3+} during aging needs further investigation.

Based on the BCR protocol, F2 contained the cerium bound to Fe-Mn oxides in soil. Fe-Mn oxides primarily exist in soil as secondary minerals which are normally in the clay fraction, including birnessite ($(Na_{0.3}Ca_{0.1}K_{0.1})(Mn(IV)Mn(III))_2O_4 \cdot 1.5H_2O$), ferrihydrite ($Fe_{10}O_{15} \cdot 9H_2O$), goethite (α-FeOOH), hematite (α-Fe_2O_3), lepidocrocite (γ-FeOOH), lithiophorite ($LiAl_2(OH)_6Mn(IV)_2Mn(III)O_6$), maghemite ($\gamma$-$Fe_2O_3$), magnetite ($FeFe_2O_4$), and so on.[202] According to Table 5.1, the Fe ($Fe(OH)_3$) and Mn (MnO_2 (pyrolusite)) concentrations in the soil used in this study were 11.93 mg/kg and 9.43 mg/kg respectively. So considerable amounts of Fe-Mn oxides existed in soil. The zeta potential of CeO_2NPs in water suspension at pH=7 was measured as +45.13 mV by a zetasizer (Malvern Zetasizer Nano-ZS90, NY). Due to the negative charge of Fe-Mn oxides, the positively charged uncoated CeO_2NPs and Ce cations could be adsorbed on these metal oxide surface through non-specific adsorption.[202] It was also reported that CeO_2NPs could be retained by heteroaggregation with clay colloids in soil and increase

the Ce concentration in this fraction.[178] As a result, higher F2 concentration in CeO_2NPs dosed soils than in control soil was expected. At stable pH, temperature, humidity, and organic matter content, the weathering process of these minerals would be slow (timescale in years).[202, 210] Thus the effects of seven months of aging on F2 might be very minimal and cannot be reflected by the BCR method in this study.

The relative percentage of Ce in F3 was similar in all soils and fell in the range of 7.59% to 9.31% (Figure 5.2). When the actual Ce concentration in F3 was compared across the treatments, it showed the same pattern as F1 and F2 that although Ce concentrations in Fresh and Aged soil were significantly higher than that in control soil, no significant difference existed between the F3 Ce concentrations in the two dosed soils (Figure 5.3). F3 is associated with the organic matter in soil. The batch soil system (no organic matter source) and stable environmental condition such as relatively stable pH, temperature, and humidity of soil, might keep the organic matter stable during the aging process and led to non-significant difference of F3 in the Fresh and Aged soils.

F4 was the dominant fraction of Ce in all three soils. The percentage increased significantly from 52.9% in the control soil to 80.4% and 81.0% in the Fresh and Aged soil respectively after the introduction of CeO_2NPs, yet no significant difference was observed between these two dosed soils. In summary, the BCR sequential extraction results indicated that the introduction of CeO_2NPs significantly increased the Ce concentrations in all fractions, and the majority of added CeO_2NPs stayed in the residual fraction F4, which was hardly bioavailable to plants. The insignificant differences of Ce concentrations between the Fresh and Aged soils demonstrated that aging effects on Ce

fractionation in soil could not be reflected by BCR sequential extraction method. However, based on the EDTA partial extraction results, it can be seen that the dosed CeO_2NPs were able to release Ce^{3+}, and aging led to greater release of Ce^{3+}.

In addition to the Ce fractionation in soil, the aging effects on Ce uptake by plants was examined. The previous studies reported in Chapter IV demonstrated that the Ce concentration in radish storage roots and the sum of first three fractions of CeO_2NPs in soil are linearly correlated. The similarity of the sum of the first three fractions in the Fresh and Aged soils (Figure 5.4) might be the primary reason for the comparable Ce concentration in the storage root grown in both soils. The previous investigation also showed that the Ce concentration in radish shoots only exhibited strong correlation with F1. Considering the higher Ce concentration in the shoots of radish grown in Aged soil and higher Ce^{3+} concentration in this soil, the higher concentration of Ce in radish shoots grown in Aged soil could be attributed to the higher Ce^{3+} in the Aged soil. Thus, the Ce^{3+} fraction extracted by EDTA could be a better indicator of bioavailability of CeO_2NPs to plant shoots rather than the acetic acid extracted fraction through BCR method. Gui et al.[68] reported that Ce in the roots of lettuce treated with 50 – 1000 mg/kg CeO_2NPs in potting soil presented a mixed oxidation states of Ce^{3+} and Ce^{4+}, implying the transformation of CeO_2NPs to Ce^{3+}. Schwabe et al.[76] proposed that the Ce^{3+} could be released from CeO_2NPs in plant rhizosphere and taken up by plant roots. The results in Chapter III confirmed that Ce^{3+} could be released from CeO_2NPs on the root surface because of the low molecular weight organic acid in plant exudates and the ions are readily transported to radish shoots. While it is still unclear why aging enhanced the

dissolution of CeO_2NPs, it is possible that biological activities which result in the increase of low weight organic molecules in Aged soil may contribute to this process. Regardless of the mechanisms, it is clear now that the significantly higher Ce^{3+} in the Aged soil, which was more bioavailable to plants, is deemed as a significant source of Ce in the radish shoots.

When the plant physiological status was evaluated, neither the freshly spiked nor the aged CeO_2NPs was found to cause any significant differences in plant transpiration. However, the treatment with freshly spiked and aged CeO_2NPs increased the average fresh biomass of radish shoots by 5.65% and 10.41% respectively; and the biomass of fresh storage root by 1.27% and 6.10% respectively compared with control plants, even though the increase was not statistically significant (Figure 5.8). Chapter IV shows that the dry biomass of radish shoots and storage root was unaffected by 1000 mg/kg CeO_2NPs in the same silt loam soil. However, several previous studies, including the investigation in Chapter III, have shown that low concentrations of CeO_2NPs could enhance plant growth.[68, 74, 114] Notably, the Aged soil exhibited a more beneficial effect on radish growth than Fresh soil. Based on our analysis, the Ce^{3+} concentrations was significantly higher in the Aged soil than in Fresh soil. Water soluble Ce at low concentrations is generally not phytotoxic and has been used as fertilizers for crops.[169] Therefore, the beneficial effect of CeO_2NPs on plant biomass, albeit insignificant, could be partially attributed to the higher concentrations of Ce^{+3} in these soils.

Plant nutrients can be divided into two general categories: macronutrients and micronutrients. Macronutrients such as carbohydrate, protein, and fat provide calories or

energy, while micronutrients consisting both macrominerals (*e.g.* Ca, P, Mg, K, Na, Cl, and S) and microminerals (*e.g.* Fe, Mn, Zn, Cu, Cr, Co, F, I, Mo, and Se) as well as vitamins play important roles in maintaining the physiological and biochemical functions of plants.[211] Table 5.2 showed that CeO_2NPs at 1000 mg/kg did not cause any significant changes on plant nutritional status, including the concentrations of several major macro/micro-nutrients in the storage roots. Zhao et al.[77] investigated the effects of CeO_2NPs on cucumber fruit quality and found that the CeO_2NPs at 800 mg/kg did not cause any significant changes on the concentrations of several macro- and micronutrients in cucumber. Rico et al.[74] also reported that minerals (with the exception of sulfur) in the grains of wheat were not affected by CeO_2NPs at 125 and 500 mg/kg. Although the underlying mechanisms for the interactions between CeO_2NPs and nutrient uptake are unclear, this study agrees well with previous reports that the nutrients in the edible tissues of several crops, including radish, was not significantly affected by CeO_2NPs.

In summary, the aging process of CeO_2NPs in soil did not cause any significant differences of Ce fractionation in soil as determined through the BCR sequential extraction. However, the aging process significantly enhanced the releasing of Ce^{3+} from CeO_2NPs and resulted in significantly higher Ce concentration in radish shoots. The results also indicated that the biomass of radish tissues and the nutritional status were not affected by either freshly spiked or aged CeO_2NPs.

CHAPTER VI

THE INTERACTION BETWEEN CEO2NPS AND SOIL PARTICLES

Introduction

Literature as well as the results from previous chapters have shown that CeO_2NPs can be taken up by edible plants and transferred through the food chain, posing potential risks to humans. The risks associated with the trophic transfer of CeO_2NPs in soils depend on the mobility of CeO_2NPs in soil and their bioavailability to organisms.[212]

Soil properties such as the soil texture and the content of organic matters strongly affect the fate and transport of ENMs in soil.[213-215] The soil texture, defined by the percentages of sand, silt, and clay, is a key factor governing ENMs mobility and bioavailability in soil. For example, Schlich and Hund-Rinke[215] suggested that the sand and clay content is the most important parameter affecting the mobility and bioavailability of AgNPs to microorganisms in soils. Cai et al.[213] investigated the combined effects of ionic strength and clay particles (bentonite and kaolinite) on the transport of titanium oxide nanoparticles (TiO_2NPs) in quartz sand column and found that clay particles could alter the mobility of TiO_2NPs. Therefore, it is critical to further investigate the interactions of ENMs with different components of soil particles to gain further mechanistic understanding on the mobility and bioavailability of ENMs in soil.

The literature is inconsistent with regard to the use of terminology in the investigation of the interactions between ENMs and soil particles. For example, both heteroaggregation[216] and adsorption[213, 214, 217] were used in studies with ENMs and clay

particles. In this chapter, due to the large size difference between nano-scale ENMs and micron-scale soil particles, their interaction was defined as an adsorption process of spherical ENMs onto a flat surface of sand or clay.

The adsorption of ENMs on soil particles could be affected by many factors including the surrounding pH and surface charge of the nanoparticles and soil particles.[178, 214, 218] This chapter focused on investigating the adsorption of both positively charged CeO_2NPs (CeO_2NPs(+)) and negatively charged CeO_2NPs (CeO_2NPs(-)) onto sand and clay. Ottawa sand and kaolin were used to represent the sand and clay particles in soil. Ottawa sand is almost entirely composed of naturally rounded grains of nearly pure quartz. Kaolin is one of the most common clay minerals and is mainly made of kaolinite that is composed of Al-substituted octahedral sheets and Si-substituted tetrahedral sheets in a 1:1 relationship. Due to the unique properties of ENMs compared with conventional environmental pollutants, the extended Derjaguin-Landau-Verwey-Overbeek (XDLVO) theory was employed to model the adsorption of CeO_2NPs onto soil particles and the homoaggregation of CeO_2NPs themselves, in addition to the measurement and model fitting of the adsorption isotherms. The classic DLVO method calculates the thermodynamic surface interactions between two particles or between a particle and a surface by summing van der Waals and electric double-layer potentials to determine the net interaction force. The DLVO model has been successfully used to calculate the interaction energies between ENMs and soil particles. For example, Sotirelis and Chrysikopoulos[219] constructed the DLVO potential energy profiles between graphene oxide (GO) nanoparticles and quartz sand and successfully explained the

significant impact of ionic strength on the adsorption of GO nanoparticles onto quartz sand using the DLVO model. Buettner et al.[220] also employed the DLVO theory to predict the aggregation of CeO_2NPs in NaCl and $CaCl_2$ electrolytes. However, the application of classic DLVO model for ENM soil interactions may be an oversimplification because other short range interactions (such as short range hydration forces, structure forces, and specific chemical interaction) may play important roles in the particle-surface and particle-particle interactions. In this study, the CeO_2NPs(-) were coated with Polyvinylpyrrolidone (PVP). With the adsorbed polymer layer, classic DLVO model is insufficient to accurately predict the ENMs-soil interactions.[218, 221] Therefore, the steric repulsion force defined as the sum of osmotic and elastic repulsive energies was also considered. Song et al.[222] and Stebounova et al.[223] have successfully applied the XDLVO to model the interactions between PVP-coated AgNPs and biological hydrophobic surfaces and provided the fundamental methodology for the application of XDLVO theory for PVP coated CeO_2NPs in this chapter.

The aims of this study were to (1) to determine the impact of surface properties of CeO_2NPs on their interactions with sand and kaolin and the homoaggregation of the nanoparticles; (2) to assess the feasibility of three adsorption isotherm models for data fitting on the interactions of CeO_2NPs with sand and clay; and (3) to investigate the adsorption mechanisms of CeO_2NPs onto sand and kaolin using XDLVO model.

Materials and Methods

Nanoparticles preparation and characterization

Two types of CeO_2NPs were used: CeO_2NPs(+) without coating and CeO_2NPs(-) coated with PVP. The CeO_2NPs(+) dispersion (10 wt. % in H_2O <25 nm particle size) was purchased from Sigma-Aldrich (St. Louis, MO), while CeO_2NPs(-) dispersion (20 wt. % in H_2O 30-50 nm particle size) was purchased from US Research Nanomaterials Inc. (Houston, TX). The shape and size of both CeO_2NPs were determined by a Tecnai G2 F20 Transmission Electron Microscope (TEM) (FEI, Hillsboro, OR). Six concentrations of CeO_2NPs dispersions were prepared: control (0 µg/L), 500 µg/L, 5 mg/L, 50 mg/L, 200 mg/L, and 500 mg/L. The zeta potentials of both CeO_2NPs at the concentrations mentioned above were measured by a dynamic light scattering instrument (Malvern Zetasizer Nano-ZS90, Worcestershire, UK).

Sand and kaolin characterization

The Ottawa sand obtained from U.S. silica (Ottawa, IL) and the kaolin purchased from Acros Organics (Geel, Belgium) were used to represent sand and clay in soil. The Ottawa sand was sieved through Mesh No. 35 and collected on Mesh No. 45 to obtain sand particles within the size range of 355 to 500 µm in diameter. The sieved sand was submerged in 10% (v/v) HNO_3 in a flask and placed on a shaker at 150 rpm for two hours to remove impurities on sand surface. The acid washed sand was then rinsed by DI water until the pH of rinsing water was approximately the same as the unused DI water. The clean sand was then dried at 105 °C overnight. The kaolin powder with particle

sizes of 1.0 to 1.8 μm was used as received. The density of the kaolin provided by the manufacturer was 1.8×10^3 - 2.6×10^3 kg/m^3.

The specific surface area (SSA) of the Ottawa sand was estimated based on the assumption that all sand particles were spherical with an average diameter of 427 μm. The SSA of kaolin was estimated based on the density and particle size of the kaolin particles provided by the manufacturer.

The point of zero charge (PZC) of Ottawa sand determined from streaming potential experiments using conductivity water as streaming solution (KCl solution, conductivity < 0.1 $\mu\Omega^{-1}cm^{-1}$) was below 2 [224]. The PZC of kaolin was measured by potentiometric acid-base titration using NaCl for ionic strength control. Before titration, the DI water used in titration was boiled for 10 minutes to remove all dissolved CO_2. The temperature was controlled at 25 °C during the titration process. Three solutions were prepared: a blank without kaolin, two kaolin dispersions at 100 mg/L concentration with different ionic strengths (0.1 M and 0.15 M). The titration was performed by gradually adding 0.1 M NaOH to increase pH of three solutions from 3 to 9. The surface charge density (σ_0) of kaolin was then calculated with the following equations:[225]

$$\Gamma_{H^+} - \Gamma_{OH^-} = \frac{c_{NaOH}(v_b - v_d)}{s \cdot \gamma \cdot V} \quad \text{Equation 6.1}$$

$$\sigma_0 = F(\Gamma_{H^+} - \Gamma_{OH^-}) \quad \text{Equation 6.2}$$

where Γ_{H^+}- Γ_{OH^-} represents the net uptake of H^+ ions or release of OH^- ions; c_{NaOH} is the concentration of titrant; v_b is the volume of the titrant added in the blank titration and v_d is the volume of the titrant added to the kaolin dispersion to achieve the same pH as in the blank solution; s is the specific surface area of kaolin; γ is the mass concentration of

kaolin (mass of kaolin divided by the volume of the total liquid medium *V*); and *F* is the Faraday constant. The PZC was the pH at which the σ_0 was zero.

Adsorption study

A batch experiment was carried out in 50 mL polypropylene centrifuge tubes. The temperature was controlled at 25 °C. Approximately 5 g of washed sand or 0.5 g of kaolin was added to the 50 mL polypropylene tubes. Thirty mL of CeO_2NPs dispersions at different concentrations (500 µg/L, 5 mg/L, 50 mg/L, 200 mg/L, and 500 mg/L) was then added to the tubes. All tubes were shaken at 250 rpm for 7 days on an Excella E24 incubator shaker (New Brunswick Scientific, Enfield, CT) and kept stationary for 3 days. The supernatant of each tube was carefully collected and digested by aqua regia following the ISO11466 protocol with slight modifications: 6 mL of HCl (12.0 M) and 2 mL of HNO_3 (15.8 M) was added drop-wise to 1 mL of the supernatant; the mixture was left at room temperature for 16 hours and then was transferred to a 50 mL reaction vessel connected to a reflux condenser; the reaction vessel was heated until the reflux condition was reached (condensation zone was lower than 1/3 of the height of the condenser) and was continuously heated for 2 hours. The concentration of Ce content in the digested solution was quantified by a NexION 300 inductively coupled plasma-mass spectrometry (ICP-MS) (Perkin Elmer, Waltham, MA). All adsorption samples were replicated three times.

A separate set of CeO_2NPs dispersions at the same concentrations as used in the batch experiment (500 µg/L to 500 mg/L) were prepared without any sand or kaolin and digested by aqua regia similarly. The Ce concentrations of the digested solutions

measured by ICP-MS were used to obtain a digestion efficiency calibration curve. The actual cerium concentration in the supernatant at the end of adsorption study was calibrated from the digestion efficiency curve. The amount of cerium attached to the sand or koalin at termination was defined as q_e (mg/g), and the concentration of Ce remaining in the liquid was defined as C_e (mg/L). q_e was calculated from C_e based on the mass balance of cerium in each tube.

Imaging of adsorbents

Scanning electron microcopy (SEM) photographs were used to examine the size, morphology of CeO_2NPs and surface structure of the sand or koalin after adsorption. The sand or kaolin mixed with 500 mg/L CeO_2NPs dispersion were carefully collected from the polypropylene tubes after the batch experiment and air-dried for 1 week. The air-dried particles were fixed on a double-sided adhesive tape, attached to the specimen holder, and were analyzed using a SEM equipped with an energy dispersive spectroscopy (EDS) detector (FEI Quanta FEG450 SEM, Hillsboro, OR).

XDLVO calculation

XDLVO was used to calculate the interaction energies between CeO_2NPs and sand/kaolin (sphere-plate), as well as between CeO_2NPs and CeO_2NPs (sphere-sphere) at 25 °C. The ionic strength of all CeO_2NPs dispersions were relatively low and assumed to be 0.1 mM, which adapted from previous studies.[226, 227] The sphere-plate interaction energies that equal to the sum of the four interactions (electrostatic double layer repulsion, Van de Waals attraction, osmotic repulsion, and elastic repulsion) were calculated using the following equations:[221]

$$V_{XDLVO}(h) = V_{EDL}(h) + V_{VDW}(h) + V_{OSM} + V_{ELAS} \quad \text{Equation 6.3}$$

$$V_{EDL}(h) = \pi\varepsilon_0\varepsilon r_p \left\{2\psi_p\psi_c \ln\left[\frac{1+\exp(-\kappa h)}{1-\exp(-\kappa h)}\right] + \left(\psi_p^2 + \psi_c^2\right)\ln[1-\exp(-2\kappa h)]\right\}$$

Equation 6.4

$$V_{VDW}(h) = -\frac{A_{123} r_p}{6h\left(1+\frac{14h}{\lambda}\right)} \quad \text{Equation 6.5}$$

$$V_{OSM}(h) = \begin{cases} \frac{4\pi r_p k_B T \Phi_P^2}{v_1}\left(\frac{1}{2}-\chi\right)d^2\left(\frac{h}{2d}-\frac{1}{4}-\ln\left(\frac{h}{d}\right)\right), & h < d \\ \frac{4\pi r_p k_B T \Phi_P^2}{v_1}\left(\frac{1}{2}-\chi\right)\left(d-\frac{h}{2}\right)^2, & d \le h < 2d \\ 0, & h \ge 2d \end{cases} \quad \text{Equation 6.6}$$

$$V_{ELAS}(h) = \begin{cases} \frac{2\pi r_p \Phi_P d^2 \rho_P k_B T}{M_w}\left\{\frac{h}{d}\ln\left[\frac{h}{d}\left(\frac{3-h/d}{2}\right)^2\right]\right\} - 6\ln\left(\frac{3-s/d}{2}\right) + 3\left(1+\frac{s}{d}\right), & h < d \\ 0, & h \ge d \end{cases}$$

Equation 6.7

For sphere-sphere calculations (homoaggregation), the interaction energies of electrostatic double layer and Van der Waals forces were calculated as follows:

$$V_{EDL}(h) = 2\pi\varepsilon_0\varepsilon r_p\psi_p^2\, k_B T\ln[1+\exp(-\kappa h)] \quad \text{Equation 6.8}$$

$$V_{VDW}(h) = -\frac{A_{121} r_p k_B T}{12h\left(1+\frac{14h}{\lambda}\right)} \quad \text{Equation 6.9}$$

where V_{XDLVO}, V_{EDL}, V_{VDW}, V_{OSM}, and V_{ELAS} denotes the total, electrostatic double layer repulsion, ,Van de Waals attraction, osmotic repulsion, and elastic repulsion respectively; h is the separation distance between the CeO_2NPs and the interface; ε_0 is the vacuum permittivity (8.854×10^{-12} $C^2\,N^{-1}\,m^{-2}$); ε is the dielectric constant of the water (78.5 for water at 25 °C); κ is the inverse Debye length (1/m); ψ_p and ψ_c are the surface potentials of the particles (CeO_2NPs) and the collector (sand/clay); r_p is the average radius of CeO_2NPs; λ is the characteristic wavelength, which is often assumed to

be 100 nm;[228] A_{123} and A_{121} are the Hamaker constants for the particle-water-collector (1.0×10^{-20} J for CeO_2NPs across water) and particle-water-particle (5.57×10^{-20} J for CeO_2-CeO_2)[229] respectively; d is the thickness of the polymer layer (assumed to be the stern layer thickness of 1.5 nm); Φ_P is the volume fraction of polymer (calculated to be 0.1 for PVP based on the NP size and PVP thickness and assumed to be 0 for CeO_2NPs(+)); v_1 is the volume of water molecule (2.99×10^{-29} m^3); χ is the Flory-Huggins solvency parameter (assumed to be 0.45 for PVP)[230]; M_w is the molecular weight of polymer (average 4×10^4 g/mol for PVP); ρ_P is the density of polymer (1.2 g/cm^3). The total interaction energy is dimensionless after dividing V_{XDLVO} by the product of the Boltzmann constant k_B (1.38×10^{-23} J K^{-1}) and the absolute temperature T (297 K).

Model fitting with adsorption isotherms

Three commonly used adsorption isotherm models were assessed for their feasibility to fit the adsorption data obtained in the batch study: (1) Langmuir; (2) Freundlich; (3) Dubinin-Radushkevich (D-R) model.

The Langmuir model describes the formation of a monolayer adsorbate on a perfectly flat surface of the adsorbent with no corrugation, and assumes that no further adsorption and interactions between adsorbate and adsorbent takes place.[231] This model assumes that the adsorption sites on the surface of adsorbent are homogenous. Langmuir adsorption parameters were determined by transforming the Langmuir equation into a linear form

$$\frac{1}{q_e} = \frac{1}{Q_0} + \frac{1}{Q_0 K_L C_e} \qquad \text{Equation 6.10}$$

where Q_0 is the maximum monolayer adsorption capacity (mg/g) and K_L is the Langmuir isotherm constant (L/mg).

Freundlich isotherm is a semi-empirical model that describes the adsorption on a heterogeneous surface and is mathematically expressed as Equation 6.11:[217]

$$\log q_e = \log K_f + \frac{1}{n}\log C_e \qquad \text{Equation 6.11}$$

where K_f indicates the adsorption capacity $(mg/g)(L/g)^n$ and n the adsorption affinity.

D-R isotherm describes the adsorption process onto a heterogeneous surface following a pore filling mechanism.[232] The linear expression of D-R isotherm model is illustrated as:

$$\ln q_e = \ln q_s - k_{ad}\varepsilon^2 \qquad \text{Equation 6.12}$$

$$\varepsilon = RT \ln\left[1 + \frac{1}{C_e}\right] \qquad \text{Equation 6.13}$$

$$E = \frac{1}{\sqrt{2k_{ad}}} \qquad \text{Equation 6.14}$$

where q_s is the theoretical adsorption capacity (mg/g); k_{ad} is the D-R isotherm constant related to the free energy of sorption per mole of the sorbate as it migrates to the surface of the adsorbent from infinite distance in the solution (mol^2/kJ^2); ε is the characteristic energy derived from D-R equation (kJ^2/ mol^2); E is the free energy of the adsorption (J/mol) and reflects the nature of adsorption (e.g. physical vs. chemical adsorption).

Results

Characterization of CeO_2NPs, Ottawa sand, and kaolin

The TEM images and particle size distributions of CeO_2NPs(+) and CeO_2NPs(-) are shown in Figure 6.1. Both CeO_2NPs have irregular polygonal shape. The size distributions and average sizes of both particles were obtained by measuring individual nanoparticles on the TEM images with an image processing software ImageJ 1.49. Most CeO_2NPs(+) fell in the size range of 10-20 nm, with an average size of 15.5 nm, consistent with the sizes reported by the vendor. On the other hand, the CeO_2NPs(-) had a wider size distribution and larger average size than reported by the manufacturer. , the size of CeO_2NP(-) ranged from 20-90 nm, with the average size of 62.5 nm.

The pH of CeO_2NPs dispersion at different concentrations and the zeta potential of CeO_2NPs in the corresponding dispersion are tabulated in Table 6.1. The PZC of uncoated CeO_2NPs has a theoretical value of 7 and was experimentally reported to be 6.8±0.1.[233, 234] The surface charge of CeO_2NPs(+) as represented by the zeta potential fell in the range of +41.33 to +48.23 at pH<6, indicating the high stability of the dispersion. The zeta potential of CeO_2NPs(+) decreased to +20.63 mV as pH increased to 6.1 at the lowest concentration. Because of the PVP coating, the zeta potential of CeO_2NPs(-) was strongly negative at pH near 7, ranging from -35.3 to -51.57.

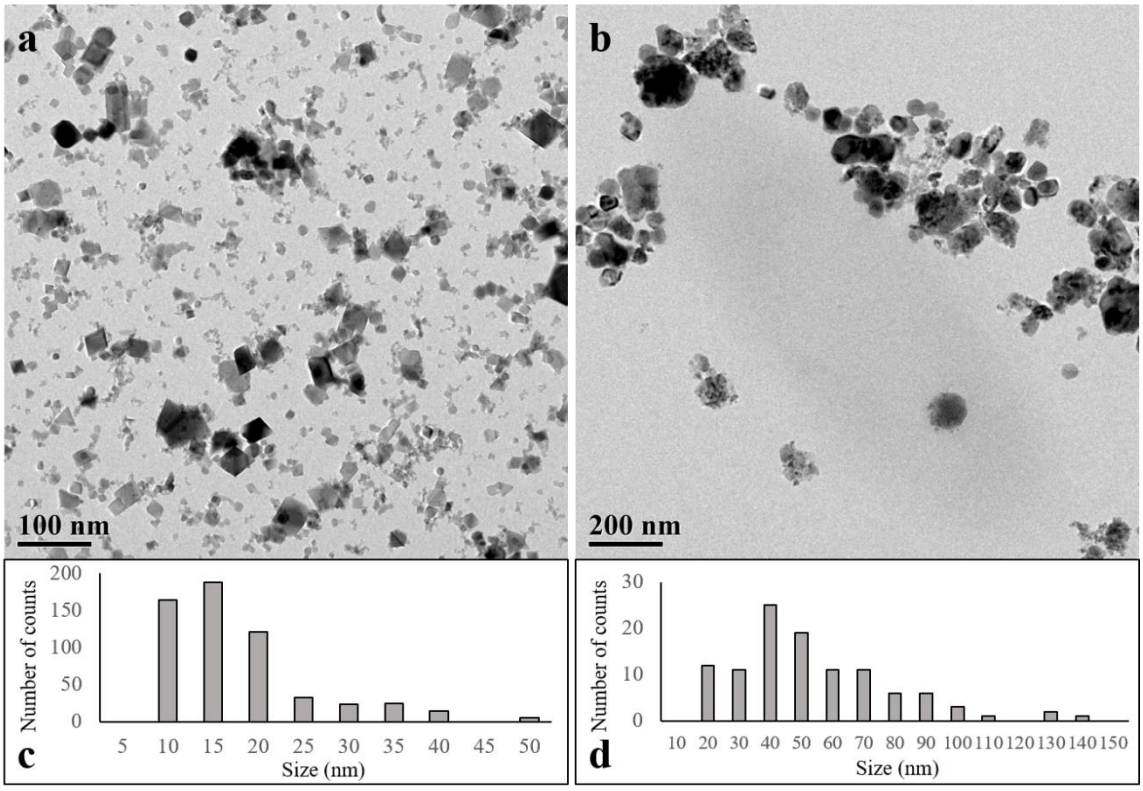

Figure 6.1. TEM images and particle size distributions of CeO_2NPs(+) (a & c) and CeO_2NPs(-) (b & d).

Table 6.1. The pH of CeO_2NPs dispersion at different concentrations and the zeta potential of CeO_2NPs in corresponding dispersion.

	pH		Zeta potential (mV)	
	CeO_2NPs(+)	CeO_2NPs(-)_	CeO_2NPs(+)	CeO_2NPs(-)
500 µg/L	6.10	7.04	+20.63	-35.3
5 mg/L	5.98	7.04	+41.33	-40
50 mg/L	5.10	7.05	+48.23	-45.43
200 mg/L	4.85	7.13	+47.3	-51.8
500 mg/L	4.63	7.2	+45.13	-51.57

The PZC of kaolin measured in this study was around 3.7-4 (Figure 6.2), in agreement with the previously reported values of 3-6.[235, 236] Therefore, both Ottawa sand and kaolin in CeO_2NPs dispersions displayed a negative surface charge in the experimental conditions. The results are summarized in Table 6.2.

Table 6.2. Surface properties of Ottawa sand and kaolinite.

Material	Specific surface area (m^2/g)	PZC	Zeta potential at pH=7 (mV)	Zeta potential at pH=4.6 (mV)
Ottawa sand	0.0053	<2[224]	-31[224]	-23[224]
Kaolinite	18	3.7-4	-34[236]	-29[236]

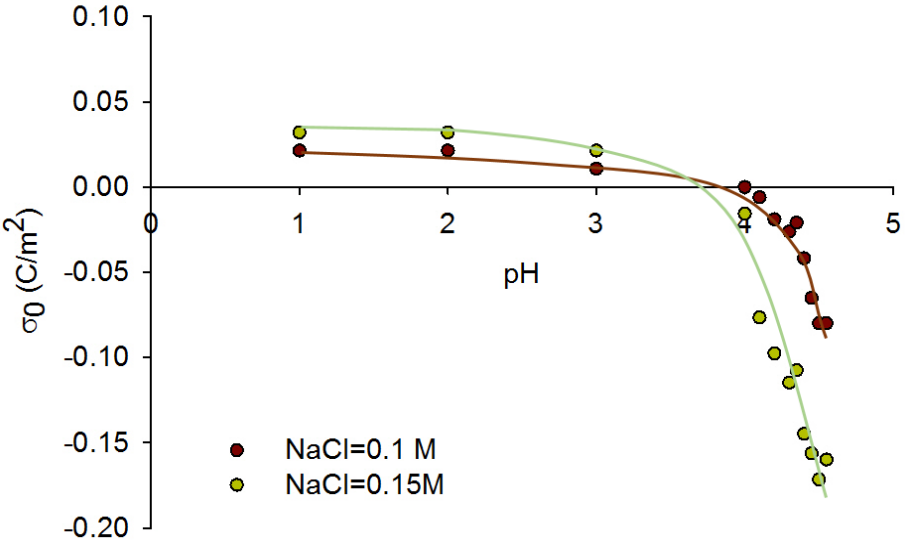

Figure 6.2. Potentiometric titration curves of kaolin. Supporting electrolyte, NaCl: (1) 0.1 M, (2) 0.15 M.

Adsorption and homoaggregation study

The adsorption isotherms for CeO_2NPs and sand/clay are shown in Figure 6.3. CeO_2NPs(+) demonstrated greatest adsorption with kaolin, followed by the CeO_2NPs(-) and kaolin. Strong electrostatic attraction between the oppositely charged nanoparticles and kaolin surface as well as the large SSA of kaolin relative to the sand were ascribed as key factors for the strong adsorption between CeO2NPs (+) and kaolin. The adsorption between CeO_2NPs and sand was significantly weaker than the adsorption between CeO_2NPs and kaolin, regardless of surface charge on CeO_2NPs. CeO_2NPs(-) showed lowest adsorption with sand.

Figure 6.4 and Figure 6.5 show the SEM images of sand and kaolin before and after the adsorption in 500 mg/L CeO_2NPs dispersion, with the corresponding EDS spectrums in selected areas. Figure 6.5 illustrates that both types of CeO_2NPs mostly concentrated on the concave and convex areas of sand after adsorption. The average size of CeO_2NPs(+) in Figure 6.4, as measured using ImageJ 1.49, increased from 15.5 nm to 52.6 nm and 47.7 nm on sand surface and kaolin surface respectively. Similarly, the average size of CeO_2NPs(-) increased from 62.5 nm to 76.7 nm and 204 nm on sand surface and kaolin surface respectively. The homoaggregated CeO_2NPs(+) were densely and evenly distributed on the kaolinite surface, while the homoaggregated of CeO_2NPs(-) were scattered on the kaolinite surface.

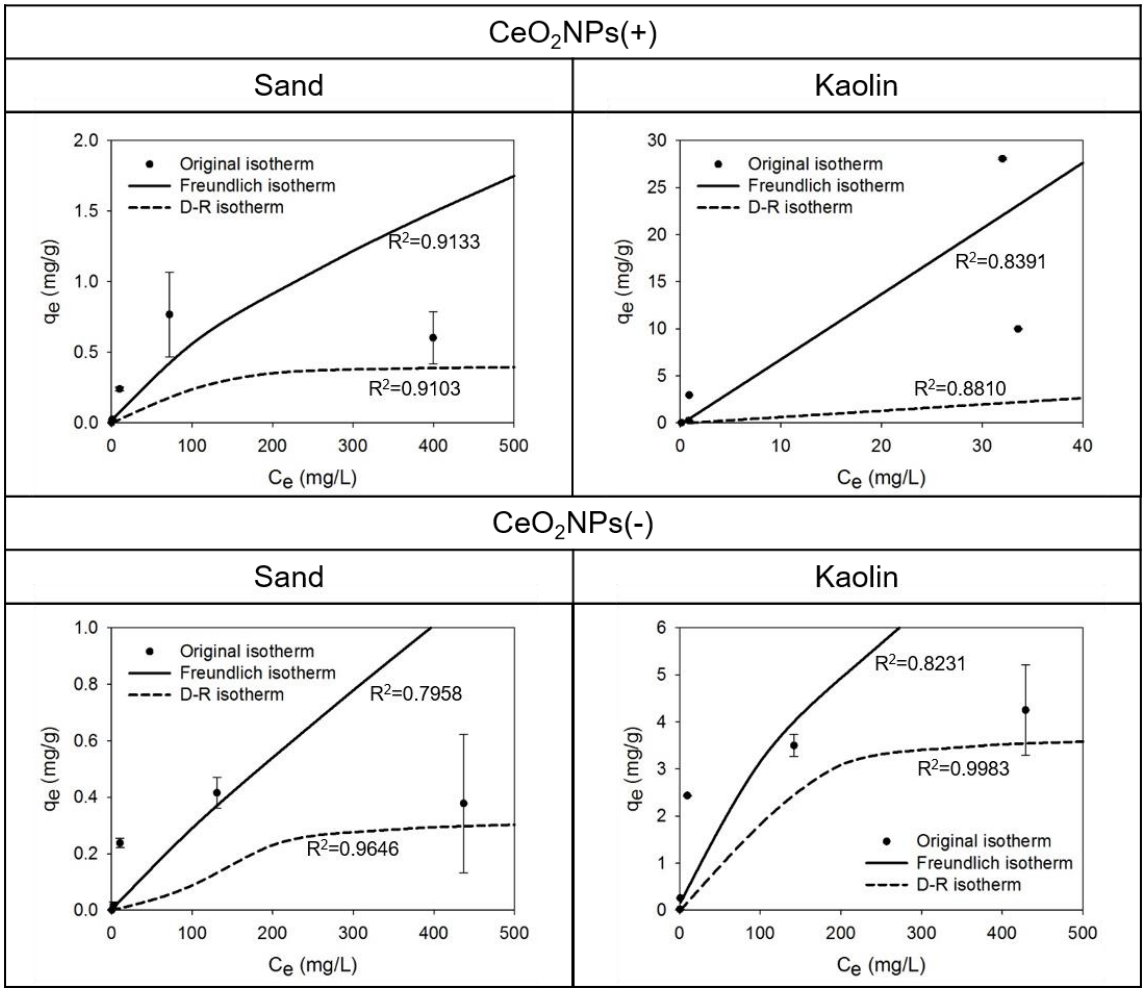

Figure 6.3. The original, Freundlich, and D-R isotherms for the adsortpion of CeO_2NPs onto sand and kaolin. q_e (mg/g) is the amount of Ce adsorbed per unit weight of adsorbent at equilibrium, and C_e (mg/L) is the equilibrium concentration of Ce remaining in the liquid. The error bars represent the standard error (n=3). Points without error bars indicate that the error bars are too small to see in the figures.

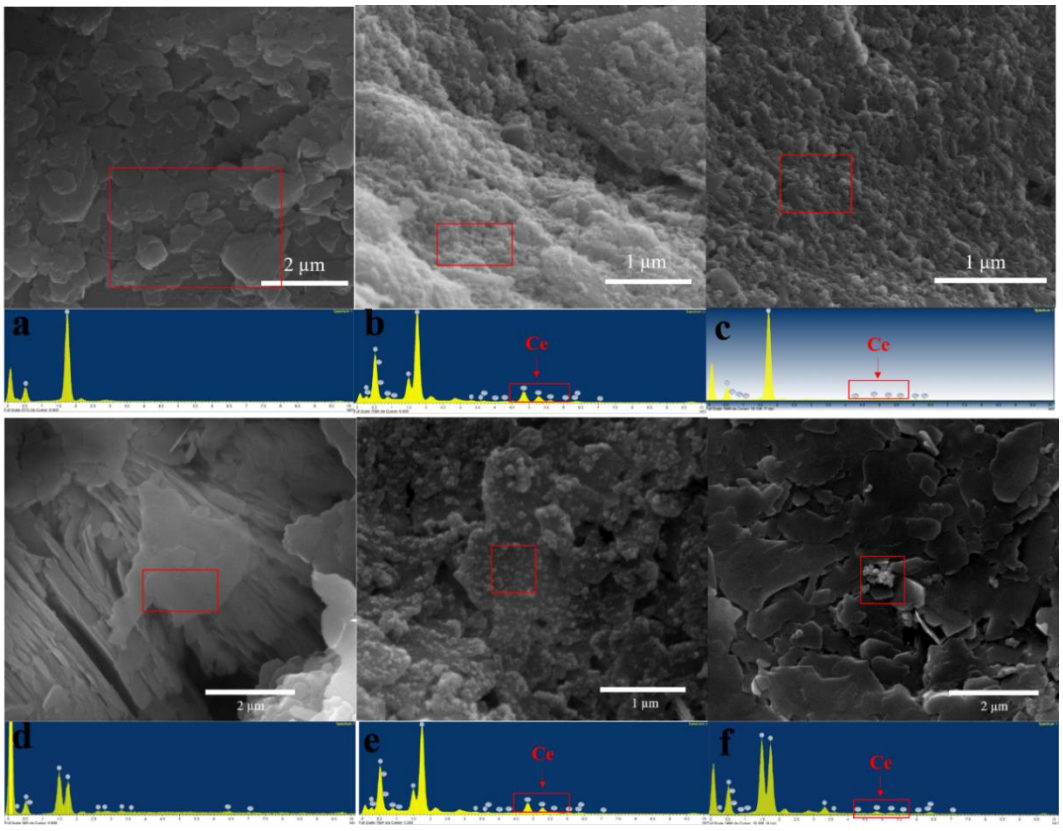

Figure 6.4. The SEM images of sand and kaolin before and after the adsorption by 500 mg/L CeO_2NPs dispersion with the corresponding EDS spectrum in selected areas: (a) sand without CeO_2NPs; (b) sand with CeO_2NPs(+); (c) sand with CeO_2NPs(-); (d) kaolin without CeO_2NPs; (e) kaolin with CeO_2NPs(+); (f) kaolin with CeO_2NPs(-).

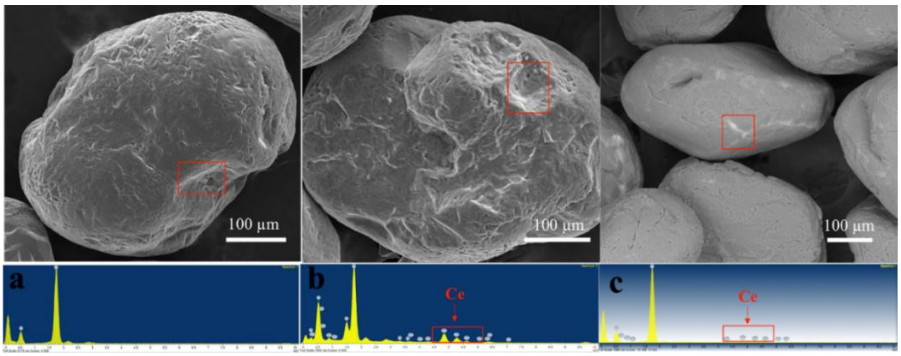

Figure 6.5. The SEM images of sand mixed with 500 mg/L CeO_2NPs dispersion with corresponding EDS spectum: (a) sand without CeO_2NPs; (b) sand with CeO_2NPs(+); (c) sand with CeO_2NPs(-).

Table 6.3. The model constants and correlation coefficients of Langmuir isotherm, Freundlich isotherm, and D-R isotherm for the adsorption of CeO_2NPs onto sand and Kaolin.

Adsorbate	CeO_2NPs(+)		CeO_2NPs(-)	
Adsorbent	Sand	Kaolin	Sand	Kaolin
Langmuir				
Q_o (mg/g)	-3.3289	-0.4487	-0.0116	-0.4146
K_L (L/mg)	-0.0071	-0.3715	-0.1041	-0.2151
R^2	0.9999	0.9824	0.9786	0.9521
Freundlich				
K_f (mg/g $(L/mg)^{1/n}$)	0.0215	0.4962	0.0046	0.1630
n	1.4128	0.9282	1.1115	1.5538
R^2	0.9133	0.8391	0.7958	0.8231
D-R				
k_{ad} (mol^2/J^2)	0.0009	0.0013	0.0022	0.0012
q_s (mg/g)	0.4018	14.0385	0.3190	3.6881
E (J/mol)	23.5702	19.6116	15.0756	20.4124
R^2	0.9103	0.8810	0.9646	0.9983

Adsorption isotherm

The adsorption parameters from model fitting are listed in Table 6.3. Langmuir isotherm led to negative adsorption capacities, indicating that the adsorption process did not follow the monolayer adsorption of Langmuir model. Freundlich isotherm fitted the adsorption data favorably but derived a low value of adsorption affinity (*n*) for the

system of CeO_2NPs(+) and kaolin. Based on R^2, D-R isotherm showed the best fit to the adsorption data. The fitting curves are shown in Figure 6.3.

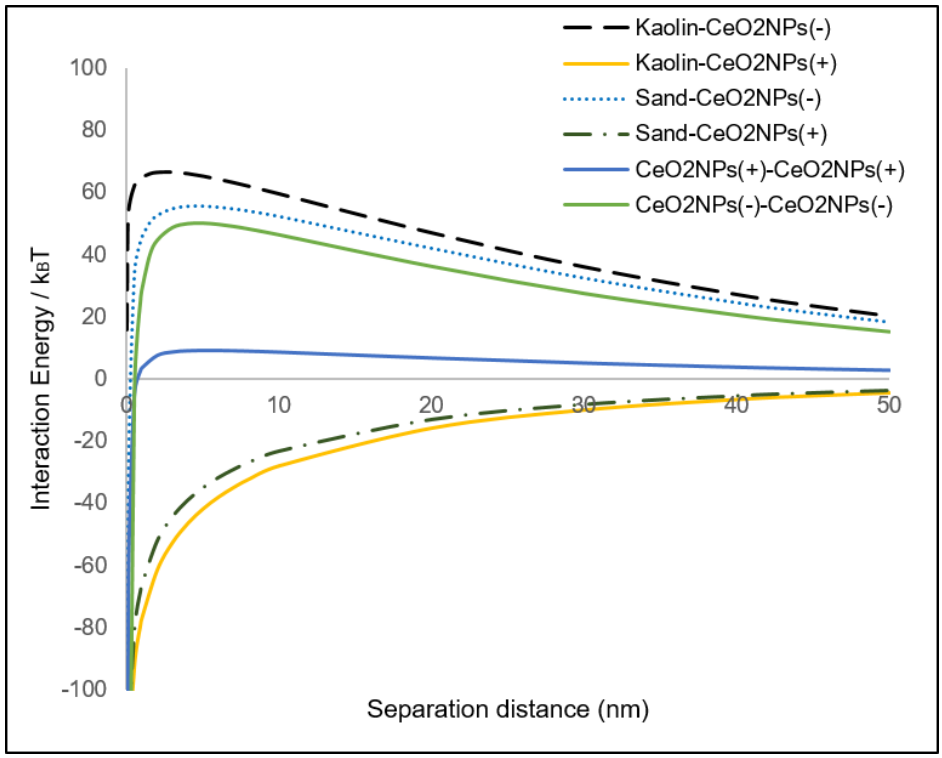

Figure 6.6. XDLVO interaction energy profiles for adsorption of CeO_2NPs onto sand and kaolin and homoaggregation of CeO_2NPs at 500 mg/L concentration as a function of the separation distance.

XDLVO modelling

The calculated XDLVO interaction energies between soil particles and CeO_2NPs and between CeO_2NPs are plotted in Figure 6.6. The primary energy barrier in kaolin-CeO_2NPs(-) system was significantly higher than that in sand-CeO_2NPs(-) system. The

interaction energy profiles for adsorption of CeO_2NPs(+) and sand/kaolin had no primary energy barrier. For homoaggregation, the primary energy barrier CeO_2NPs(-) was five times higher than that between CeO_2NPs(+).

Discussion and Conclusions

Due to the electrostatic force, the adsorption of CeO_2NPs(+) with both sand and kaolin was greater than those of CeO_2NPs(-). Not surprisingly, CeO_2NPs(+) demonstrated greatest adsorption with kaolin, while CeO_2NPs(-) had poorest adsorption with sand. Barton et al.[237] measured the nanoparticle affinity for heteroaggregation in environmental matrices and reported similar results that CeO_2NPs(+) had higher affinity to negatively charged activated sludge than CeO_2NPs(-). The differences on the adsorption of these two types of CeO_2NPs on sand and clay generally agreed with the interaction energy profiles calculated by the XDLVO along the surface charge line of CeO_2NPs (Figure 6.6a). However, the energy barrier appeared to contradict with the high adsorption of CeO_2NPs on kaolin. We attributed the phenomenon to the much larger SSA of kaolin. To gain further insights on the mechanisms, the concentration of CeO_2NPs on solid was normalized on SSA and the normalized adsorption isotherms based on adsorbent surface area are shown in Figure 6.7. The higher normalized adsorption capacity of sand for CeO_2NPs(-) compared to that of kaolin (Figure 6.7) was in line with the finding in Figure 6.6 that the energy barrier of the sand-CeO_2NPs(-) interaction was lower than that of the kaolin-CeO_2NPs(-) interaction.

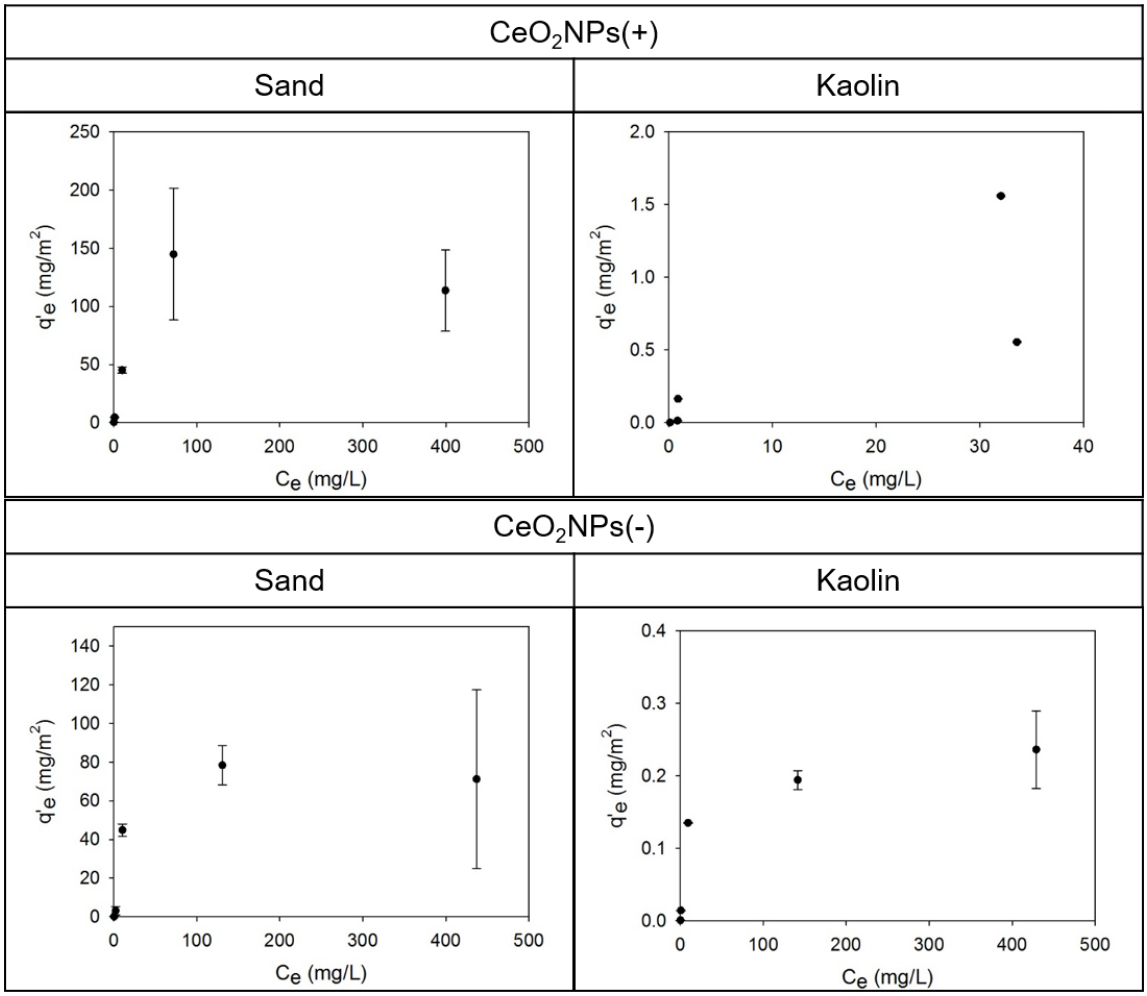

Figure 6.7. The normolized adsorption isotherms based on the adsorbent suface area. q'_e (mg/m^2) is the amount of Ce adsorbed per unit surface area of adsorbent at equilibrium, and C_e (mg/L) is the equilibrium concentration of Ce remaining in the liquid. The error bars represent the standard error (n=3). Points without error bars indicate that the error bars are too small to see in the figures.

The absence of the energy barriers for the interactions between CeO_2NPs(+) and sand/kaolin implied that CeO_2NPs(+) could be easily attracted onto sand and kaolin and agreed with the observation that most of CeO_2NPs(+) absorbed onto kaolin. Due to the

low SSA of sand and the unevenly distributed surface charge, sand adsorbed significantly fewer CeO_2NPs(+) than kaolin did, but still adsorbed around two times more of CeO_2NPs(+) than CeO_2NPs(-).

Because of the absence of the energy barriers, CeO_2NPs(+) would adsorb onto sand and kaolin without preference and the normalized adsorption capacities of kaolin and sand for CeO_2NPs(+) should be comparable. However, the normalized adsorption capacity of CeO_2NPs(+) on kaolin was only about one-hundredth of that on sand (Figure 6.7). It is likely that the aggregation of kaolin particles during adsorption process that caused the reduction of the accessible surface area of kaolin might be one reason for the hundredfold differences between SSA-normalized adsorption capacities of these two materials.

Irrespective of higher energy barriers, the net adsorption of CeO_2NPs on unit mass of kaolin was greater than onto sand. Kim et al.[238] reported similar results that zero-valent iron nanoparticles retained to a larger extent on kaolinite surfaces than reactive surfaces of sand at pH=6. The results agreed well with the earlier observation that the retention of ENMs is higher in fine-textured soils containing more clays and less sand.[239] For example, Cornelis et al.[214] reported that the retention of silver nanoparticles (AgNPs) in natural soils was strongly correlated with the soil clay content because of the adsorption of AgNPs on clay minerals. Zhou et al.[240] reached the same conclusion after studying the interactions of TiO_2NPs and AgNPs with clay (montmorillonite) that clay particles are capable of destabilizing and immobilizing ENMs in aqueous environments by electrostatic attraction. Our previous study in Chapter IV showed that the

bioavailability of CeO_2NPs to radish roots, which was strongly associated with the mobility of CeO_2NPs in soil, was lower in silt loam soil (19.6% clay) than in loamy sand soil (6.27% clay).[208] Although other factors, such as the natural organic matter and microorganisms in soil could also affect the bioavailability of CeO_2NPs, the strong adsorption of CeO_2NPs onto clay observed in this study reveals another mechanism for the reduced bioavailability of CeO_2NPs in soil. From this perspective, clay particles may be potentially used as an ENMs controlling agent by limiting the transport of ENMs in soil.[240]

During the adsorption process, the stability of the suspended ENMs could be disrupted by soil particles.[240] Wang et al.[241] demonstrated that kaolin particles could destabilize TiO_2NPs and AgNPs in aqueous environments and cause homoaggregation of ENMs. The homoaggregation is a critical process that governs the size distribution, solubility, and toxicity of ENMs. Our results also showed the increase of the CeO_2NPs size on the surface of sand and clay particles, suggesting homoaggregation of CeO_2NPs (Figure 6.4). This phenomenon can be interpreted by the XDLVO interaction energy profiles as well. The energy barriers illustrated in Figure 6.6 indicate the energy required to form homoaggregation of CeO_2NPs. The low energy barrier of CeO_2NPs(+) curve implied that the homoaggregation could be easily formed during the adsorption. The energy needed for homoaggregation of CeO_2NPs(-) was significantly higher than that of CeO_2NPs(+), but still lower than the energies required to form sand- CeO_2NPs(-) and kaolin-CeO_2NPs(-) adsorption, indicating the inevitability of homoaggregation. Based on the SEM images of the adsorbates, the size of CeO_2NPs(+) increased by 239.4% after

interacting with sand, while the size of CeO2NPs(-) only increased by 22.7% on the sand surface after homoaggregation (Figure 6.4). Although the size increases of CeO_2NPs(+) (207.7%) and CeO_2NPs(-) (226.4%) on kaolin surface were comparable, significantly more homoaggregated CeO_2NPs(+) were found on the kaolin surface than the homoaggregated CeO_2NPs(-). The above observations from SEM images were consistent with the conclusion from the comparison of two energy barriers that the homoaggregation of CeO_2NPs(+) could be more easily formed than that of CeO_2NPs(-).

The adsorption between CeO_2NPs(-) and soil particles, as well as the homoaggregation of CeO_2NPs(-) highly depend on the volume fraction of the coating polymer (PVP) when the interaction distance was less than the coating thickness. Equation 6.8 indicates that the volume fraction of PVP is a function of the maximum surface concentration of PVP on the particles. In this chapter, the volume fraction of the PVP was calculated to be 0.1, which was relatively conservative compared to previous reports.[222, 242] The steric repulsion would increase rapidly with the increase of maximum surface concentration of PVP, and makes the adsorption of CeO_2NPs(-) onto soil particles more difficult than the adsorption of CeO_2NPs(+) onto corresponding particles. Therefore, the surface conditions of ENMs was as critical as the surface charge when assessing the interactions between ENMs and soil particles.

The bioavailability and risks of CeO_2NPs to plants were demonstrated to be strongly correlated to the nanoparticle size in Chapter II and III. The homoaggregation of CeO_2NPs during the adsorption process significantly increased the particle size of CeO_2NPs and hence could reduce the bioavailability of CeO_2NPs in soil. Moreover, the

XDLVO modeling implied the significance of the CeO_2NPs surface coating on their homoaggregation process and suggested that the modification of CeO_2NPs surface chemistry could alter the level of their homoaggregation and affect the bioavailability of CeO_2NPs in soil as well.

Heavy metal contaminants are retained by soil through three main mechanisms: adsorption, surface precipitation, and chemical bonding.[202] Among these three mechanisms, adsorption is considered as the dominant mechanism for the transport processes of metal contaminants.[243] For the transport and attachment of ENMs to environmentally relevant surfaces, adsorption was also proposed as a controlling process.[244] To determine whether the adsorption is the dominant mechanism for the adsorption of ENMs on soil particles, three commonly used adsorption isotherm models were employed to fit the adsorption data. Clearly, based on the discussion above, the assumption of monolayer adsorption by the Langmuir model does not apply to the interactions of ENMs and sand or kaolin due to the homoaggregation of CeO_2NPs and the uneven energy distribution on the sand and kaolin surfaces. Huang et al.[245] reported that the surface charge distribution of sand strongly correlates with its morphology. Regions with more complex morphology, including the concave and convex parts, have greater charge density. The SEM images of sand before and after CeO_2NPs adsorption indicated that the CeO_2NPs mostly concentrated on the concave and convex parts of sand (Figure 6.5). For the kaolin, Tombacz and Szekeres[246] stated that the entire platelet of kaolinite would be negatively charged with a non-uniform charge density at pH higher than the PZC. In another word, the energy distribution on the surfaces of sand and kaolin

is uneven. Thus, the Langmuir isotherm failed to predict the adsorption of CeO_2NPs onto sand and kaolin. In Freundlich isotherm, K_f is directly proportional to the adsorption capacity. The K_f of the CeO_2NPs(+) kaolin binary system was the highest, while the K_f of the CeO_2NPs(-) sand binary system was the lowest, consistent with the experimental observation. Another parameter in the Freundlich isotherm, the calculated adsorption intensity *n*, indicates the degree of favorability of adsorption. Treybal[247] stated that larger value of *n* implies stronger interaction between adsorbent and adsorbate, while the values of *n* in the range 1-10 indicate a favorable adsorption process. The derived values of *n* shown in Table 6.3 contradicted with the experimental observation that CeO_2NPs(+) displayed greatest adsorption onto kaolin. As a result, Freundlich isotherm is not appropriate to describe the adsorption in which the electrostatic attraction dominates. The D-R isotherm distinguishes the physical and chemical adsorption of adsorbate with its free energy, *E*. The relatively low value of *E* in all adsorption processes (<1 kJ/mol) implied a physical adsorption process.[248] The calculation of *E* was also consistent with the finding from XDLVO modeling that the physical electrostatic interactions were always dominant during the approaching process of CeO_2NPs to soil particles (Figure 6.6). Labille et al.[216] investigated the heteroaggregation of TiO_2NPs with clay colloids (smectite) and came to the same conclusion that the affinity of TiO_2NPs to clay was mainly driven by electrostatic interactions. The process of CeO_2NPs(+) adsorbing to kaolin had the highest theoretical isotherm saturation capacity (q_s), which agreed well with the experimental results. The high values of R^2 for all adsorption scenarios explored

in this study indicates that D-R isotherm successfully fitted all experimental data and could potentially model the adsorption of CeO_2NPs on soil components.

In summary, the surface charge of CeO_2NPs as well as the surface coating conditions were critical when assessing the adsorption of CeO_2NPs with soil components and homoaggregation of CeO_2NPs. Soil texture was further demonstrated as a key factor to govern the mobility of ENMs in soil and the clay content in soil must be considered when assessing the bioavailability and risks of ENMs to plants. The D-R model was found to fit the adsorption well between CeO_2NPs and soil particles. This chapter provide some insights into the interactions between CeO_2NPs and basic soil particles. However, the composition and properties of natural soil are much more complicated than the simplified soil in this experiment. Future studies should take more soil components into consideration to gain further understanding on the fate and transport of CeO_2NPs in terrestrial environment.

CHAPTER VII

CONCLUSIONS AND FUTURE STUDIES

Conclusions

The potential toxicity and accumulation of engineered nanomaterials (ENMs) in agricultural crops has become an area of great concern and intense investigation. In this dissertation, the uptake and accumulation of CeO_2NPs by *Raphanus sativus* L. (radish) have been evaluated in both hydroponic and soil systems.

The results demonstrated the complexity of Ce uptake by plants. The surface charge of CeO_2NPs, the aging process of CeO_2NPs in soil, and soil properties, including the soil texture, mineral content, and organic matter content, are all important factors governing the fractionation of CeO_2NPs in soil and subsequent bioavailability to radish. The intact CeO_2NPs could be taken up by the radish fine roots, but the upward transport to the shoots was limited. The transformation of CeO_2NPs to ionic Ce (Ce^{3+}) on the radish fine root surface or rhizosphere was confirmed in this study and the low molecular organic acids exuded from fine roots were deemed as a key factor for the enhanced transformation. The aging process of CeO_2NPs in soil could also enhance the transformation of CeO_2NPs to ionic Ce and lead to higher Ce^{3+} concentration in bulk soil. The ionic Ce, which could cause potential risks to radish plants, was found to be more readily transported to and accumulated in the radish shoots and can reform particulate Ce salt within plant tissues.

Future Studies

Because of many restraints during the investigation, some questions remain and deserve more detailed investigations in future studies. From the aspect of phytotoxicity, the genomic responses of plants to ENMs exposure would worth studying to gain an in-depth understanding of the toxicity of ENMs to plants. The low molecular weight organic acids in root exudates were found to be able to enhance the dissolution of CeO_2NPs. However, whether the enhancement by organic acids is a general and critical mechanism for the metallic ENMs is still unknown. The underlying chemical mechanisms of the interactions between ENMs and organic acids are still elusive and worth clarifying in the future. Root exudates are known to differ with plant developmental stage, both in composition and in relative quantities of each compound. Thus, the uptake efficiency of metallic ENMs for plants might be significantly affected by the developmental stages and worth further investigation if it is the case that root exudates play a critical role in the uptake of ENMs. In addition, the significance of microbial community to the uptake of ENMs worth investigation. In most of the previous uptake studies, either in the hydroponic system or in the soil system, the effects of microorganisms, such as bacteria, fungi, and algae, were often overlooked. However, the unique exudate cocktails released by plants could attract a specific microorganism community and influence the rhizosphere environment, hence affect the uptake of ENMs by plants. Moreover, whether the unique attributes of ENMs, such as particle size, particle surface charge, and crystal structure of ENMs, will be able to minimize or facilitate the accumulation of ENMs in plants based on the mechanisms for ENMs to

penetrate into plant tissues needs to be further tested. From this perspective, the improvement of nano-fertilizers (in terms of the active ingredient delivery efficiency) might be a new direction of ENMs uptake study and a promising application of the nanotechnology.

REFERENCES

1. Taniguchi, N. In *On the basic concept of nanotechnology*, Proceedings International Conference on Production Engineering, Part II, Tokyo, Japan, 1974; Japan Society of Precision Engineering: 1974; pp 18-23.

2. Aithal, P., Nanotechnology Innovations & Business Opportunities: A Review. *International Journal of Management, IT and Engineering* **2016,** *6*, (1), 182-204.

3. NIOSH, Approaches to safe nanotechnology: managing the health and safety concerns associated with engineered nanomaterials. In Services, D. o. H. a. H., Ed. DHHS (NIOSH) Publication: Cincinnati, Ohio, 2009.

4. De Volder, M. F.; Tawfick, S. H.; Baughman, R. H.; Hart, A. J., Carbon nanotubes: present and future commercial applications. *Science* **2013,** *339*, (6119), 535-539.

5. Magrez, A.; Kasas, S.; Salicio, V.; Pasquier, N.; Seo, J. W.; Celio, M.; Catsicas, S.; Schwaller, B.; Forró, L., Cellular toxicity of carbon-based nanomaterials. *Nano Letters* **2006,** *6*, (6), 1121-1125.

6. Hussain, F.; Hojjati, M.; Okamoto, M.; Gorga, R. E., Review article: polymer-matrix nanocomposites, processing, manufacturing, and application: an overview. *Journal of Composite Materials* **2006,** *40*, (17), 1511-1575.

7. Mody, V. V.; Siwale, R.; Singh, A.; Mody, H. R., Introduction to metallic nanoparticles. *Journal of Pharmacy And Bioallied Sciences* **2010,** *2*, (4), 282-289.

8. Mody, V. V.; Nounou, M. I.; Bikram, M., Novel nanomedicine-based MRI contrast agents for gynecological malignancies. *Advanced Drug Delivery Reviews* **2009,** *61*, (10), 795-807.

9. Ajayan, P. M.; Zhou, O. Z., Applications of carbon nanotubes. In *Carbon nanotubes*, Springer: 2001; pp 391-425.

10. Nishijima, H.; Kamo, S.; Akita, S.; Nakayama, Y.; Hohmura, K. I.; Yoshimura, S. H.; Takeyasu, K., Carbon-nanotube tips for scanning probe microscopy: Preparation by a controlled process and observation of deoxyribonucleic acid. *Applied Physics Letters* **1999,** *74*, (26), 4061-4063.

11. Zanello, L. P.; Zhao, B.; Hu, H.; Haddon, R. C., Bone cell proliferation on carbon nanotubes. *Nano Letters* **2006,** *6*, (3), 562-567.

12. Allen, N. S.; Edge, M.; Sandoval, G.; Verran, J.; Stratton, J.; Maltby, J., Photocatalytic coatings for environmental applications. *Photochemistry and Photobiology* **2005,** *81*, (2), 279-290.

13. Puddu, V.; Choi, H.; Dionysiou, D. D.; Puma, G. L., TiO 2 photocatalyst for indoor air remediation: influence of crystallinity, crystal phase, and UV radiation intensity on trichloroethylene degradation. *Applied Catalysis B: Environmental* **2010,** *94*, (3), 211-218.

14. Balasubramanian, G.; Dionysiou, D. D.; Suidan, M. T.; Baudin, I.; Laîné, J.-M., Evaluating the activities of immobilized TiO 2 powder films for the photocatalytic degradation of organic contaminants in water. *Applied Catalysis B: Environmental* **2004,** *47*, (2), 73-84.

15. Weir, A.; Westerhoff, P.; Fabricius, L.; Hristovski, K.; Von Goetz, N., Titanium dioxide nanoparticles in food and personal care products. *Environmental Science & Technology* **2012,** *46*, (4), 2242-2250.

16. Popov, A. P.; Kirillin, M. Y.; Priezzhev, A. V.; Lademann, J.; Hast, J.; Myllyla, R. In *Optical sensing of titanium dioxide nanoparticles within horny layer of human skin and their protecting effect against solar UV radiation*, Biomedical Optics 2005, 2005; International Society for Optics and Photonics: 2005; pp 113-122.

17. Cassee, F. R.; van Balen, E. C.; Singh, C.; Green, D.; Muijser, H.; Weinstein, J.; Dreher, K., Exposure, health and ecological effects review of engineered nanoscale cerium and cerium oxide associated with its use as a fuel additive. *Critical Reviews in Toxicology* **2011,** *41*, (3), 213-229.

18. Dahle, J. T.; Arai, Y., Environmental geochemistry of cerium: Applications and toxicology of cerium oxide nanoparticles. *International Journal of Environmental Research and Public Health* **2015,** *12*, (2), 1253-1278.

19. Celardo, I.; Pedersen, J. Z.; Traversa, E.; Ghibelli, L., Pharmacological potential of cerium oxide nanoparticles. *Nanoscale* **2011,** *3*, (4), 1411-1420.

20. Das, S.; Dowding, J. M.; Klump, K. E.; McGinnis, J. F.; Self, W.; Seal, S., Cerium oxide nanoparticles: applications and prospects in nanomedicine. *Nanomedicine* **2013,** *8*, (9), 1483-1508.

21. Hirst, S. M.; Karakoti, A. S.; Tyler, R. D.; Sriranganathan, N.; Seal, S.; Reilly, C. M., Anti‐inflammatory Properties of Cerium Oxide Nanoparticles. *Small* **2009,** *5*, (24), 2848-2856.

22. Boisselier, E.; Astruc, D., Gold nanoparticles in nanomedicine: preparations, imaging, diagnostics, therapies and toxicity. *Chemical Society Reviews* **2009,** *38*, (6), 1759-1782.

23. Zeng, S.; Yong, K.-T.; Roy, I.; Dinh, X.-Q.; Yu, X.; Luan, F., A review on functionalized gold nanoparticles for biosensing applications. *Plasmonics* **2011,** *6*, (3), 491-506.

24. Baruah, S.; Dutta, J., Nanotechnology applications in pollution sensing and degradation in agriculture: a review. *Environmental Chemistry Letters* **2009,** *7*, (3), 191-204.

25. Sondi, I.; Salopek-Sondi, B., Silver nanoparticles as antimicrobial agent: a case study on E. coli as a model for Gram-negative bacteria. *Journal of Colloid and Interface Science* **2004,** *275*, (1), 177-182.

26. Bergeson, L. L., Nanosilver: US EPA's pesticide office considers how best to proceed. *Environmental Quality Management* **2010,** *19*, (3), 79-85.

27. Becheri, A.; Dürr, M.; Nostro, P. L.; Baglioni, P., Synthesis and characterization of zinc oxide nanoparticles: application to textiles as UV-absorbers. *Journal of Nanoparticle Research* **2008,** *10*, (4), 679-689.

28. Sabir, S.; Arshad, M.; Chaudhari, S. K., Zinc oxide nanoparticles for revolutionizing agriculture: synthesis and applications. *The Scientific World Journal* **2014,** *2014*, 1-8.

29. Cheng, H.-M.; Chiu, W.-H.; Lee, C.-H.; Tsai, S.-Y.; Hsieh, W.-F., Formation of branched ZnO nanowires from solvothermal method and dye-sensitized solar cells applications. *The Journal of Physical Chemistry C* **2008,** *112*, (42), 16359-16364.

30. Prasad, T.; Sudhakar, P.; Sreenivasulu, Y.; Latha, P.; Munaswamy, V.; Reddy, K. R.; Sreeprasad, T.; Sajanlal, P.; Pradeep, T., Effect of nanoscale zinc oxide particles on the germination, growth and yield of peanut. *Journal of Plant Nutrition* **2012,** *35*, (6), 905-927.

31. Ren, G.; Hu, D.; Cheng, E. W.; Vargas-Reus, M. A.; Reip, P.; Allaker, R. P., Characterisation of copper oxide nanoparticles for antimicrobial applications. *International Journal of Antimicrobial Agents* **2009,** *33*, (6), 587-590.

32. Rui, M.; Ma, C.; Hao, Y.; Guo, J.; Rui, Y.; Tang, X.; Zhao, Q.; Fan, X.; Zhang, Z.; Hou, T., Iron Oxide Nanoparticles as a Potential Iron Fertilizer for Peanut (Arachis hypogaea). *Frontiers in Plant Science* **2016,** *7*, 1-10.

33. Pankhurst, Q. A.; Connolly, J.; Jones, S. K.; Dobson, J., Applications of magnetic nanoparticles in biomedicine. *Journal of Physics D: Applied Physics* **2003,** *36*, (13), R167.

34. Piccinno, F.; Gottschalk, F.; Seeger, S.; Nowack, B., Industrial production quantities and uses of ten engineered nanomaterials in Europe and the world. *Journal of Nanoparticle Research* **2012,** *14*, (9), 1-11.

35. Zheng, X.; Chen, Y.; Wu, R., Long-term effects of titanium dioxide nanoparticles on nitrogen and phosphorus removal from wastewater and bacterial

community shift in activated sludge. *Environmental Science & Technology* **2011,** *45*, (17), 7284-7290.

36. Bystrzejewska-Piotrowska, G.; Golimowski, J.; Urban, P. L., Nanoparticles: their potential toxicity, waste and environmental management. *Waste Management* **2009,** *29*, (9), 2587-2595.

37. Ward, N. I., Multielement contamination of British motorway environments. *Science of the Total Environment* **1990,** *93*, 393-401.

38. Kaegi, R.; Ulrich, A.; Sinnet, B.; Vonbank, R.; Wichser, A.; Zuleeg, S.; Simmler, H.; Brunner, S.; Vonmont, H.; Burkhardt, M., Synthetic TiO 2 nanoparticle emission from exterior facades into the aquatic environment. *Environmental Pollution* **2008,** *156*, (2), 233-239.

39. Benn, T. M.; Westerhoff, P., Nanoparticle silver released into water from commercially available sock fabrics. *Environmental Science & Technology* **2008,** *42*, (11), 4133-4139.

40. Geranio, L.; Heuberger, M.; Nowack, B., The behavior of silver nanotextiles during washing. *Environmental Science & Technology* **2009,** *43*, (21), 8113-8118.

41. Yokel, R. A.; MacPhail, R. C., Engineered nanomaterials: exposures, hazards, and risk prevention. *Journal of Occupational Medicine and Toxicology* **2011,** *6*, (7), 6673-6676.

42. Auffan, M.; Rose, J.; Wiesner, M. R.; Bottero, J.-Y., Chemical stability of metallic nanoparticles: a parameter controlling their potential cellular toxicity in vitro. *Environmental Pollution* **2009,** *157*, (4), 1127-1133.

43. Navarro, E.; Baun, A.; Behra, R.; Hartmann, N. B.; Filser, J.; Miao, A.-J.; Quigg, A.; Santschi, P. H.; Sigg, L., Environmental behavior and ecotoxicity of engineered nanoparticles to algae, plants, and fungi. *Ecotoxicology* **2008,** *17*, (5), 372-386.

44. Kosynkin, V.; Arzgatkina, A.; Ivanov, E.; Chtoutsa, M.; Grabko, A.; Kardapolov, A.; Sysina, N., The study of process production of polishing powder based on cerium dioxide. *Journal of Alloys and Compounds* **2000,** *303*, 421-425.

45. Melard, P.; Peltier, M.; Tastu, F. Cerium based glass polishing compositions. US4601755 A, 1986.

46. Yoshida, M.; Ashizawa, T.; Terazaki, H.; Kurata, Y.; Matsuzawa, J.; Tanno, K.; Ootuki, Y. Cerium oxide abrasive and method of polishing substrates. US6221118 B1, 2001.

47. Feng, X.; Sayle, D. C.; Wang, Z. L.; Paras, M. S.; Santora, B.; Sutorik, A. C.; Sayle, T. X.; Yang, Y.; Ding, Y.; Wang, X., Converting ceria polyhedral nanoparticles into single-crystal nanospheres. *Science* **2006,** *312*, (5779), 1504-1508.

48. Goharshadi, E. K.; Samiee, S.; Nancarrow, P., Fabrication of cerium oxide nanoparticles: characterization and optical properties. *Journal of Colloid and Interface Science* **2011,** *356*, (2), 473-480.

49. Dutta, P.; Pal, S.; Seehra, M.; Shi, Y.; Eyring, E.; Ernst, R., Concentration of Ce3+ and oxygen vacancies in cerium oxide nanoparticles. *Chemistry of Materials* **2006,** *18*, (21), 5144-5146.

50. Wang, Y.; Duncan, K.; Wachsman, E.; Ebrahimi, F., Effects of oxygen vacancy concentration on mechanical properties of cerium oxide. *ECS Transactions* **2006,** *1*, (7), 23-31.

51. Perullini, M.; Bilmes, S. A. A.; Jobbágy, M., Cerium oxide nanoparticles: structure, applications, reactivity, and eco-toxicology. In *Nanomaterials: A Danger or a Promise?*, Springer: 2013; pp 307-333.

52. Deshpande, S.; Patil, S.; Kuchibhatla, S. V.; Seal, S., Size dependency variation in lattice parameter and valency states in nanocrystalline cerium oxide. *Applied Physics Letters* **2005,** *87*, (13), 133113-133113.

53. Schwabe, F.; Schulin, R.; Rupper, P.; Rotzetter, A.; Stark, W.; Nowack, B., Dissolution and transformation of cerium oxide nanoparticles in plant growth media. *Journal of Nanoparticle Research* **2014,** *16*, (10), 1-11.

54. Park, B.; Martin, P.; Harris, C.; Guest, R.; Whittingham, A.; Jenkinson, P.; Handley, J., Initial in vitro screening approach to investigate the potential health and environmental hazards of Envirox™–a nanoparticulate cerium oxide diesel fuel additive. *Particle and Fibre Toxicology* **2007,** *4*, (1), 12.

55. Sajith, V.; Sobhan, C.; Peterson, G., Experimental investigations on the effects of cerium oxide nanoparticle fuel additives on biodiesel. *Advances in Mechanical Engineering* **2010,** *2010*, 1-6.

56. Colon, J.; Hsieh, N.; Ferguson, A.; Kupelian, P.; Seal, S.; Jenkins, D. W.; Baker, C. H., Cerium oxide nanoparticles protect gastrointestinal epithelium from radiation-induced damage by reduction of reactive oxygen species and upregulation of superoxide

dismutase 2. *Nanomedicine: Nanotechnology, Biology and Medicine* **2010,** *6*, (5), 698-705.

57. Das, M.; Patil, S.; Bhargava, N.; Kang, J.-F.; Riedel, L. M.; Seal, S.; Hickman, J. J., Auto-catalytic ceria nanoparticles offer neuroprotection to adult rat spinal cord neurons. *Biomaterials* **2007,** *28*, (10), 1918-1925.

58. Reed, K.; Cormack, A.; Kulkarni, A.; Mayton, M.; Sayle, D.; Klaessig, F.; Stadler, B., Exploring the properties and applications of nanoceria: is there still plenty of room at the bottom? *Environmental Science: Nano* **2014,** *1*, (5), 390-405.

59. Ivanov, V. K.; Shcherbakov, A.; Usatenko, A., Structure-sensitive properties and biomedical applications of nanodispersed cerium dioxide. *Russian Chemical Reviews* **2009,** *78*, (9), 855.

60. Korsvik, C.; Patil, S.; Seal, S.; Self, W. T., Superoxide dismutase mimetic properties exhibited by vacancy engineered ceria nanoparticles. *Chemical Communications* **2007**, (10), 1056-1058.

61. Pirmohamed, T.; Dowding, J. M.; Singh, S.; Wasserman, B.; Heckert, E.; Karakoti, A. S.; King, J. E.; Seal, S.; Self, W. T., Nanoceria exhibit redox state-dependent catalase mimetic activity. *Chemical Communications* **2010,** *46*, (16), 2736-2738.

62. Nelson, B. C.; Johnson, M. E.; Walker, M. L.; Riley, K. R.; Sims, C. M., Antioxidant cerium oxide nanoparticles in biology and medicine. *Antioxidants* **2016,** *5*, (2), 15.

63. Leppänen, M.; Lyyränen, J.; Järvelä, M.; Auvinen, A.; Jokiniemi, J.; Pimenoff, J.; Tuomi, T., Exposure to CeO2 nanoparticles during flame spray process. *Nanotoxicology* **2012,** *6*, (6), 643-651.

64. Pietroiusti, A.; Magrini, A., Engineered nanoparticles at the workplace: current knowledge about workers' risk. *Occupational Medicine* **2014,** *64*, (5), 319-330.

65. Oberdörster, G.; Maynard, A.; Donaldson, K.; Castranova, V.; Fitzpatrick, J.; Ausman, K.; Carter, J.; Karn, B.; Kreyling, W.; Lai, D., Principles for characterizing the potential human health effects from exposure to nanomaterials: elements of a screening strategy. *Particle and Fibre Toxicology* **2005,** *2*, (1), 8.

66. Dudka, S.; Miller, W., Accumulation of potentially toxic elements in plants and their transfer to human food chain. *Journal of Environmental Science & Health Part B* **1999,** *34*, (4), 681-708.

67. Corredor, E.; Testillano, P. S.; Coronado, M.-J.; González-Melendi, P.; Fernández-Pacheco, R.; Marquina, C.; Ibarra, M. R.; de la Fuente, J. M.; Rubiales, D.; Pérez-de-Luque, A., Nanoparticle penetration and transport in living pumpkin plants: in situ subcellular identification. *BMC Plant Biology* **2009,** *9*, (1), 45.

68. Gui, X.; Zhang, Z.; Liu, S.; Ma, Y.; Zhang, P.; He, X.; Li, Y.; Zhang, J.; Li, H.; Rui, Y., Fate and phytotoxicity of CeO 2 nanoparticles on lettuce cultured in the potting soil environment. *PloS One* **2015,** *10*, (8), e0134261.

69. Hu, X.; Ding, Z.; Chen, Y.; Wang, X.; Dai, L., Bioaccumulation of lanthanum and cerium and their effects on the growth of wheat (*Triticum aestivum* L.) seedlings. *Chemosphere* **2002,** *48*, (6), 621-629.

70. López-Moreno, M. L.; de la Rosa, G.; Hernández-Viezcas, J. Á.; Castillo-Michel, H.; Botez, C. E.; Peralta-Videa, J. R.; Gardea-Torresdey, J. L., Evidence of the differential biotransformation and genotoxicity of ZnO and CeO2 nanoparticles on soybean (*Glycine max*) plants. *Environmental Science & Technology* **2010,** *44*, (19), 7315-7320.

71. Ma, Y.; Zhang, P.; Zhang, Z.; He, X.; Zhang, J.; Ding, Y.; Zhang, J.; Zheng, L.; Guo, Z.; Zhang, L., Where Does the Transformation of Precipitated Ceria Nanoparticles in Hydroponic Plants Take Place? *Environmental Science & Technology* **2015,** *49*, (17), 10667-10674.

72. Majumdar, S.; Almeida, I. C.; Arigi, E. A.; Choi, H.; VerBerkmoes, N. C.; Trujillo-Reyes, J.; Flores-Margez, J. P.; White, J. C.; Peralta-Videa, J. R.; Gardea-Torresdey, J. L., Environmental effects of nanoceria on seed production of common bean (*Phaseolus vulgaris*): a proteomic analysis. *Environmental Science & Technology* **2015,** *49*, (22), 13283–13293.

73. Rico, C. M.; Hong, J.; Morales, M. I.; Zhao, L.; Barrios, A. C.; Zhang, J.-Y.; Peralta-Videa, J. R.; Gardea-Torresdey, J. L., Effect of cerium oxide nanoparticles on rice: a study involving the antioxidant defense system and in vivo fluorescence imaging. *Environmental Science & Technology* **2013,** *47*, (11), 5635-5642.

74. Rico, C. M.; Lee, S. C.; Rubenecia, R.; Mukherjee, A.; Hong, J.; Peralta-Videa, J. R.; Gardea-Torresdey, J. L., Cerium oxide nanoparticles impact yield and modify nutritional parameters in wheat (Triticum aestivum L.). *Journal of Agricultural and Food Chemistry* **2014,** *62*, (40), 9669-9675.

75. Rui, Y.; Zhang, P.; Zhang, Y.; Ma, Y.; He, X.; Gui, X.; Li, Y.; Zhang, J.; Zheng, L.; Chu, S., Transformation of ceria nanoparticles in cucumber plants is influenced by phosphate. *Environmental Pollution* **2015,** *198*, 8-14.

76. Schwabe, F.; Tanner, S.; Schulin, R.; Rotzetter, A.; Stark, W.; von Quadt, A.; Nowack, B., Dissolved cerium contributes to uptake of Ce in the presence of differently sized CeO 2-nanoparticles by three crop plants. *Metallomics* **2015,** *7*, (3), 466-477.

77. Zhao, L.; Peralta-Videa, J. R.; Rico, C. M.; Hernandez-Viezcas, J. A.; Sun, Y.; Niu, G.; Servin, A.; Nunez, J. E.; Duarte-Gardea, M.; Gardea-Torresdey, J. L., CeO2 and ZnO nanoparticles change the nutritional qualities of cucumber (Cucumis sativus). *Journal of Agricultural and Food Chemistry* **2014,** *62*, (13), 2752-2759.

78. Zhao, L.; Sun, Y.; Hernandez-Viezcas, J. A.; Servin, A. D.; Hong, J.; Niu, G.; Peralta-Videa, J. R.; Duarte-Gardea, M.; Gardea-Torresdey, J. L., Influence of CeO2 and ZnO nanoparticles on cucumber physiological markers and bioaccumulation of Ce and Zn: a life cycle study. *Journal of Agricultural and Food Chemistry* **2013,** *61*, (49), 11945-11951.

79. Andersen, C. P.; King, G.; Plocher, M.; Storm, M.; Pokhrel, L. R.; Johnson, M. G.; Rygiewicz, P. T., Germination and early plant development of ten plant species exposed to TiO2 and CeO2 nanoparticles. *Environmental Toxicology and Chemistry* **2016,** *35*, (9), 2223-2229.

80. Hernandez-Viezcas, J. A.; Castillo-Michel, H. A.; Peralta-Videa, J. R.; Gardea-Torresdey, J. L., Interactions between CeO2 nanoparticles and the desert plant mesquite:

A spectroscopy approach. *ACS Sustainable Chemistry & Engineering* **2016,** *4*, (3), 1187-1192.

81. Wang, Q.; Ebbs, S. D.; Chen, Y.; Ma, X., Trans-generational impact of cerium oxide nanoparticles on tomato plants. *Metallomics* **2013,** *5*, (6), 753-759.

82. Zhao, L.; Sun, Y.; Hernandez-Viezcas, J. A.; Hong, J.; Majumdar, S.; Niu, G.; Duarte-Gardea, M.; Peralta-Videa, J. R.; Gardea-Torresdey, J. L., Monitoring the environmental effects of CeO2 and ZnO nanoparticles through the life cycle of corn (Zea mays) plants and in situ μ-XRF mapping of nutrients in kernels. *Environmental Science & Technology* **2015,** *49*, (5), 2921-2928.

83. López-Moreno, M. L.; de la Rosa, G.; Hernández-Viezcas, J. A.; Peralta-Videa, J. R.; Gardea-Torresdey, J. L., X-ray absorption spectroscopy (XAS) corroboration of the uptake and storage of CeO2 nanoparticles and assessment of their differential toxicity in four edible plant species. *Journal of Agricultural and Food Chemistry* **2010,** *58*, (6), 3689-3693.

84. Wang, Q.; Ma, X.; Zhang, W.; Pei, H.; Chen, Y., The impact of cerium oxide nanoparticles on tomato (Solanum lycopersicum L.) and its implications for food safety. *Metallomics* **2012,** *4*, (10), 1105-1112.

85. Zhang, Z.; He, X.; Zhang, H.; Ma, Y.; Zhang, P.; Ding, Y.; Zhao, Y., Uptake and distribution of ceria nanoparticles in cucumber plants. *Metallomics* **2011,** *3*, (8), 816-822.

86. Schwab, F.; Zhai, G.; Kern, M.; Turner, A.; Schnoor, J. L.; Wiesner, M. R., Barriers, pathways and processes for uptake, translocation and accumulation of nanomaterials in plants–critical review. *Nanotoxicology* **2016,** *10*, (3), 257-278.

87. Basavaraju, P.; Shetty, N. P.; Shetty, H. S.; De Neergaard, E.; Jørgensen, H. J. L., Infection biology and defence responses in sorghum against Colletotrichum sublineolum. *Journal of Applied Microbiology* **2009,** *107*, (2), 404-415.

88. Carpita, N. C.; Gibeaut, D. M., Structural models of primary cell walls in flowering plants: consistency of molecular structure with the physical properties of the walls during growth. *The Plant Journal* **1993,** *3*, (1), 1-30.

89. Carpita, N.; Sabularse, D.; Montezinos, D.; Delmer, D. P., Determination of the pore size of cell walls of living plant cells. *Science* **1979,** *205*, (4411), 1144-1147.

90. McCann, M.; Wells, B.; Roberts, K., Direct visualization of cross-links in the primary plant cell wall. *Journal of Cell Science* **1990,** *96*, (2), 323-334.

91. Geisler-Lee, J.; Wang, Q.; Yao, Y.; Zhang, W.; Geisler, M.; Li, K.; Huang, Y.; Chen, Y.; Kolmakov, A.; Ma, X., Phytotoxicity, accumulation and transport of silver nanoparticles by Arabidopsis thaliana. *Nanotoxicology* **2012,** *7*, (3), 323-337.

92. Lucas, W. J.; Lee, J.-Y., Plasmodesmata as a supracellular control network in plants. *Nature Reviews Molecular Cell Biology* **2004,** *5*, (9), 712-726.

93. Zhai, G.; Walters, K. S.; Peate, D. W.; Alvarez, P. J.; Schnoor, J. L., Transport of gold nanoparticles through plasmodesmata and precipitation of gold ions in woody poplar. *Environmental Science & Technology Letters* **2014,** *1*, (2), 146-151.

94. Mezitt, L. A.; Lucas, W. J., Plasmodesmal cell-to-cell transport of proteins and nucleic acids. In *Post-Transcriptional Control of Gene Expression in Plants*, Springer: 1996; pp 251-273.

95. Roberts, A.; Oparka, K., Plasmodesmata and the control of symplastic transport. *Plant, Cell & Environment* **2003,** *26*, (1), 103-124.

96. Lucas, W. J.; Ham, B.-K.; Kim, J.-Y., Plasmodesmata–bridging the gap between neighboring plant cells. *Trends in Cell Biology* **2009,** *19*, (10), 495-503.

97. Steudle, E.; Frensch, J., Water transport in plants: role of the apoplast. *Plant and Soil* **1996,** *187*, (1), 67-79.

98. Lee, W. M.; An, Y. J.; Yoon, H.; Kweon, H. S., Toxicity and bioavailability of copper nanoparticles to the terrestrial plants mung bean (Phaseolus radiatus) and wheat (Triticum aestivum): plant agar test for water‐insoluble nanoparticles. *Environmental Toxicology and Chemistry* **2008,** *27*, (9), 1915-1921.

99. Ma, Y.; He, X.; Zhang, P.; Zhang, Z.; Guo, Z.; Tai, R.; Xu, Z.; Zhang, L.; Ding, Y.; Zhao, Y., Phytotoxicity and biotransformation of La2O3 nanoparticles in a terrestrial plant cucumber (Cucumis sativus). *Nanotoxicology* **2011,** *5*, (4), 743-753.

100. Sun, D.; Hussain, H. I.; Yi, Z.; Siegele, R.; Cresswell, T.; Kong, L.; Cahill, D. M., Uptake and cellular distribution, in four plant species, of fluorescently labeled mesoporous silica nanoparticles. *Plant Cell Reports* **2014,** *33*, (8), 1389-1402.

101. Tripathi, S.; Kapri, S.; Datta, A.; Bhattacharyya, S., Influence of the morphology of carbon nanostructures on the stimulated growth of gram plant. *RSC Advances* **2016,** *6*, (50), 43864-43873.

102. Ma, Y.; Kuang, L.; He, X.; Bai, W.; Ding, Y.; Zhang, Z.; Zhao, Y.; Chai, Z., Effects of rare earth oxide nanoparticles on root elongation of plants. *Chemosphere* **2010,** *78*, (3), 273-279.

103. Zhang, P.; Ma, Y.; Zhang, Z.; He, X.; Zhang, J.; Guo, Z.; Tai, R.; Zhao, Y.; Chai, Z., Biotransformation of ceria nanoparticles in cucumber plants. *ACS Nano* **2012,** *6*, (11), 9943-9950.

104. Zhang, P.; Ma, Y.; Liu, S.; Wang, G.; Zhang, J.; He, X.; Zhang, J.; Rui, Y.; Zhang, Z., Phytotoxicity, uptake and transformation of nano-CeO 2 in sand cultured romaine lettuce. *Environmental Pollution* **2017,** *220*, 1400–1408.

105. Majumdar, S.; Peralta-Videa, J. R.; Bandyopadhyay, S.; Castillo-Michel, H.; Hernandez-Viezcas, J.-A.; Sahi, S.; Gardea-Torresdey, J. L., Exposure of cerium oxide nanoparticles to kidney bean shows disturbance in the plant defense mechanisms. *Journal of Hazardous Materials* **2014,** *278*, 279-287.

106. Hong, J.; Peralta-Videa, J. R.; Rico, C.; Sahi, S.; Viveros, M. N.; Bartonjo, J.; Zhao, L.; Gardea-Torresdey, J. L., Evidence of translocation and physiological impacts of foliar applied CeO2 nanoparticles on cucumber (Cucumis sativus) plants. *Environmental Science & Technology* **2014,** *48*, (8), 4376-4385.

107. Hong, J.; Wang, L.; Sun, Y.; Zhao, L.; Niu, G.; Tan, W.; Rico, C. M.; Peralta-Videa, J. R.; Gardea-Torresdey, J. L., Foliar applied nanoscale and microscale CeO 2 and CuO alter cucumber (Cucumis sativus) fruit quality. *Science of The Total Environment* **2016,** *563*, 904-911.

108. Birbaum, K.; Brogioli, R.; Schellenberg, M.; Martinoia, E.; Stark, W. J.; Günther, D.; Limbach, L. K., No evidence for cerium dioxide nanoparticle translocation in maize plants. *Environmental Science & Technology* **2010,** *44*, (22), 8718-8723.

109. Wang, H.; Wu, F.; Meng, W.; White, J. C.; Holden, P. A.; Xing, B., Engineered nanoparticles may induce genotoxicity. *Environmental Science & Technology* **2013,** *47*, (23), 13212-13214.

110. Ma, C.; Chhikara, S.; Xing, B.; Musante, C.; White, J. C.; Dhankher, O. P., Physiological and Molecular Response of Arabidopsis thaliana (L.) to Nanoparticle Cerium and Indium Oxide Exposure. *ACS Sustainable Chemistry & Engineering* **2013,** *1*, (7), 768-778.

111. Pagano, L.; Servin, A. D.; De La Torre-Roche, R.; Mukherjee, A.; Majumdar, S.; Hawthorne, J.; Marmiroli, M.; Maestri, E.; Marra, R. E.; Isch, S. M., Molecular response of crop plants to engineered nanomaterials. *Environmental Science & Technology* **2016,** *50*, (13), 7198-7207.

112. Morales, M. I.; Rico, C. M.; Hernandez-Viezcas, J. A.; Nunez, J. E.; Barrios, A. C.; Tafoya, A.; Flores-Marges, J. P.; Peralta-Videa, J. R.; Gardea-Torresdey, J. L., Toxicity assessment of cerium oxide nanoparticles in cilantro (Coriandrum sativum L.) plants grown in organic soil. *Journal of Agricultural and Food Chemistry* **2013,** *61*, (26), 6224-6230.

113. Ma, X.; Wang, Q.; Rossi, L.; Ebbs, S. D.; White, J. C., Multigenerational exposure to cerium oxide nanoparticles: Physiological and biochemical analysis reveals transmissible changes in rapid cycling Brassica rapa. *NanoImpact* **2016,** *1*, 46-54.

114. Ma, X.; Wang, Q.; Rossi, L.; Zhang, W., Cerium Oxide Nanoparticles and Bulk Cerium Oxide Leading to Different Physiological and Biochemical Responses in Brassica rapa. *Environmental Science & Technology* **2015,** *50*, (13), 6793-6802.

115. Hale, M. G.; Orcutt, D. M., *The physiology of plants under stress*. John Wiley & Sons.: 1987.

116. Mittler, R., Oxidative stress, antioxidants and stress tolerance. *Trends in Plant Science* **2002,** *7*, (9), 405-410.

117. Sharma, P.; Jha, A. B.; Dubey, R. S.; Pessarakli, M., Reactive oxygen species, oxidative damage, and antioxidative defense mechanism in plants under stressful conditions. *Journal of Botany* **2012,** *2012*, 1-27.

118. Fruehauf, J. P.; Meyskens, F. L., Reactive oxygen species: a breath of life or death? *Clinical Cancer Research* **2007,** *13*, (3), 789-794.

119. Bailey-Serres, J.; Mittler, R., The roles of reactive oxygen species in plant cells. *Plant Physiology* **2006,** *141*, (2), 311-311.

120. Brooker, R. J., *Genetics: analysis & principles*. 5th ed.; McGraw-Hill Education: New York, 2014.

121. Scandalios, J. G., Molecular biology of superoxide dismutase. In *Plant Responses to the Gaseous Environment*, Springer: 1994; pp 147-164.

122. Lindqvist, Y.; Brändén, C., The active site of spinach glycolate oxidase. *Journal of Biological Chemistry* **1989,** *264*, (6), 3624-3628.

123. Dat, J.; Vandenabeele, S.; Vranová, E.; Van Montagu, M.; Inzé, D.; Van Breusegem, F., Dual action of the active oxygen species during plant stress responses. *Cellular and Molecular Life Sciences CMLS* **2000,** *57*, (5), 779-795.

124. Gupta, D. K.; Palma, J. M.; Corpas, F. J., *Reactive oxygen species and oxidative damage in plants under stress*. Springer: 2015.

125. Asada, K., Production and scavenging of reactive oxygen species in chloroplasts and their functions. *Plant Physiology* **2006,** *141*, (2), 391-396.

126. Zhao, L.; Peng, B.; Hernandez-Viezcas, J. A.; Rico, C.; Sun, Y.; Peralta-Videa, J. R.; Tang, X.; Niu, G.; Jin, L.; Varela-Ramirez, A., Stress response and tolerance of Zea mays to CeO2 nanoparticles: cross talk among H2O2, heat shock protein, and lipid peroxidation. *ACS Nano* **2012,** *6*, (11), 9615-9622.

127. Rico, C. M.; Morales, M. I.; McCreary, R.; Castillo-Michel, H.; Barrios, A. C.; Hong, J.; Tafoya, A.; Lee, W.-Y.; Varela-Ramirez, A.; Peralta-Videa, J. R., Cerium oxide nanoparticles modify the antioxidative stress enzyme activities and macromolecule composition in rice seedlings. *Environmental Science & Technology* **2013,** *47*, (24), 14110-14118.

128. Hayes, S. A.; Yu, P.; O'Keefe, T. J.; O'Keefe, M. J.; Stoffer, J. O., The phase stability of cerium species in aqueous systems i. e-ph diagram for the ce hclo 4 h 2 o system. *Journal of the Electrochemical Society* **2002,** *149*, (12), C623-C630.

129. Ojalvo, I.; Rokem, J. S.; Navon, G.; Goldberg, I., 31P NMR study of elicitor treated Phaseolus vulgaris cell suspension cultures. *Plant Physiology* **1987,** *85*, (3), 716-719.

130. Babu, S.; Velez, A.; Wozniak, K.; Szydlowska, J.; Seal, S., Electron paramagnetic study on radical scavenging properties of ceria nanoparticles. *Chemical Physics Letters* **2007,** *442*, (4), 405-408.

131. Heckert, E. G.; Karakoti, A. S.; Seal, S.; Self, W. T., The role of cerium redox state in the SOD mimetic activity of nanoceria. *Biomaterials* **2008,** *29*, (18), 2705-2709.

132. Xia, T.; Kovochich, M.; Liong, M.; Mädler, L.; Gilbert, B.; Shi, H.; Yeh, J. I.; Zink, J. I.; Nel, A. E., Comparison of the mechanism of toxicity of zinc oxide and cerium oxide nanoparticles based on dissolution and oxidative stress properties. *ACS Nano* **2008,** *2*, (10), 2121-2134.

133. Amin, K. A.; Hassan, M. S.; Awad, e.-S.; Hashem, K. S., The protective effects of cerium oxide nanoparticles against hepatic oxidative damage induced by monocrotaline. *International Journal of Nanomedicine* **2011,** *6*, 143-149.

134. OECD, List of Manufactured Nanomaterials and List of Endpoints for Phase One of the Sponsorship Programme for the Testing of Manufactured Nanomaterials: Revision. Safety of manufactured nanomaterials No. 6. In Development, O. f. E. C. a., Ed. Paris, France, 2008.

135. Zhang, Y.; Chen, Y.; Westerhoff, P.; Crittenden, J., Impact of natural organic matter and divalent cations on the stability of aqueous nanoparticles. *Water Research* **2009,** *43*, (17), 4249-4257.

136. Nowack, B.; Bucheli, T. D., Occurrence, behavior and effects of nanoparticles in the environment. *Environmental Pollution* **2007,** *150*, (1), 5-22.

137. Ma, X.; Geisler-Lee, J.; Deng, Y.; Kolmakov, A., Interactions between engineered nanoparticles (ENPs) and plants: phytotoxicity, uptake and accumulation. *Science of the Total Environment* **2010,** *408*, 3053-3061.

138. Brar, S. K.; Verma, M.; Tyagi, R.; Surampalli, R., Engineered nanoparticles in wastewater and wastewater sludge–Evidence and impacts. *Waste Management* **2010,** *30*, (3), 504-520.

139. Pelletier, D. A.; Suresh, A. K.; Holton, G. A.; McKeown, C. K.; Wang, W.; Gu, B.; Mortensen, N. P.; Allison, D. P.; Joy, D. C.; Allison, M. R., Effects of engineered cerium oxide nanoparticles on bacterial growth and viability. *Applied and Environmental Microbiology* **2010,** *76*, (24), 7981-7989.

140. Rosenkranz, P.; Fernández-Cruz, M.; Conde, E.; Ramírez-Fernández, M.; Flores, J.; Fernández, M.; Navas, J., Effects of cerium oxide nanoparticles to fish and mammalian cell lines: An assessment of cytotoxicity and methodology. *Toxicology in Vitro* **2012,** *26*, (6), 888-896.

141. Stampoulis, D.; Sinha, S. K.; White, J. C., Assay-dependent phytotoxicity of nanoparticles to plants. *Environmental Science & Technology* **2009,** *43*, (24), 9473-9479.

142. Zhao, L.; Peralta-Videa, J. R.; Varela-Ramirez, A.; Castillo-Michel, H.; Li, C.; Zhang, J.; Aguilera, R. J.; Keller, A. A.; Gardea-Torresdey, J. L., Effect of surface coating and organic matter on the uptake of CeO 2 NPs by corn plants grown in soil: insight into the uptake mechanism. *Journal of Hazardous Materials* **2012,** *225*, 131-138.

143. Hoagland, D. R.; Arnon, D. I., The water-culture method for growing plants without soil. *Circular. California Agricultural Experiment Station* **1950,** *347*, (2nd edit).

144. Dionisio-Sese, M. L.; Tobita, S., Antioxidant responses of rice seedlings to salinity stress. *Plant Science* **1998,** *135*, (1), 1-9.

145. Bajji, M.; Kinet, J.-M.; Lutts, S., The use of the electrolyte leakage method for assessing cell membrane stability as a water stress tolerance test in durum wheat. *Plant Growth Regulation* **2002,** *36*, (1), 61-70.

146. DiTomaso, J. M.; Shaff, J. E.; Kochian, L. V., Putrescine-induced wounding and its effects on membrane integrity and ion transport processes in roots of intact corn seedlings. *Plant Physiology* **1989,** *90*, (3), 988-995.

147. Gomez-Garay, A.; Pintos, B.; Manzanera, J. A.; Lobo, C.; Villalobos, N.; Martín, L., Uptake of CeO2 nanoparticles and its effect on growth of Medicago arborea in vitro plantlets. *Biological Trace Element Research* **2014,** *161*, (1), 143-150.

148. Qu, C.; Gong, X.; Liu, C.; Hong, M.; Wang, L.; Hong, F., Effects of manganese deficiency and added cerium on photochemical efficiency of maize chloroplasts. *Biological Trace Element Research* **2012,** *146*, (1), 94-100.

149. Qu, C.; Liu, C.; Guo, F.; Hu, C.; Ze, Y.; Li, C.; Zhou, Q.; Hong, F., Improvement of cerium on photosynthesis of maize seedlings under a combination of potassium deficiency and salt stress. *Biological Trace Element Research* **2013,** *155*, (1), 104-113.

150. Loomis, R.; Torrey, J., Chemical control of vascular cambium initiation in isolated radish roots. *Proceedings of the National Academy of Sciences* **1964,** *52*, (1), 3-11.

151. Parida, A. K.; Das, A. B., Salt tolerance and salinity effects on plants: a review. *Ecotoxicology and Environmental Safety* **2005,** *60*, (3), 324-349.

152. Marcelis, L.; Van Hooijdonk, J., Effect of salinity on growth, water use and nutrient use in radish (Raphanus sativus L.). *Plant and Soil* **1999,** *215*, (1), 57-64.

153. Trujillo-Reyes, J.; Vilchis-Nestor, A.; Majumdar, S.; Peralta-Videa, J.; Gardea-Torresdey, J., Citric acid modifies surface properties of commercial CeO 2 nanoparticles reducing their toxicity and cerium uptake in radish (Raphanus sativus) seedlings. *Journal of Hazardous Materials* **2013,** *263*, 677-684.

154. Tassi, E.; Giorgetti, L.; Morelli, E.; Peralta-Videa, J.; Gardea-Torresdey, J.; Barbafieri, M., Physiological and biochemical responses of sunflower (Helianthus annuus L.) exposed to nano-CeO 2 and excess boron: Modulation of boron phytotoxicity. *Plant Physiology and Biochemistry* **2017,** *110*, 50-58.

155. Majumdar, S.; Peralta-Videa, J. R.; Trujillo-Reyes, J.; Sun, Y.; Barrios, A. C.; Niu, G.; Flores-Margez, J. P.; Gardea-Torresdey, J. L., Soil organic matter influences cerium translocation and physiological processes in kidney bean plants exposed to cerium oxide nanoparticles. *Science of the Total Environment* **2016,** *569*, 201-211.

156. Zhang, W.; Ebbs, S. D.; Musante, C.; White, J. C.; Gao, C.; Ma, X., Uptake and accumulation of bulk and nano-sized cerium oxide particles and ionic cerium by radish (*Raphanus sativus* L.). *Journal of Agricultural and Food Chemistry* **2015,** *63*, (2), 382–390.

157. Mittal, S.; Pandey, A. K., Cerium oxide nanoparticles induced toxicity in human lung cells: role of ROS mediated DNA damage and apoptosis. *BioMed Research International* **2014,** *2014*.

158. Zhang, W.; Dan, Y.; Shi, H.; Ma, X., Effects of Aging on the Fate and Bioavailability of Cerium Oxide Nanoparticles to Radish (Raphanus sativus L.) in Soil. *ACS Sustainable Chemistry & Engineering* **2016,** *4*, (10), 5424-5431.

159. Laborda, F.; Bolea, E.; Cepriá, G.; Gómez, M. T.; Jiménez, M. S.; Pérez-Arantegui, J.; Castillo, J. R., Detection, characterization and quantification of inorganic engineered nanomaterials: A review of techniques and methodological approaches for the analysis of complex samples. *Analytica Chimica Acta* **2016,** *904*, 10-32.

160. Loeschner, K.; Brabrand, M. S. J.; Sloth, J. J.; Larsen, E. H., Use of alkaline or enzymatic sample pretreatment prior to characterization of gold nanoparticles in animal tissue by single-particle ICPMS. *Analytical and Bioanalytical Chemistry* **2014,** *406*, (16), 3845-3851.

161. Dan, Y.; Ma, X.; Zhang, W.; Liu, K.; Stephan, C.; Shi, H., Single particle ICP-MS method development for the determination of plant uptake and accumulation of CeO2 nanoparticles. *Analytical and Bioanalytical Chemistry* **2016,** *408*, (19), 5157-5167.

162. Dan, Y.; Zhang, W.; Xue, R.; Ma, X.; Stephan, C.; Shi, H., Characterization of Gold Nanoparticle Uptake by Tomato Plants Using Enzymatic Extraction Followed by Single-Particle Inductively Coupled Plasma–Mass Spectrometry Analysis. *Environmental Science & Technology* **2015,** *49*, (5), 3007-3014.

163. LeFevre, G. H.; Hozalski, R. M.; Novak, P. J., Root exudate enhanced contaminant desorption: an abiotic contribution to the rhizosphere effect. *Environmental Science & Technology* **2013,** *47*, (20), 11545-11553.

164. Brandt, K. K.; Sjøholm, O. R.; Krogh, K. A.; Halling-Sørensen, B.; Nybroe, O., Increased pollution-induced bacterial community tolerance to sulfadiazine in soil hotspots amended with artificial root exudates. *Environmental Science & Technology* **2009,** *43*, (8), 2963-2968.

165. Henry, S.; Texier, S.; Hallet, S.; Bru, D.; Dambreville, C.; Chèneby, D.; Bizouard, F.; Germon, J.; Philippot, L., Disentangling the rhizosphere effect on nitrate reducers and denitrifiers: insight into the role of root exudates. *Environmental Microbiology* **2008,** *10*, (11), 3082-3092.

166. Barrios, A. C.; Rico, C. M.; Trujillo-Reyes, J.; Medina-Velo, I. A.; Peralta-Videa, J. R.; Gardea-Torresdey, J. L., Effects of uncoated and citric acid coated cerium oxide nanoparticles, bulk cerium oxide, cerium acetate, and citric acid on tomato plants. *Science of The Total Environment* **2016,** *563*, 956-964.

167. Yang, X.; Pan, H.; Wang, P.; Zhao, F.-J., Particle-specific toxicity and bioavailability of cerium oxide (CeO 2) nanoparticles to Arabidopsis thaliana. *Journal of Hazardous Materials* **2017,** *322*, 292-300.

168. Shyam, R.; Aery, N., Effect of cerium on growth, dry matter production, biochemical constituents and enzymatic activities of cowpea plants [Vigna unguiculata (L.) Walp.]. *Journal of Soil Science and Plant Nutrition* **2012,** *12*, (1), 1-14.

169. Pang, X.; Li, D.; Peng, A., Application of rare-earth elements in the agriculture of China and its environmental behavior in soil. *Environmental Science and Pollution Research* **2002,** *9*, (2), 143-148.

170. Liu, D.; Wang, X.; Lin, Y.; Chen, Z.; Xu, H.; Wang, L., The effects of cerium on the growth and some antioxidant metabolisms in rice seedlings. *Environmental Science and Pollution Research* **2012,** *19*, (8), 3282-3291.

171. Ma, C.; Rui, Y.; Liu, S.; Li, X.; Xing, B.; Liu, L., Phytotoxic mechanism of nanoparticles: destruction of chloroplasts and vascular bundles and alteration of nutrient absorption. *Scientific Reports* **2015,** *5*, 11618.

172. Li, K.; Zhang, W.; Huang, Y.; Chen, Y., Aggregation kinetics of CeO2 nanoparticles in KCl and CaCl2 solutions: measurements and modeling. *Journal of Nanoparticle Research* **2011,** *13*, (12), 6483-6491.

173. Bais, H. P.; Weir, T. L.; Perry, L. G.; Gilroy, S.; Vivanco, J. M., The role of root exudates in rhizosphere interactions with plants and other organisms. *Annual Review of Plant Biology* **2006,** *57*, 233-266.

174. Rovira, A. D., Plant root exudates. *The Botanical Review* **1969,** *35*, (1), 35-57.

175. Zahra, Z.; Arshad, M.; Rafique, R.; Mahmood, A.; Habib, A.; Qazi, I. A.; Khan, S. A., Metallic Nanoparticle (TiO2 and Fe3O4) Application Modifies Rhizosphere Phosphorus Availability and Uptake by Lactuca sativa. *Journal of Agricultural and Food Chemistry* **2015,** *63*, (31), 6876-6882.

176. Stegemeier, J. P.; Schwab, F.; Colman, B. P.; Webb, S. M.; Newville, M.; Lanzirotti, A.; Winkler, C.; Wiesner, M. R.; Lowry, G. V., Speciation Matters: Bioavailability of Silver and Silver Sulfide Nanoparticles to Alfalfa (Medicago sativa). *Environmental Science & Technology* **2015,** *49*, (14), 8451-8460.

177. Dewick, P. M., *Essentials of organic chemistry: for students of pharmacy, medicinal chemistry and biological chemistry*. John Wiley & Sons: New Jersey, 2006.

178. Cornelis, G.; Ryan, B.; McLaughlin, M. J.; Kirby, J. K.; Beak, D.; Chittleborough, D., Solubility and batch retention of CeO2 nanoparticles in soils. *Environmental Science & Technology* **2011,** *45*, (7), 2777-2782.

179. Um, N.; Miyake, M.; Hirato, T., Dissolution of Cerium Oxide in Sulfuric Acid. In *Zero-Carbon Energy Kyoto 2010*, Springer: 2011; pp 165-170.

180. Preston, J.; Cole, P.; Du Preez, A.; Fox, M.; Fleming, A., The recovery of rare earth oxides from a phosphoric acid by-product. Part 2: The preparation of high-purity cerium dioxide and recovery of a heavy rare earth oxide concentrate. *Hydrometallurgy* **1996,** *41*, (1), 21-44.

181. Ebbing, D.; Gammon, S. D., *General chemistry*. Cengage Learning: 2010.

182. Karp, G., *Cell and molecular biology*. Hoboken. New Jersey: John Wiley & Sons, Inc: 2008.

183. Sharpe, E.; Frasco, T.; Andreescu, D.; Andreescu, S., Portable ceria nanoparticle-based assay for rapid detection of food antioxidants (NanoCerac). *Analyst* **2013,** *138*, (1), 249-262.

184. Li, J.; Lu, Y.; Shim, H.; Deng, X.; Lian, J.; Jia, Z.; Li, J., Use of the BCR sequential extraction procedure for the study of metal availability to plants. *Journal of Environmental Monitoring* **2010,** *12*, (2), 466-471.

185. Sahuquillo, A.; Rigol, A.; Rauret, G., Overview of the use of leaching/extraction tests for risk assessment of trace metals in contaminated soils and sediments. *TrAC Trends in Analytical Chemistry* **2003,** *22*, (3), 152-159.

186. Ernst, W. H. O., Bioavailability of heavy metals and decontamination of soils by plants. *Applied Geochemistry* **1996,** *11*, (1), 163-167.

187. Zhong, X.; Zhou, S.; Zhu, Q.; Zhao, Q., Fraction distribution and bioavailability of soil heavy metals in the Yangtze River Delta—A case study of Kunshan City in Jiangsu Province, China. *Journal of Hazardous Materials* **2011,** *198*, 13-21.

188. Gleyzes, C.; Tellier, S.; Astruc, M., Fractionation studies of trace elements in contaminated soils and sediments: a review of sequential extraction procedures. *TrAC Trends in Analytical Chemistry* **2002,** *21*, (6), 451-467.

189. Ure, A. M.; Quevauvillerb, P.; Muntauc, H.; Griepinkb, B., Speciation of heavy-metals in soils and sediments - an account of the improvement and harmonization of extraction techniques undertaken under the auspices of the BCR of the Commission of the European Communities. *International Journal of Environmental Analytical Chemistry* **1993,** *51*, (1-4), 135-151.

190. Rauret, G.; Lopez-Sanchez, J.; Sahuquillo, A.; Rubio, R.; Davidson, C.; Ure, A.; Quevauviller, P., Improvement of the BCR three step sequential extraction procedure prior to the certification of new sediment and soil reference materials. *Journal of Environmental Monitoring* **1999,** *1*, (1), 57-61.

191. Bouyoucos, G. J., Hydrometer method improved for making particle size analyses of soils. *Agronomy Journal* **1962,** *54*, (5), 464-465.

192. Holden, P. A.; Klaessig, F.; Turco, R. F.; Priester, J. H.; Rico, C. M.; Avila-Arias, H.; Mortimer, M.; Pacpaco, K.; Gardea-Torresdey, J. L., Evaluation of exposure concentrations used in assessing manufactured nanomaterial environmental hazards: are they relevant? *Environmental Science & Technology* **2014,** *48*, (18), 10541-10551.

193. Antisari, L. V.; Carbone, S.; Fabrizi, A.; Gatti, A.; Vianello, G., Response of soil microbial biomass to CeO2 nanoparticles. *EQA-International Journal of Environmental Quality* **2011,** *7*, (7), 1-16.

194. Allen, B. L.; Hajek, B. F., Mineral occurrence in soil environments. *Minerals in Soil Environments* **1989,** *2*, 199-278.

195. Post, J. E., Manganese oxide minerals: Crystal structures and economic and environmental significance. *Proceedings of the National Academy of Sciences* **1999,** *96*, (7), 3447-3454.

196. Lin, D.; Tian, X.; Wu, F.; Xing, B., Fate and transport of engineered nanomaterials in the environment. *Journal of Environmental Quality* **2010,** *39*, (6), 1896-1908.

197. Ebbs, S. D.; Bradfield, S. J.; Kumar, P.; White, J. C.; Musante, C.; Ma, X., Accumulation of zinc, copper, or cerium in carrot (Daucus carota) exposed to metal oxide nanoparticles and metal ions. *Environmental Science: Nano* **2016,** *3*, 114-126.

198. Lock, K.; Janssen, C. R., Influence of aging on metal availability in soils. *Reviews of Environmental Contamination and Toxicology* **2003,** *178*, (1), 1-21.

199. Coutris, C.; Joner, E. J.; Oughton, D. H., Aging and soil organic matter content affect the fate of silver nanoparticles in soil. *Science of the Total Environment* **2012,** *420*, 327-333.

200. Jalali, M.; Khanlari, Z., Effect of aging process on the fractionation of heavy metals in some calcareous soils of Iran. *Geoderma* **2008,** *143*, (1), 26-40.

201. Diez-Ortiz, M.; Lahive, E.; George, S.; Ter Schure, A.; Van Gestel, C. A.; Jurkschat, K.; Svendsen, C.; Spurgeon, D. J., Short-term soil bioassays may not reveal the full toxicity potential for nanomaterials; bioavailability and toxicity of silver ions (AgNO 3) and silver nanoparticles to earthworm Eisenia fetida in long-term aged soils. *Environmental Pollution* **2015,** *203*, 191-198.

202. Sposito, G., *The chemistry of soils*. Oxford university press: 2008.

203. Kuchibhatla, S. V.; Karakoti, A. S.; Baer, D. R.; Samudrala, S.; Engelhard, M. H.; Amonette, J. E.; Thevuthasan, S.; Seal, S., Influence of aging and environment on nanoparticle chemistry: implication to confinement effects in nanoceria. *Journal of Physical Chemistry C* **2012,** *116*, (26), 14108-14114.

204. Cervini-Silva, J.; Fowle, D. A.; Banfield, J., Biogenic dissolution of a soil cerium-phosphate mineral. *American Journal of Science* **2005,** *305*, (6-8), 711-726.

205. Turekian, K. K.; Wedepohl, K. H., Distribution of the elements in some major units of the earth's crust. *Geological Society of America Bulletin* **1961,** *72*, (2), 175-192.

206. Liu, X.; Byrne, R. H., Rare earth and yttrium phosphate solubilities in aqueous solution. *Geochimica et Cosmochimica Acta* **1997,** *61*, (8), 1625-1633.

207. Chang, S.; Jackson, M. L., Fractionation of soil phosphorus. *Soil Science* **1957,** *84*, (2), 133-144.

208. Zhang, W.; Musante, C.; White, J. C.; Schwab, P.; Wang, Q.; Ebbs, S. D.; Ma, X., Bioavailability of cerium oxide nanoparticles to Raphanus sativus L. in two soils. *Plant Physiology and Biochemistry* **2017,** *110*, 185-193.

209. Golden, T. D.; Wang, A. Q., Anodic electrodeposition of cerium oxide thin films II. Mechanism studies. *Journal of the Electrochemical Society* **2003,** *150*, (9), C621-C624.

210. Sparks, D. L., *Environmental soil chemistry*. Academic press: 2003.

211. Berdanier, C. D.; Berdanier, L. A.; Zempleni, J., *Advanced nutrition: macronutrients, micronutrients, and metabolism*. CRC Press: 2008.

212. Peijnenburg, W.; Praetorius, A.; Scott-Fordsmand, J.; Cornelis, G., Fate assessment of engineered nanoparticles in solids dominated media–Current insights and the way forward. *Environmental Pollution* **2016,** *218*, 1365-1369.

213. Cai, L.; Tong, M.; Wang, X.; Kim, H., Influence of clay particles on the transport and retention of titanium dioxide nanoparticles in quartz sand. *Environmental Science & Technology* **2014,** *48*, (13), 7323-7332.

214. Cornelis, G.; DooletteMadeleine Thomas, C.; McLaughlin, M. J.; Kirby, J. K.; Beak, D. G.; Chittleborough, D., Retention and dissolution of engineered silver nanoparticles in natural soils. *Soil Science Society of America Journal* **2012,** *76*, (3), 891-902.

215. Schlich, K.; Hund-Rinke, K., Influence of soil properties on the effect of silver nanomaterials on microbial activity in five soils. *Environmental Pollution* **2015,** *196*, 321-330.

216. Labille, J.; Harns, C.; Bottero, J.-Y.; Brant, J., Heteroaggregation of titanium dioxide nanoparticles with natural clay colloids. *Environmental Science & Technology* **2015,** *49*, (11), 6608-6616.

217. Foo, K.; Hameed, B., Insights into the modeling of adsorption isotherm systems. *Chemical Engineering Journal* **2010,** *156*, (1), 2-10.

218. Wang, H.; Adeleye, A. S.; Huang, Y.; Li, F.; Keller, A. A., Heteroaggregation of nanoparticles with biocolloids and geocolloids. *Advances in Colloid and Interface Science* **2015,** *226*, 24-36.

219. Sotirelis, N. P.; Chrysikopoulos, C. V., Interaction between graphene oxide nanoparticles and quartz sand. *Environmental Science & Technology* **2015,** *49*, (22), 13413-13421.

220. Buettner, K. M.; Rinciog, C. I.; Mylon, S. E., Aggregation kinetics of cerium oxide nanoparticles in monovalent and divalent electrolytes. *Colloids and Surfaces A: Physicochemical and Engineering Aspects* **2010,** *366*, (1), 74-79.

221. Hotze, E. M.; Phenrat, T.; Lowry, G. V., Nanoparticle aggregation: challenges to understanding transport and reactivity in the environment. *Journal of Environmental Quality* **2010,** *39*, (6), 1909-1924.

222. Song, J. E.; Phenrat, T.; Marinakos, S.; Xiao, Y.; Liu, J.; Wiesner, M. R.; Tilton, R. D.; Lowry, G. V., Hydrophobic interactions increase attachment of gum arabic-and

PVP-coated Ag nanoparticles to hydrophobic surfaces. *Environmental Science & Technology* **2011,** *45*, (14), 5988-5995.

223. Stebounova, L. V.; Guio, E.; Grassian, V. H., Silver nanoparticles in simulated biological media: a study of aggregation, sedimentation, and dissolution. *Journal of Nanoparticle Research* **2011,** *13*, (1), 233-244.

224. Sharma, M. M.; Kuo, J.; Yen, T., Further investigation of the surface charge properties of oxide surfaces in oil-bearing sands and sandstones. *Journal of Colloid and Interface Science* **1987,** *115*, (1), 9-16.

225. Lützenkirchen, J.; Preočanin, T.; Kovačević, D.; Tomišić, V.; Lövgren, L.; Kallay, N., Potentiometric titrations as a tool for surface charge determination. *Croatica Chemica Acta* **2012,** *85*, (4), 391-417.

226. Saleh, N.; Kim, H.-J.; Phenrat, T.; Matyjaszewski, K.; Tilton, R. D.; Lowry, G. V., Ionic strength and composition affect the mobility of surface-modified Fe0 nanoparticles in water-saturated sand columns. *Environmental Science & Technology* **2008,** *42*, (9), 3349-3355.

227. Zhang, W.; Morales, V. L.; Cakmak, M. E.; Salvucci, A. E.; Geohring, L. D.; Hay, A. G.; Parlange, J.-Y.; Steenhuis, T. S., Colloid transport and retention in unsaturated porous media: Effect of colloid input concentration. *Environmental Science & Technology* **2010,** *44*, (13), 4965-4972.

228. Abu-Lail, N. I.; Camesano, T. A., Role of Ionic Strength on the Relationship of Biopolymer Conformation, DLVO Contributions, and Steric Interactions to Bioadhesion of P seudomonas p utida KT2442. *Biomacromolecules* **2003,** *4*, (4), 1000-1012.

229. Karimian, H.; Babaluo, A., Halos mechanism in stabilizing of colloidal suspensions: Nanoparticle weight fraction and pH effects. *Journal of the European Ceramic Society* **2007,** *27*, (1), 19-25.

230. Einarson, M. B.; Berg, J. C., Electrosteric stabilization of colloidal latex dispersions. *Journal of Colloid and Interface Science* **1993,** *155*, (1), 165-172.

231. Masel, R. I., *Principles of adsorption and reaction on solid surfaces*. John Wiley & Sons: 1996; Vol. 3.

232. Dubinin, M.; Radushkevich, L., Equation of the characteristic curve of activated charcoal. *Chemisches Zentralblatt* **1947,** *1*, (1), 875.

233. Jolivet, J.-P.; Henry, M.; Livage, J., *Metal oxide chemistry and synthesis: from solution to solid state*. Wiley-Blackwell: 2000.

234. Oriekhova, O.; Stoll, S., Effects of pH and fulvic acids concentration on the stability of fulvic acids–cerium (IV) oxide nanoparticle complexes. *Chemosphere* **2016,** *144*, 131-137.

235. Kosmulski, M., The pH-dependent surface charging and points of zero charge: V. Update. *Journal of Colloid and Interface Science* **2011,** *353*, (1), 1-15.

236. Yukselen, Y.; Kaya, A., Zeta potential of kaolinite in the presence of alkali, alkaline earth and hydrolyzable metal ions. *Water, Air, and Soil Pollution* **2003,** *145*, (1-4), 155-168.

237. Barton, L. E.; Therezien, M.; Auffan, M.; Bottero, J.-Y.; Wiesner, M. R., Theory and methodology for determining nanoparticle affinity for heteroaggregation in

environmental matrices using batch measurements. *Environmental Engineering Science* **2014,** *31*, (7), 421-427.

238. Kim, H.-J.; Phenrat, T.; Tilton, R. D.; Lowry, G. V., Effect of kaolinite, silica fines and pH on transport of polymer-modified zero valent iron nano-particles in heterogeneous porous media. *Journal of Colloid and Interface science* **2012,** *370*, (1), 1-10.

239. Rodrigues, S.; Trindade, T.; Duarte, A.; Pereira, E.; Koopmans, G.; Römkens, P., A framework to measure the availability of engineered nanoparticles in soils: Trends in soil tests and analytical tools. *TrAC Trends in Analytical Chemistry* **2016,** *75*, 129-140.

240. Zhou, D.; Abdel-Fattah, A. I.; Keller, A. A., Clay particles destabilize engineered nanoparticles in aqueous environments. *Environmental Science & Technology* **2012,** *46*, (14), 7520-7526.

241. Wang, H.; Dong, Y.-n.; Zhu, M.; Li, X.; Keller, A. A.; Wang, T.; Li, F., Heteroaggregation of engineered nanoparticles and kaolin clays in aqueous environments. *Water Research* **2015,** *80*, 130-138.

242. Phenrat, T.; Saleh, N.; Sirk, K.; Kim, H.-J.; Tilton, R. D.; Lowry, G. V., Stabilization of aqueous nanoscale zerovalent iron dispersions by anionic polyelectrolytes: adsorbed anionic polyelectrolyte layer properties and their effect on aggregation and sedimentation. *Journal of Nanoparticle Research* **2008,** *10*, (5), 795-814.

243. Ghorbel-Abid, I.; Trabelsi-Ayadi, M., Competitive adsorption of heavy metals on local landfill clay. *Arabian Journal of Chemistry* **2015,** *8*, (1), 25-31.

244. Lecoanet, H. F.; Bottero, J.-Y.; Wiesner, M. R., Laboratory assessment of the mobility of nanomaterials in porous media. *Environmental Science & Technology* **2004,** *38*, (19), 5164-5169.

245. Huang, L.; Fang, H.; Chen, M., Experiment on surface charge distribution of fine sediment. *Science China Technological Sciences* **2012,** *55*, (4), 1146-1152.

246. Tombácz, E.; Szekeres, M., Surface charge heterogeneity of kaolinite in aqueous suspension in comparison with montmorillonite. *Applied Clay Science* **2006,** *34*, (1), 105-124.

247. Treybal Robert, E., *Mass-transfer operations*. McGraw-Hill New York: 1980; Vol. 3.

248. Dada, A.; Olalekan, A.; Olatunya, A.; Dada, O., Langmuir, Freundlich, Temkin and Dubinin–Radushkevich isotherms studies of equilibrium sorption of Zn2+ unto phosphoric acid modified rice husk. *Journal of Applied Chemistry* **2012,** *3*, (1), 38-45.